

The Pennsylvania State University

The Graduate School

Eberly College of Science

**THE STABILITY OF HABITABLE PLANETARY ENVIRONMENTS**

A Thesis in

Astronomy and Astrophysics

by

Darren M. Williams

Copyright 1998 Darren M. Williams

Submitted in Partial Fulfillment  
of the Requirements  
for the Degree of

Doctor of Philosophy

May 1998

We approve the thesis of Darren M. Williams.

Date of Signature

---

James F. Kasting  
Professor of Geosciences and Meteorology  
Thesis Advisor  
Co-chair of Committee

---

Richard A. Wade  
Associate Professor of Astronomy and Astrophysics  
Co-chair of Committee

---

Pablo Laguna  
Assistant Professor of Astronomy and Astrophysics

---

Jorge Pullin  
Associate Professor of Physics

---

Alexander Wolszczan  
Distinguished Professor of Astronomy and Astrophysics

---

Peter Mészáros  
Professor of Astronomy and Astrophysics  
Head of Department of Astronomy and Astrophysics

## ABSTRACT

The recent discoveries of extrasolar planets have generated widespread anticipation of detecting a life-supporting environment, such as an Earth-like planet or moon, around a nearby solar-type star. Future observations will enable life on such worlds to be detected remotely through the spectral identification of  $\text{CH}_4$ ,  $\text{O}_3$ , and  $\text{H}_2\text{O}$  vapor in their atmospheres. This thesis addresses the climatic and dynamic factors affecting whether an Earth-like biosphere might exist around another star and, hence, the likelihood that extraterrestrial life will be discovered in the foreseeable future.

To remain habitable for billions of years, a planetary body must be large enough to form and retain an atmosphere. Earth's Moon ( $\sim 0.01M_\oplus$ ) does not satisfy this basic criterion. Objects with atmospheres must orbit their stars within the habitable zone (HZ) for liquid water to exist on their surfaces. Otherwise habitable worlds can have their climates destabilized by the slow brightening of their stars as the age, or by chaotic variability of their orbits and obliquities over time. Earth's  $23.5^\circ$ -obliquity is presently stable, but the spin-stability of extrasolar Earths will depend on the masses and proximity of satellites and neighboring planets.

Climates of planets with high obliquities are investigated using an energy-balance climate model. At high obliquity, Earth's climatic zonation is reversed so that the lower latitudes are permanently frozen and the poles are subjected to extraordinary swings in seasonal temperature. Planets within the outer HZs around their stars are less affected by obliquity because they develop dense- $\text{CO}_2$  atmospheres as a result of the carbonate-silicate geochemical cycle. Efficient heat transport within such atmospheres reduce latitudinal temperature gradients and limit the amplitudes of seasonal temperature extremes.

Geologic evidence for low-latitude glaciation during the Precambrian era sug-

gests that the obliquity of early-Earth may have been much higher than it is today. Earth's obliquity could have been reduced to its present value as a consequence of obliquity-oblateness feedback. In this process, obliquity-driven changes to continental ice volume and oblateness may have caused a secular downward drift in obliquity of  $\sim 30^\circ$  between 600 Ma and 500 Ma. Such an event may account for the present non-zero inclination of the lunar orbit.

# TABLE OF CONTENTS

LIST OF FIGURES .....	viii
LIST OF TABLES .....	x
ACKNOWLEDGMENTS .....	xi
Chapter 1. INTRODUCTION .....	1
1.1 Stars With Planetary Systems .....	1
1.2 Habitable Zones .....	2
1.3 Extrasolar Planets .....	6
1.4 Orbital Stability of Terrestrial Planets .....	10
1.5 Spin Stability and Climate .....	12
1.6 Thesis Outline .....	14
Chapter 2. THE EFFECT OF HIGH OBLIQUITY ON PLANETARY CLIMATE .....	16
2.1 Overview .....	16
2.2 Model Description .....	17
2.2.1 Energy-Balance Methods .....	17
2.2.2 Diurnally-Averaged Incident Solar Flux (S) .....	18
2.2.3 Top-of-Atmosphere Albedo (A) .....	20
2.2.4 Surface Albedo ( $a_s$ ) .....	23
2.2.5 Effective Heat Capacity (C) .....	25
2.2.6 Outgoing Infrared Flux (I) .....	26
2.2.7 The Carbonate-Silicate Weathering Cycle .....	28
2.2.8 Dynamic Heat Transport .....	30
2.2.9 CO <sub>2</sub> Clouds .....	33
2.2.10 Solving the Model .....	35
2.3 Results .....	36
2.3.1 Earth's Present Climate .....	36
2.3.2 Earth at 90° Obliquity .....	37
2.3.3 Effects of Changing the Geography .....	40
2.3.4 Dense CO <sub>2</sub> Atmospheres and the HZ Outer Edge .....	43
2.3.5 Temperature Gradients and Seasonal Cycles at 1.4 AU .....	45
2.4 Discussion .....	48

Chapter 3. THE EQUATIONS OF PRECESSION .....	51
3.1 Preface .....	51
3.2 Torques on Earth's Equatorial Bulge .....	52
3.3 Averaging the Torques Over an Orbit .....	54
3.4 The Moving Ecliptic Plane .....	58
3.5 Converting to the Notation of Laskar .....	62
3.6 The Laplace-Lagrange Variables $\mathbf{h}$ , $\mathbf{k}$ , $\mathbf{p}$ , and $\mathbf{q}$ .....	64
3.7 Solving the Precession Equations .....	67
Chapter 4. THE SYMPLECTIC ORBIT INTEGRATOR <i>SWIFT</i> .....	70
4.1 Symplectic Integration .....	70
4.2 Phase Error .....	71
4.3 SWIFT .....	72
4.4 Numerical Precision and Choice of Time Step .....	73
Chapter 5. HIGH OBLIQUITY AS AN EXPLANATION FOR LOW- LATITUDE GLACIAL CLIMATES OF THE EARLY EARTH .....	74
5.1 Overview .....	74
5.2 Climate Friction .....	76
5.3 Changes to Oblateness During an Ice Age .....	80
5.4 Drift Dependence on the Ice-Sheet-Formation Phase Lag .....	87
5.5 Results .....	90
5.6 Explaining the Inclination of the Lunar Orbit .....	92
Chapter 6. THE SUSCEPTIBILITY OF EARTH-LIKE PLANETS TO LARGE OBLIQUITY VARIATIONS .....	95
6.1 Motion of Earth's Spin Axis .....	95
6.2 Influence of the Moon on Precession .....	98
6.3 Planet Spacing and Orbit Precession .....	100
6.4 Earth's Position Within the Habitable Zone .....	107
6.5 Extrasolar Earths .....	107
Chapter 7. HABITABLE MOONS AROUND EXTRASOLAR GIANT PLANETS .....	111
7.1 Moons as Life-Supporting Environments .....	111
7.2 Volatile Endowments .....	113
7.3 Atmospheric Retention .....	115
7.3.1 Thermal Escape .....	115

7.3.2 Escape by Dissociative Recombination .....	116
7.3.3 Loss of Atmosphere by Sputtering .....	117
7.4 Tidal Locking and Spin .....	118
7.5 Eccentric Orbits .....	118
7.6 Climate Stabilization and the Carbonate-Silicate Cycle .....	119
7.7 Tidal Heating .....	120
Chapter 8. CONCLUSIONS .....	121
8.1 Opening Summary .....	121
8.2 Obliquity and Climate – Chapter 2 .....	122
8.3 Obliquity-Oblateness Feedback – Chapter 5 .....	123
8.4 Precession and Obliquity – Chapter 6 .....	124
8.5 Moons Around Giant Planets – Chapter 7 .....	125
8.6 Directions For Future Research .....	126
REFERENCE LIST .....	128

## LIST OF FIGURES

1.1 The approximate width of the habitable zone around low-mass stars .....	5
1.2 Conditions for orbital stability in 3-body systems .....	11
2.1 Zonal energy fluxes calculated by the energy-balance climate model .....	18
2.2 Low- and high-temperature model fits to top-of-atmosphere albedo .....	21
2.3 Model fits to outgoing infrared flux .....	27
2.4 Representative seasonal temperature cycles for Earth .....	38
2.5 Variations in the global-mean weathering rate over a seasonal cycle .....	41
2.6 Carbonate-silicate cycle equilibrium CO <sub>2</sub> levels (solid line) for Earth at a variety of positions within the HZ .....	44
2.7 Latitudinal temperature profiles for Earth at 1.0 AU and 1.4 AU .....	46
2.8 Seasonal temperature cycles for Earth at 1.4 AU, and with 90° obliquity .....	47
3.1 The Earth-Sun (or Earth-Moon) configuration of maximum precessional torque .....	52
3.2 Variables used in averaging the precessional torques over an orbit .....	54
3.3 Planes and variables of precession .....	59
4.1 The principle of the symplectic orbit integrator <i>SWIFT</i> .....	71
5.1 Diurnally-averaged, summer-solstice insolation received at 45°N latitude .....	78
5.2 Oblateness response to a hypothetical, sinusoidal obliquity cycle .....	79
5.3 Geometry for the calculation of the ice-age change to oblateness .....	82
5.4 Change to Earth's oblateness ( $\Delta J_2/J_2$ ) from continental ice loading and a lowering of sea level .....	86
5.5 Rate and direction of obliquity drift for different values of the phase lag ( $\xi_i$ ) ..	88

5.6 Insolation and relative sea level for the period defining the last deglaciation ..	89
5.7 Secular drift in obliquity over 100 Myr spanning the Late Proterozoic-Cambrian boundary .....	91
5.8 Momentum exchange between the Earth and Moon as a consequence of their tidal evolution .....	93
6.1 The obliquity of Earth over 1 Myr with the Moon (A) and without the Moon (B) .....	96
6.2 The leading orbit-precession frequencies for Earth in the present Solar System, with Jupiter at 5.2 AU .....	97
6.3 Fourier spectrum of Earth's orbit precession frequencies .....	98
6.4 Zone of chaotic behavior for the motion of Earth's spin axis .....	99
6.5 Dependence of the precession constant $\alpha$ on satellite mass .....	100
6.6 Variation in Earth's obliquity over 1 Myr as a function of Jupiter's orbital position .....	102
6.7 Fourier spectrum of Earth's orbital precession frequencies with Jupiter at 4.1 AU .....	103
6.8 Earth's obliquity over 1 Myr with Jupiter at 4.1 AU .....	104
6.9 Fourier spectrum of Earth's orbital precession frequencies with Jupiter at 3.1 AU .....	105
6.10 Earth's obliquity over 1 Myr with Jupiter at 3.1 AU .....	106
6.11 Range of Earth's obliquity over 1 Myr as a function of Earth's orbital position within the HZ .....	108
6.12 Obliquity variations of a hypothetical Earth-like planet orbiting at 1.0 AU from stars: (a) 47 UMa and (b) $\rho$ CrB .....	109
7.1 Locations of recently discovered or confirmed companions to nearby stars with respect to the HZ .....	112

## LIST OF TABLES

1.1 Physical parameters of known extrasolar planets .....	8
2.1 Latitudinal land-sea fractions for three model geographies .....	23
2.2 Model surface albedo ( $a_S$ ) and heat capacity ( $C = C_1$ for land) .....	26
2.3 Model output with Earth at 1.0 AU .....	37
2.4 Model output with Earth at 1.4 AU .....	45

## ACKNOWLEDGEMENTS

This thesis was made possible by the financial, academic, and personal support of many people. I would first like to express my professional indebtedness to the people of the National Aeronautics and Space Administration who provided me the three-year Graduate Student Researchers Program Fellowship to work on my chosen thesis topic of planetary habitability. This award enabled me the financial means to travel to key conferences, purchase text books and various other academic supplies, and support my family. All that I have learned and accomplished in the last three years was made possible by this grant.

I have greatly benefited from the orbital- and precession-integration software provided by Martin Duncan (University of Toronto, CAN) and Hal Levison (Southwest Research Inst., Boulder CO), and Jacques Laskar (Bureau de Longitudes, Paris FRA), respectively. I also gratefully acknowledge the helpful collaborative efforts of Ken Caldeira (Lawrence Livermore National Lab., San Francisco), Larry Frakes (University of Adelaide, AUS), Jim Kasting (Dept. of Geosciences, Penn State University), and Richard Wade (Dept. of Astronomy and Astrophysics, Penn State University).

During my six years at Penn State, I have received valuable financial and academic help from many faculty and staff. My sincerest thanks are hereby given: to members of my thesis committee, Jim Kasting, Richard Wade, Pablo Laguna, Jorge Pullin, and Alex Wolszczan for keeping me on track, for sitting through all those committee meetings, and for reading my thesis; to Richard Wade for supporting me financially for one year while engaging me in interesting research involving binary stars; to Peter Mészáros for his commitment and attention to the departmental outreach program; and to Jim Kasting, Richard Wade, Don Schneider, Jane Charlton, Dan Weedman, and Peter Mészáros for writing more than twenty letters of recommen-

mentation on my behalf to prospective employers.

Here I also wish to acknowledge the helpful administrative assistance of the front-office staff, including Christine Selders, Cathy Lutz, Wendy Donley, Kerry Kubalak, Deb Detweiler (geosciences), and many others who have since moved on to other positions. I would also like to express my gratitude to Larry Strickler for his help with the department planetarium and other favors, and to George Weaver, the departmental computer administrator, for his patience and for his undying willingness to help the technically naive. Thanks also to all faculty, students, and staff in the astronomy, geoscience, and meteorology departments who have befriended me over the years with conversations, gifts, and smiles.

On a more personal note, I would like to thank my thesis advisor, Jim Kasting, for over five years of academic guidance and friendship. I am especially indebted to Jim for his help and inspiration in formulating the ideas for this thesis. In this sense, this work is as much his as it is mine. I also thankfully acknowledge the grant monies Jim gave me for travel, as well as the helpful and enjoyable companionship on several conference excursions. I will not soon forget the many extracurricular activities (tennis, raquetball, jogging) we enjoyed together. Thank you Jim.

I would also like to express my personal indebtedness to my family for their steadfast love and support through the entire graduate school process. My sincerest thanks go: to my father, Richard A. Williams, for pointing out planets, stars, and comets to me at a young age and encouraging my sense of wonder, for taking me to the Toronto Science Center when I was fifteen years old and to a lecture given by Carl Sagan in Toronto when I was in college, and for introducing me to astronomy through books and television; to my mother, Carolyn E. Williams, for rewarding me with smiles, hugs, and many gifts for my academic successes, and for encouraging me throughout my education while at the same time lacking a good answer to her

question, “So what does an astronomer do anyway?”; to both my mother and father and to my Grandma and Grandfather Williams for helping me afford two years of higher education; to my Grandma Haller, brothers David and Douglas and sister Christine for their love and for their enthusiasm and interest in what I do; to my inlaws Beth and Kent Black and their children for gifts and encouragement, and for permitting their daughter (sister) to marry an astronomer.

Most importantly, I would like to thank my wife Jody for her steadfast love, patience, friendship, gifts, encouragement, and her many personal sacrifices that have enabled me to start and to complete this work. I am especially indebted to Jody for believing in a dream I had ten years ago about wanting to be a professional astronomer, for always listening to me as I attempted to describe what I was up to, for carrying me through times troubled by diabetes, for preparing thousands of tasty meals, for her valuable assistance with astronomy outreach activities, and for sitting through many academic talks with me that turned out to be not so interesting. For all of these things, and many more unrecorded, thank you Jody Beth.

In the beginning, when God created the heavens and the earth, the earth was a formless wasteland and darkness covered the abyss, while a mighty wind swept over the waters. .... Thus the heavens and the earth and all their array were completed.

—Genesis 1:1-2;2:1

That there are many Suns — perhaps 400 billion of them in our Galaxy — we can readily grant. But are there many planets, many Earths, many biospheres?

—Carl Sagan

Circumstellar Habitable Zones: An Introduction  
Doyle (1996)

# Chapter 1

## INTRODUCTION

### 1.1 Stars With Planetary Systems

Astronomers are now taking inventory of planetary systems in the near-solar neighborhood of the Galaxy with the common goal of finding planetary environments capable of supporting life. The size of the region of space in which it is currently possible to detect planets around Sun-like stars is  $\sim 1$  Kpc in radius, assuming that milli-arcsecond resolution is possible from the ground with good adaptive-optics technology (Angel 1994). Microlensing might yield more distant detections, but the locations of planets would be effectively lost after the lensing event (Peale 1997). Thus, the volume of space probed by planet surveys that would enable follow-up observations is  $\sim 10^{-6}$  the volume of the entire Galaxy. It is on this small region of space that I will focus my attention.

The present-day stellar mass function indicates that there are  $\sim 50$  million stars within 1 Kpc of the Sun, but only a fraction of these stars will survive long enough to form planets having terrestrial surfaces that might potentially harbor life. The terrestrial planet-formation process itself may require  $10^7 - 10^8$  years to reach completion (Wetherill 1996), which excludes from these considerations stars in spectroscopic classes earlier than  $\sim A5$  ( $\sim 10^6$  stars), which have lifetimes comparable to or shorter than this.

Once a terrestrial planet has formed, the time scale for the subsequent evolution of life on its surface is difficult to determine precisely. On Earth, the age of the earliest

fossils ( $\sim 3.5$  Gyr) is approximately coincident with (and was perhaps enabled by) the end of late-heavy bombardment of the terrestrial planets by rock/ice planetesimals (Sleep et al. 1989). Life could, in principle, have appeared earlier on Earth and survived up to the present, given a milder impact history and an adequate amount of liquid water. The time scale for primitive life to develop is not useful for this discussion, however, as only long-lived biospheres may be unambiguously recognized from space. Primitive life might be detected by looking for  $\text{CH}_4$  in a planet's atmosphere, but  $\text{CH}_4$  can also be produced abiotically. A stronger case for extraterrestrial life could be made with the spectral identification of  $\text{O}_2$ , which is produced biogenically on Earth, or  $\text{O}_3$  which is formed from photochemical reactions involving  $\text{O}_2$ . Hence, for the purpose of remote detection either through spectroscopic analysis of a planet's atmosphere or by direct radio communication, life may need to occupy a planetary surface for 1-5 Gyr; it took  $\sim 2$  Gyr for life on Earth to produce a spectroscopically strong ozone signature (Kasting 1996b) and  $\sim 4.6$  Gyr for life to develop the means to send radio signals into space. Excluding stars with shorter main-sequence lifetimes (stars earlier than F0, or  $\sim 5 \times 10^6$  stars), leaves  $\sim 45$  million stars within 1 Kpc of the Sun that may have habitable planets.

## 1.2 Habitable Zones

The concept of the *habitable zone* (HZ), or the region around a star in which planets might be able to support life, has been discussed in the scientific literature for many years (Huang 1959, 1960; Dole 1964; Shklovski and Sagan 1966; Hart 1979), although the subject has recently seen renewed attention (Kasting, Whitmire and Reynolds 1993 – henceforth KWR; Kasting 1996a and accompanying references in the same volume). Common to all of these works is the assumption that “habitability”

and “life” refer to organisms having chemistries with which we are familiar and that depend on liquid water for survival. The HZ, then, is the range of orbital distances from a star in which a planet (or moon) with an atmosphere can maintain liquid water on its surface.

One of the simplest assumptions to make is that the atmospheres of habitable environments will resemble the atmospheres of terrestrial planets in the Solar System. Thus, the model atmospheres of KWR contain  $N_2$  and  $CO_2$ , plus  $H_2O$  vapor from standing bodies of liquid water ( $O_2$  is sometimes left out of model atmospheres since its high concentration in Earth’s atmosphere is a result of biology.) Under these assumptions, KWR demonstrated that an Earth-like planet would warm and begin to accumulate significant amounts of stratospheric water vapor if it were only 5% closer to the Sun than Earth is now, or 0.95 AU (Astronomical Units). At 0.84 AU, such planets would experience global evaporation of oceans, followed by photodissociation of  $H_2O$  vapor and loss of  $H_2$  to space (Kasting 1988). These events may help to explain the high D/H ratio and low  $H_2O$  vapor concentration in Venus’ present atmosphere. Thus, KWR viewed 0.84 AU to be the least conservative value for the HZ inner edge around the Sun.

The HZ outer edge is approximately the orbital distance at which the planet-mean temperature falls below the freezing point of water. On Earth, such a catastrophe would be prevented for small, positive, radial displacements in its orbit by the negative feedback response of the carbonate-silicate cycle (Walker et al. 1981) to falling surface temperatures, which would result in a build-up of atmospheric  $CO_2$ . The carbonate-silicate cycle relies on heat in a planet’s interior to drive plate tectonics and to vent  $CO_2$  stored in the crust through volcanos at plate margins. To keep this climate-stabilizing cycle going for  $> 2$  Gyrs, a planet (or moon) must be larger than Mars

(see Chapter 7). (Smaller bodies would lose their internal heat too quickly and would become tectonically inactive.) Elevated CO<sub>2</sub> levels might be able to keep Earth warm out to 1.67 AU, at which point the surface would be cooled by scattering of light away from its overlying dense, CO<sub>2</sub> atmosphere (Kasting 1991). The HZ outer-edge may be closer in (KWR; see also Chapter 2) or farther out depending on whether CO<sub>2</sub> clouds, which form in the atmospheres of planets at such distances, act to cool or warm planetary surfaces (Forget and Pierrehumbert 1997).

Complicating the above discussion is the fact that the luminosities of main-sequence stars evolve with time. The Sun was perhaps only 70% its present brightness upon entering the main sequence at 4.6 Ga (Gough 1981). The gradual increase in luminosity over a star's main sequence lifetime is a consequence of nuclear fusion, which reduces the particle density within the core. The reduction in pressure enables the core to shrink, which causes core temperature and energy production rate to increase with time. The brightening of a star causes its HZ to move outward. Thus, if a planet is to maintain equable surface temperatures for billions of years, it must lie within the continuously habitable zone (CHZ), or the HZ defined for a certain length of time. According to KWR, the inner edge of the Sun's 4.6-Gyr CHZ is the HZ inner edge today ( $\sim 0.95$  AU), and the CHZ outer edge is the HZ outer edge when the Sun first entered the main sequence ( $\sim 1.15$  AU). Thus, the CHZ for the Solar System is 0.2 AU in width, which is  $\sim 1/2$  the mean-planet separation (0.4 AU) of the terrestrial planets. This implies that the probability of finding a planet within the CHZ of the Sun, and similar stars, is  $\sim 50\%$  (KWR).

The HZ limits for stars of different masses and, hence, luminosities are shown in Fig. 1.1. Stars with luminosities less than the Sun (K-M) have narrower HZs that are closer in than the limits reported here, while stars of greater luminosity

Figure 1.1: The approximate width of the habitable zone around low-mass stars. Dashed lines mark the region in which terrestrial planets are likely to accrete and the dotted line is the orbital distance for tidal locking. Borrowed from KWR.

have wider HZs that are farther out. However, the width of HZs around all stars is approximately equivalent on a logarithmic distance scale. Thus, stars of different luminosities should have roughly equivalent numbers of planets within their HZs if their planets are spaced logarithmically, as they are in the Solar System.

Also shown in Fig. 1.1 is the orbital distance for tidal-locking; planets to the left of this line will have their rotations captured by their stars within 4.6 Gyr. Therefore, all of the planets within the HZs of M stars ( $\sim 70\%$  of stars within 1 Kpc of the Sun) should have synchronous rotations. This condition is a possible threat to planetary habitability because such a planet might have its atmosphere condense out on its cold, permanently-shaded side. One way to prevent atmospheric freeze-out is to have enough heat transported away from the sub-stellar side to the dark side by winds to keep the planet warm. (Another solution is to have a close-in planet rotate non-

synchronously in a spin-orbit resonance, as does Mercury.) Simple energy-balance models (Haberle et al. 1996) indicate that a 100-mbar CO<sub>2</sub>-H<sub>2</sub>O atmosphere is all that would be required to make this work, so at least some planets subjected to tidal locking might still be suitable for life.

### 1.3 Extrasolar Planets

*As the search for planets and brown dwarfs around nearby stars accelerates, we should expect to be surprised.* Guillot et al. (1996)

The unconstrained theories pertaining to life-bearing planets around other stars were paid little notice until observations showed that extrasolar planets do in fact exist. The first extrasolar planets were found in orbit around a pulsar – PSR B1257+12 (Wolczszan 1994), a rapidly-spinning neutron star which completes one rotation in  $\sim 6$  milliseconds. The planets were detected through their gravitational tug on the pulsar, which causes minute, but measurable, variations in the star’s otherwise highly regular wave train of pulses. The radial-velocity amplitudes ( $\sim 1 \text{ m sec}^{-1}$  at the pulsar) and periods of the timing perturbations on the very accurate pulsar clock enables one to estimate the masses and orbital distances of the three planets. The planetary masses (assuming zero orbital inclination relative to our line of sight) are  $0.015 M_{\oplus}$ ,  $3.4 M_{\oplus}$ , and  $2.8 M_{\oplus}$ , and orbital distances are 0.19 AU, 0.36 AU, and 0.47 AU, respectively.

The temperatures of the pulsar planets are affected by the radiative and charged particle fluxes coming from PSR B1257+12. Most of the pulsar’s thermal energy is in the form of X-rays. For an X-ray luminosity of  $10^{31} \text{ ergs sec}^{-1}$  (Becker and Truemper 1997), the effective radiating temperatures of the three pulsar planets (assuming zero

X-ray albedo) are 144 K, 104 K, and 98 K, respectively. The surface temperatures of these planets could be slightly higher if they were somehow able to form atmospheres and warm themselves through the greenhouse effect. Alternatively, the planets might be warmed by charged particles from the pulsar. If the charged particle luminosity of the pulsar is  $\sim 10^{34}$  ergs sec<sup>-1</sup> (Taylor et al. 1993), or  $\sim 5$  times the solar bolometric luminosity, then the effective temperatures of the planets increase to 875 K, 636 K, and 557 K, respectively. Unfortunately, few of the pulsar's physical parameters are known with enough confidence to enable more than these speculative remarks concerning the habitability of these worlds.

Soon after the pulsar planets were discovered, radial velocity searches (sensitive to the 10 m sec<sup>-1</sup> level) began revealing the presence of giant planets in orbit about Sun-like stars. Beginning in September of 1995, when the discovery paper of a Jupiter-sized planet orbiting the star 51 Pegasi went to press (Mayor and Queloz 1995), one extrasolar planet detection or confirmation was announced every month, on average, over a 6-month time period. The number of main-sequence stars with possible planetary companions has now grown to 10. Some important physical parameters of the new planetary systems are listed in Table 1.1.

All of the new planetary objects have masses of at least 0.5 M<sub>J</sub>, although the actual masses could be much larger than the values indicated in Table 1.1 if their orbits are inclined to our line of sight. Current planet searches are biased in favor of finding such high-mass objects because the stellar reflex motion from smaller planets is presently below the observation detection limits (see Boss 1996b). Surprisingly, many of the giant planets are closer to their stars than Mercury and Venus are to the Sun, contrary to the theoretical expectations of Boss (1995), and just about everyone else.

star	M* ( $\odot$ )	L* ( $\odot$ )	M <sub>p</sub> sini (M <sub>J</sub> )	a (AU)	e	reference
HD-	0.73	1.75	12±1	0.34	0.25±0.06	Latham et al. 1989
114762			12±1	0.34	0.380±0.015	Cochran et al. 1991
			9±1	0.34	0.35±0.05	Mazeh et al. 1996
51 Peg	1.0	1.24	0.47±0.02	0.05	0.09±0.06	Mayor & Queloz 1995
			0.45±0.01	0.05	0.012±0.01	Marcy et al. 1997
70 Vir	0.92	0.667	6.6±0.1	0.43	0.40±0.01	Marcy & Butler 1996
47 UMa	1.05	1.43	2.39±0.24	2.11	0.03±0.06	Butler & Marcy 1996
Lal 21185	0.39	0.006	0.9	2.5	unknown	Gatewood 1996
55 ρ <sup>1</sup> Cnc	0.85	0.58	0.84	0.11	0.051±0.013	Butler et al. 1996
τ Boo	1.2	4.41	3.87	0.046	0.018±0.016	Butler et al. 1996
ν And	1.2	5.92	0.68	0.057	0.109±0.04	Butler et al. 1996
16 Cyg B	1.0	1.0	1.5	1.6	0.634±0.082	Cochran et al. 1997
ρ CrB	1.0	1.77	1.1	0.23	0.028±0.040	Noyes et al. 1997

Table 1.1: Physical parameters of known extrasolar planets. Columns two and three are the adopted stellar masses and luminosities relative to the Sun. Adjacent columns list minimum planetary masses (expressed M<sub>p</sub> sin *i*) relative to the mass of Jupiter (M<sub>J</sub>), orbit semi-major axes in astronomical units, and orbit eccentricities, *e*.

According to standard theory (Podolak et al. 1993), the giant planets in the Solar System were formed by gravitational collapse of solar nebula gases onto a rock-ice core of at least 10-15 M<sub>⊕</sub>. It is difficult to explain, however, how core masses could grow to this size by pair-wise accretion of planetesimals in the inner protoplanetary disk before the nebula was cleared of gas by stellar winds. Calculations by Wetherill (1996) suggest that the collisional accumulation of terrestrial planets ( $\sim 1M_{\oplus}$ ) from a planetesimal swarm in a protoplanetary disk may require  $\sim 10^8$  years, which is an order of magnitude longer than the observed lifetimes of protostellar disks. The preferred scenario is to form large core masses beyond the water condensation radius in the protoplanetary disk (Boss 1995) where relative Keplerian velocities of planetesimals are small and where the volatile-rich planetesimals tend to stick together, rather than fragment, in collision.

Many attempts have been made to reconcile this theory with observations. Gray (1997) has argued that the observed periodic variation in the spectra of star 51 Pegasi

is a consequence of stellar pulsations rather than planets, although this claim has recently been retracted (Gray 1998, Hatzes et al. 1998). Others who have tackled the problem have universally sided with the standard theory by accepting that the basic picture of where giant planets form must be correct. Thus, the extrasolar planets are assumed to have first formed beyond the water-condensation radius at several AU from their stars, and later moved inward to their present orbits. One possible mechanism for moving the planets inward is dissipative tidal interaction between a planet and a long-lived, viscous protoplanetary disk (Lin et al. 1996, Rasio et al. 1996). This explanation, however, requires a very special set of circumstances to park the planets at small orbital distances without having them fall onto their stars. Another possibility is that giant planets on crossing orbits experience a close encounter which sends one planet inward toward the star and the other on a nearly parabolic trajectory away from the star (Rasio and Ford 1996). This theory has the advantage of also being able to explain giant planets on tightly-bound eccentric orbits (e.g., HD114762 B, and 70 Vir B), which is a typical result of such dynamical interactions. It has been argued most recently (Tremaine 1998) that planetary migration could also occur as a result of momentum exchange between a giant planet and a disk of planetesimals in which it is embedded. The outward scattering of planetesimals may have similarly reduced (although to a lesser extent) the orbital radii of Jupiter and Saturn in the early Solar System (Fernandez and Ip 1984). Such migration would naturally cease once a planet entered the region of the close-inner disk, which should be relatively devoid of planetesimals.

The orbital eccentricities of extrasolar planets are also difficult to explain. Table 1.1 shows that three planets (HD114762 B, 70 Virginis B, and 16 Cygni Bb) have orbital eccentricities  $> 0.4$ ; by comparison, the largest eccentricity of any planet in the Solar System is that of Pluto (0.25). Circular orbits are expected of planets which

form by pair-wise accretion of planetesimals in a protoplanetary disk. Eccentric orbits suggest that extrasolar planets either experienced a close encounter with objects of comparable mass early in their histories, or that they formed in a way more akin to stellar objects, such as through fragmentation and collapse of a protoplanetary nebula (Boss 1996b). Recently, Black (1997) has argued on similar grounds that objects with high eccentricities are actually brown dwarfs. Some of the objects in Table 1.1 could very well be brown dwarfs, with masses  $> 13M_J$  (Saumon et al. 1996), if their orbits are slightly inclined to our line of sight, as should be expected.

## 1.4 Orbital Stability of Terrestrial Planets

Could any terrestrial-sized planets also be present around the stars listed in Table 1.1? More importantly, are there any terrestrial planets that orbit within the HZs, or CHZs, of these stars? The presence of such a planet within an extrasolar HZ does not, by itself, guarantee that it is fit for life. It is also important to know whether its orbit is stable over geologic time scales. The discovery of extrasolar giant planets within what is the terrestrial-planet region of the Solar System suggests that many planetary systems may not be as well configured for orbital stability. In the simplest sense, a terrestrial planet could have a stable orbit in the new planetary systems if the giant planet and terrestrial planet are initially well separated, as in Figs. 1.2a and 1.2b.

The condition for long-lived orbital stability would also be satisfied if a terrestrial planet were in orbit about a giant planet or brown dwarf, as illustrated in Fig. 1.2c. Such moons would need to orbit within the larger object's Hill Sphere, or sphere of influence (see Roy 1988), to avoid being pulled away by the gravity of the parent star. Since the limits for the orbital stability of moons are well known, most of the

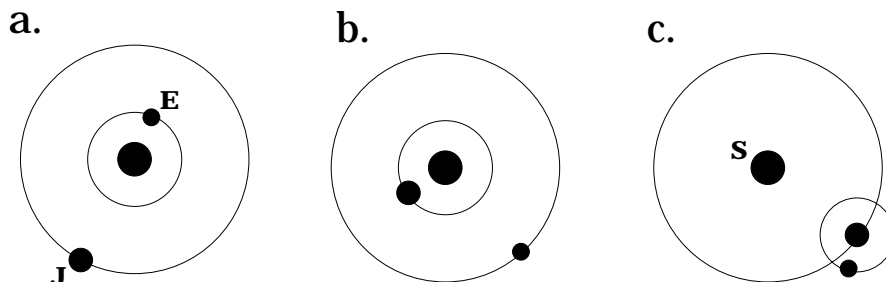


Figure 1.2: Conditions for orbital stability in 3-body systems containing one Jupiter-sized planet (J) and one Earth-sized planet (E) in orbit around a Sun-like star (S).

discussion pertaining to such objects (Chapter 7) will concern their size limits for being able to hold an atmosphere over long periods of time.

The minimum orbital separation limits of systems 1.2a and 1.2b are not known (and, in fact, cannot be known) precisely because the limits depend on all six of the orbital osculating elements, as well as the masses of planet (J) and planet (E). Even if this information were available, the 3-body planetary problem cannot be solved analytically without restricting the planets to circular, co-planar orbits. Nevertheless, some useful information about orbital stability may be obtained through numerical integrations. Orbital simulation experiments have traditionally suffered from rapid accumulation of error, so that the time taken to perform integrations of sufficient accuracy and duration is often prohibitively long. Here, we have used the method of symplectic integration (Gladman et al. 1991; Wisdom and Holman 1991,1992), which conserves energy and momentum to within machine precision, to study the evolution of planetary systems for 1-100 Myr. While integrations lasting 100 Myr do not yield precise information about planetary positions (accumulation of error in orbital phase is still very rapid), they do provide usefully accurate information on the long-term evolution of planetary orbits. Integrations of the Solar System and of hypothetical, extrasolar planetary systems were performed here to enable long-term integrations

of the equations of precession. Some simulations of closely-spaced planets have also been performed, but a detailed exposition of these results is not possible at this time.

## 1.5 Spin Stability and Climate

Laskar and Robutel (1993) complicated the discussion of planetary habitability with their discovery that the obliquities (spin-axis inclinations) of the terrestrial planets in the Solar System undergo large-amplitude, chaotic fluctuations on time scales of  $\sim 10$  Myr. The reasons for obliquity variations are well understood. A gravitational couple exerted by the Sun (and the Moon in the case of Earth) on a planet's equatorial bulge causes precession of the spin axis about the orbit normal, as well as nutation, which changes the obliquity. Gravitational interactions with other planets cause orbit normals themselves to nutate and precess about the normal to the Solar System's invariable plane (the plane defined by the combined angular momenta of all the planets). When the rates of precession of the spin axis and orbit axis come into resonance, large and unpredictable excursions in obliquity occur.

This behavior has been well studied in the case of Mars (e.g., Ward 1973, 1979, 1991), whose spin axis fluctuates between  $15^\circ$  and  $35^\circ$  with dominant periods of 0.12 and 1.2 Myr. Mars' obliquity may possibly reach  $45^\circ$  or  $50^\circ$  if a spin-orbit resonance is encountered (Ward 1991, Touma and Wisdom 1993). Laskar and Robutel (1993) predict chaotic obliquity fluctuations in the range  $0^\circ$  to  $60^\circ$  for Mars in spin-orbit resonance. A companion paper (Laskar et al. 1993a) showed that Earth's obliquity would vary even more radically ( $0^\circ$  to  $85^\circ$ ) were it not for the stabilizing presence of the Moon. Nearly  $2/3$  of Earth's couple on its oblate figure is contributed by the Moon, with the remainder contributed by the Sun. Consequently, Earth precesses faster than any of the other terrestrial planets and so avoids the numerous secular

resonances that exist at lower frequencies. Thus, the present variation in Earth's obliquity is small,  $\pm 1.5^\circ$  about a  $23.3^\circ$  mean.

Ward (1974) was perhaps first to mention that Earth's obliquity would vary by much more than it does today if the Moon were not present. Although the variation found by Ward for a moon-less Earth was relatively small ( $\pm 10^\circ$ ), he recognized that larger hypothetical variations would profoundly affect climate. For example, if Earth's obliquity ever exceeded  $54^\circ$ , the planet would receive more annual-average insolation at the poles than at the equator. Seasonal cycles at high latitudes also become very pronounced when a planet's obliquity is high. The discovery that Earth might possibly reach an obliquity as high as  $85^\circ$  led Laskar et al. (1993a) to suggest (albeit implicitly) that accompanying changes to climate might render Earth uninhabitable. The number of habitable planets around other stars may, therefore, be proportional to the fraction of planets with sizeable moons. Earth's moon is currently thought to have been formed as a result of a glancing collision with a Mars-sized object during the latter stages of accretion (Hartmann et al. 1986). Such moon-forming collisions may be relatively improbable events: Earth is the only terrestrial planet with a large moon. If most Earth-sized planets lack large moons, and if the climatic excursions caused by the obliquity variations are too severe, the chances of finding life elsewhere in the galaxy may be significantly reduced.

These arguments, however, rely on the assumption that all extrasolar terrestrial planets will encounter a spin-orbit resonance at approximately the same frequency of spin precession, which is not always true. The specific frequency for spin-orbit resonance is set by the value of the main frequency of orbit precession, which is a function of the configuration of planets in a planetary system. Earth's dominant frequency of orbit precession is much smaller than its main frequency of spin precession and, consequently, the spin axis is quite stable. Planets in other systems with differ-

ent orbital configurations may have larger orbit precession rates than the terrestrial planets do within the Solar System, especially if giant and terrestrial planets orbit in close proximity, as may be the case in the newly discovered planetary systems. In this case, rapid spin precession resulting from large satellites may be a threat to spin stability. This problem will be examined in more detail in Chapter 6.

Finally, it will be demonstrated here (see Chapter 5) that an otherwise stable spin axis can also change significantly on time scales of  $10^8$  years through the influence of large, continental ice structures on planetary oblateness. Geologic evidence of low-latitude glaciation during the Precambrian era suggests that Earth's own obliquity may have been significantly higher than its present value. Here we consider the possibility that the cyclic advance and retreat of polar ice sheets may have enabled Earth's high obliquity to drift downward to its present value during the Late Proterozoic glacial period (850-500 Ma). The direction of obliquity drift depends on climatic parameters which vary with time and from planet to planet, so ice sheets could either raise or lower obliquities of terrestrial planets in other systems. Thus, planets with otherwise stable spin axes might also be subject to the climatic problems associated with high obliquity.

## 1.6 Thesis Outline

The topics addressed by the remainder of this thesis are as follows. In Chapter 2, a climate model is used to examine the temperature threats to Earth-like planets at high obliquity for different continental topographies and orbital positions within the habitable zone. Chapter 3 includes a detailed discussion and derivation of the equations of precession, as well as a short description of the precession code obtained from Jacques Laskar and used in Chapters 5 and 6. Chapter 4 contains a short in-

roduction to symplectic integration, as well as a brief discussion of computational error and the workings of the computer code *SWIFT* used in Chapters 5 and 6. In Chapter 5, the equations of precession are modified to account for periodic changes to Earth's oblateness during an ice age. The obliquity is integrated over 100 Myr to determine if Earth may have had its early obliquity (which was possibly much higher than it is today) reduced to its present value as a consequence obliquity-oblateness feedback. The effect that this change in obliquity would have on the lunar orbit is also considered. Chapter 6 shows the results of orbital and precessional simulation experiments of Earth, both with and without a moon, in hypothetical planetary systems. In Chapter 7, moons belonging to extrasolar giant planets are considered as possible abodes for extraterrestrial life. Included is a synopsis of the important climatic and dynamic factors (e.g., longevity of an atmosphere, variable insolation, tidal heating) which could influence whether such moons might be habitable for billions of years. Thesis conclusions and directions for future research are in Chapter 8.

Portions of the thesis text are unedited excerpts of text appearing in papers by Williams and Kasting (1997; Secs. 1.5 and 8.2, and Chapter 2), Williams et al. (1997; Chapter 7), and Williams et al. (1998; Chapter 5). I gratefully acknowledge textual contributions and edits from Jim Kasting and Richard Wade. Figures 2.4-2.8 and Tables 2.1-2.4 are borrowed directly from Williams and Kasting (1997). Figure 1.1 is borrowed from Kasting et al. (1993). Figures 6.3 and 6.5 are borrowed from Laskar et al. (1993a) and from Laskar and Robutel (1993), respectively.

## Chapter 2

# THE EFFECT OF HIGH OBLIQUITY ON PLANETARY CLIMATE

### 2.1 Overview

A one-dimensional energy-balance climate model was used (Williams and Kasting 1997) to investigate the effects of large obliquity fluctuations on climate and to formulate a reply to the suggestion made by Laskar et al. (1993a), that Earth-like planets would be inhospitable if their obliquities were much greater than Earth's is today ( $23.5^\circ$ ). Early versions of the model (Williams et al. 1996) gave surprisingly pessimistic results: Monstrous seasonal cycles for planets with high obliquities yielded opposing solstice temperatures of 220 K and 430 K on high-latitude continents. Here, we show that an Earth-like planet can have its seasonal cycles damped and equator-to-pole temperature gradient reduced, provided it possesses a dense  $\text{CO}_2$  atmosphere built up in response to the carbonate-silicate cycle. Such an atmosphere is expected to exist on planets located toward the outer edge of the HZ. Weathering on tectonically active planets enforces a balanced exchange of  $\text{CO}_2$  between the atmosphere and the carbonate-rock reservoir within the crust. Less than  $\sim 0.001\%$  of Earth's 60-bar subsurface  $\text{CO}_2$  inventory resides in the atmosphere; however, Earth-like planets within the outer HZ (1.1-1.4 AU) might lose over 2% of their crustal carbonate in forming  $\text{CO}_2$ -rich atmospheres, provided they demonstrate similar amounts of volcanic activity. Many of these planets could have relatively stable climates even if

they were subject to large obliquity variations. By demonstrating this explicitly here, we show that obliquity variations are not an insurmountable obstacle to life being present around other stars.

## 2.2 Model Description

### 2.2.1 Energy-Balance Methods

The model employed for this study is a zonally-averaged energy-balance climate model (EBCM), of the kind described in detail by North and Coakley (1979), and North et al. (1981) [see also Caldeira and Kasting (1992)]. The operating principle of EBCMs is straightforward: Planets in thermal equilibrium must on average radiate as much long-wave energy to space as they receive at UV, visible, and near-IR wavelengths from stars. Radiative energy fluxes entering or leaving a particular region are balanced by dynamic fluxes of heat transported into or away from the region by winds (see Fig. 2.1). Our model divides Earth into 18 latitudinal zones, each  $10^\circ$  wide. We express radiative and dynamic energy-balance for each zone by

$$C \frac{\partial T(x, t)}{\partial t} - \frac{\partial}{\partial x} D(1 - x^2) \frac{\partial T(x, t)}{\partial x} + I = S(1 - A), \quad (2.1)$$

where  $x$  is the sine of latitude and  $T$  is the zonally-averaged surface temperature. The terms in the energy-balance equation represent, from right to left: the absorbed fraction of incident solar flux,  $S$ , where  $A$  is the top-of-atmosphere albedo; outgoing infrared flux to space,  $I$ ; dynamic heat-transport flux (modeled as diffusion); and the rate of seasonal heating and cooling. The thermal inertia is determined by the effective heat capacity,  $C$ , of the surface ocean and atmosphere. The diffusion coefficient,  $D$ , is a measure of the transport efficiency, which is assumed to depend on atmospheric pressure (as will be discussed in Sec. 2.2.8).

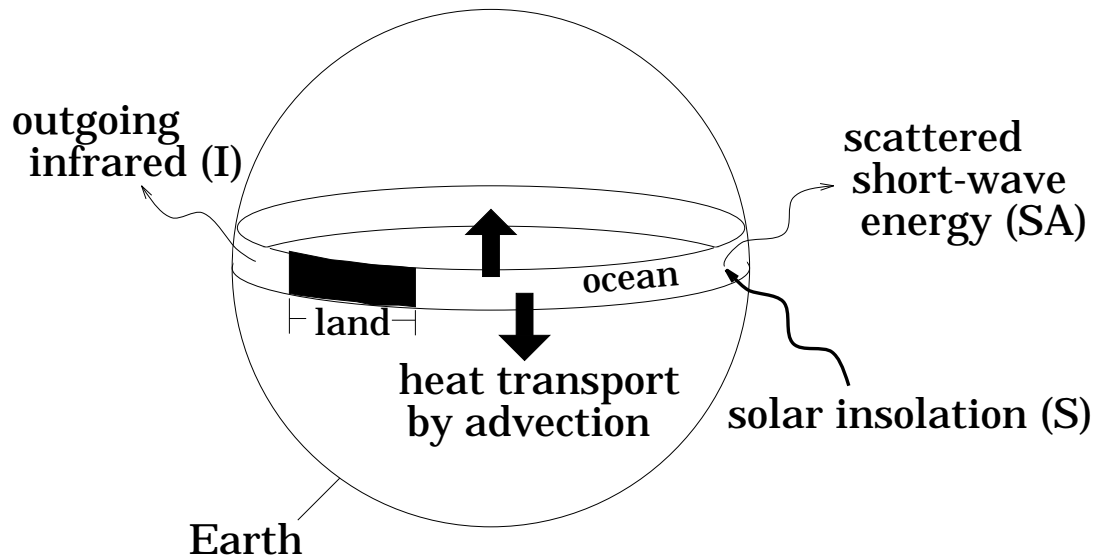


Figure 2.1: Zonal energy fluxes calculated by the energy-balance climate model.

### 2.2.2 Diurnally-Averaged Incident Solar Flux ( $S$ )

The bolometric solar flux at 1.0 AU,  $q_0$ , is  $\sim 1360 \text{ Wm}^{-2}$ . Changes in solar flux over Earth's eccentric orbit were included in the actual calculation, but eccentricity will be neglected in the following discussion. The instantaneous solar flux received by a particular latitude is  $q_0 \cos Z$ , where  $Z$  is the solar zenith angle and  $\cos Z = \mu$ , which is written as

$$\mu = \sin \theta \sin \delta + \cos \theta \cos \delta \cos h. \quad (2.2)$$

Here,  $\theta$  is latitude,  $\delta$  is solar declination, and  $h$  is solar hour angle. Solar declination,  $\delta$ , depends on obliquity, expressed here as  $\delta_0$ , and orbital longitude,  $L_s$ , through the equation

$$\sin \delta = -\sin \delta_0 \cos(L_s + \pi/2), \quad (2.3)$$

where orbital longitude for circular orbits is a simple function of time  $t$ :

$$L_s = \omega t. \quad (2.4)$$

In Eqn. 2.4,  $\omega$  is the planet's angular velocity, found from Kepler's third law,

$$\omega = 1.721 \times 10^{-20} (GM_\odot)^{1/2} \left( \frac{a}{1.0AU} \right)^{-3/2}, \quad (2.5)$$

where  $G$  and  $M_\odot$  are the gravitational constant and Sun's mass in cgs units, respectively, and  $a$  is the planet semi-major axis in AU. The diurnally-averaged solar flux is  $S = q_0 \bar{\mu}$ , and the averaging of  $\mu$  is over a complete rotation. Averaging first over the sunlit portion of rotation, i.e., over solar hour angle from  $h = -H$  to  $+H$ , where  $H$  is the radian half-day length given by

$$\cos H = -\tan \theta \tan \delta, \quad \text{for } 0 < H < \pi, \quad (2.6)$$

we obtain

$$\begin{aligned} \bar{\mu} &= \frac{\int_{-H}^H dh (\sin \theta \sin \delta + \cos \theta \cos \delta \cos h)}{\int_{-H}^H dh} \\ &= (\sin \theta \sin \delta + \cos \theta \cos \delta \frac{\sin H}{H}). \end{aligned} \quad (2.7)$$

Now, the averaging of  $\mu$  over the entire diurnal cycle is completed by scaling Eqn. 2.7 by the factor  $H/\pi$ , because  $H = \pi$  if the Sun remains above the horizon for a complete rotation. The diurnally-averaged solar flux,  $S$ , may then be written as

$$\begin{aligned} S &= q_0 \left( \frac{H}{\pi} \right) \bar{\mu} \\ &= \frac{q_0}{\pi} (H \sin \theta \sin \delta + \cos \theta \cos \delta \sin H), \end{aligned} \quad (2.8)$$

which may be expressed for any planet having an orbital semi-major axis,  $a$ , as

$$S = \frac{q_0}{\pi} \left( \frac{1.0AU}{a} \right)^2 (H \sin \theta \sin \delta + \cos \theta \cos \delta \sin H). \quad (2.9)$$

### 2.2.3 Top-Of-Atmosphere Albedo (A)

The fraction of short-wave solar energy returned to space as a consequence of atmospheric or surface scattering is the top-of-atmosphere (TOA) albedo. TOA albedo depends both on the distance photons travel through the atmosphere, which is set by the solar zenith angle, and on the surface albedo. Levels of  $\text{CO}_2$  and  $\text{H}_2\text{O}$  affect TOA albedo by their respective contributions to Rayleigh scattering and absorption.  $\text{CO}_2$  raises the albedo significantly because its cross section for Rayleigh scattering is over 2.5 times that of nitrogen.  $\text{H}_2\text{O}$  is an efficient Rayleigh scatterer, but it is also a good absorber in the near IR. Hence, for the low temperatures and small  $\text{H}_2\text{O}$  mixing ratios encountered by our model, the dominant effect of  $\text{H}_2\text{O}$  is to decrease albedo by raising atmospheric absorption. The water vapor contribution to Rayleigh scattering does not begin to dominate its contribution to absorption until surface temperatures exceed  $\sim 360$  K and the stratospheric  $\text{H}_2\text{O}$  mixing ratio becomes large (Kasting 1988).

For these calculations, the atmosphere was assumed to consist of 1.0 bar  $\text{N}_2$ , and variable amounts of  $\text{CO}_2$  and  $\text{H}_2\text{O}$ . The stratosphere was assumed to be isothermal, following Kasting (1991), and the troposphere was assumed to be fully saturated with water vapor. Using a more realistic (for present Earth) distribution of relative humidity would have complicated the model without changing any of our basic conclusions. We chose to exclude  $\text{O}_2$  from the calculations because we wanted to give equal consideration to planets without photosynthetic life from which Earth's present oxygen level is derived. Again, the model results are only weakly sensitive to this assumption.

Following Caldeira and Kasting (1992), we parameterized TOA albedo as a 2nd-order polynomial of four variables:  $\text{pCO}_2$  (here referred to as  $p$ ),  $\mu$ , surface temperature,  $T$ , and surface albedo,  $a_s$ . We obtained best fits to the results of over 24,000 runs of the radiative-convective climate model used by Kasting and Ackerman (1986),

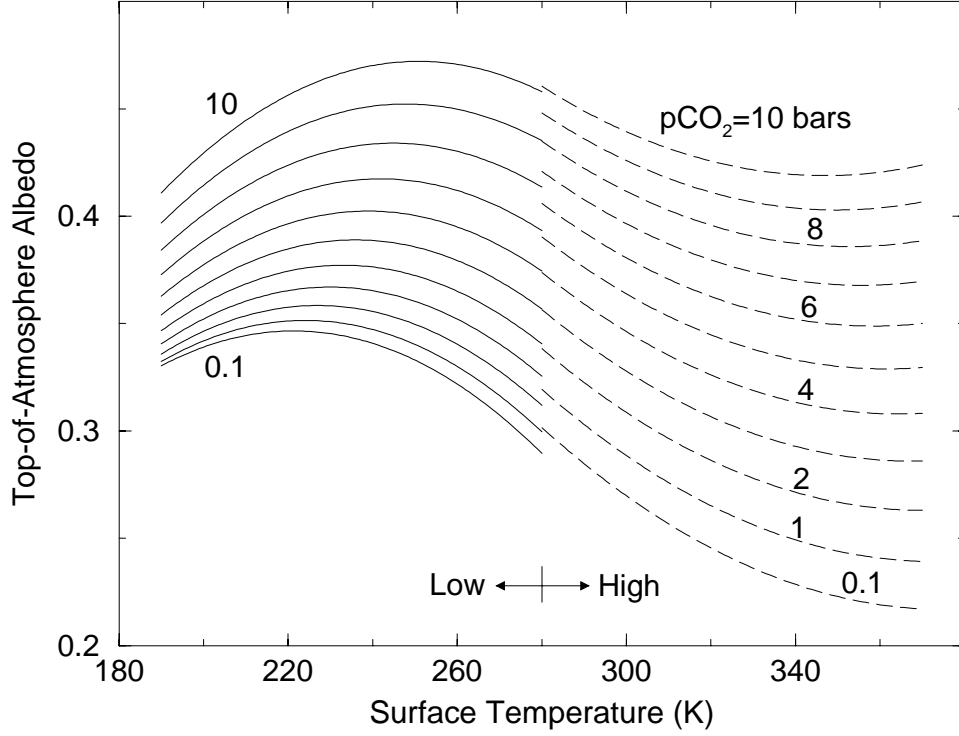


Figure 2.2: Low- and high-temperature model fits to top-of-atmosphere albedo for different surface temperatures and  $\text{CO}_2$  partial pressures. Surface albedo was taken to be 0.3 and solar zenith angle was set to  $60^\circ$ .  $\text{CO}_2$  partial pressure was started at 0.1 bar and then varied from 1 to 10 bars in steps of 1 bar. The low-temperature fits (solid) were calculated using Eqn 2.10 and the high-temperature fits were calculated using Eqn 2.11

and Kasting (1988,1991). We made separate fits for temperatures above and below  $T = 280$  K (see Fig. 2.2) to yield smaller rms errors than was possible with one fit over the entire temperature range ( $190 \text{ K} < T < 370 \text{ K}$ ). The fits we obtained may be applied confidently for  $10^{-5} \text{ bars} < p < 10 \text{ bars}$ ,  $0 < a_s < 1$ , and  $0 < \mu < 1$ . In the temperature range  $190 \text{ K} < T < 280 \text{ K}$ ,

$$\begin{aligned}
 A = & -6.8910 \times 10^{-1} + 1.0460a_s + 7.8054 \times 10^{-3}T - 2.8373 \times 10^{-3}p - \\
 & 2.8899 \times 10^{-1}\mu - 3.7412 \times 10^{-2}a_s p - 6.3499 \times 10^{-3}\mu p + \\
 & 2.0122 \times 10^{-1}a_s \mu - 1.8508 \times 10^{-3}a_s T + 1.3649 \times 10^{-4}\mu T +
 \end{aligned}$$

$$\begin{aligned}
& 9.8581 \times 10^{-5} pT + 7.3239 \times 10^{-2} a_s^2 - 1.6555 \times 10^{-5} T^2 + \\
& 6.5817 \times 10^{-4} p^2 + 8.1218 \times 10^{-2} \mu^2,
\end{aligned} \tag{2.10}$$

and for  $280 \text{ K} < T < 370 \text{ K}$ ,

$$\begin{aligned}
A = & 1.1082 + 1.5172 a_s - 5.7993 \times 10^{-3} T + 1.9705 \times 10^{-2} p - \\
& 1.8670 \times 10^{-1} \mu - 3.1355 \times 10^{-2} a_s p - 1.0214 \times 10^{-2} \mu p + \\
& 2.0986 \times 10^{-1} a_s \mu - 3.7098 \times 10^{-3} a_s T - 1.1335 \times 10^{-4} \mu T + \\
& 5.3714 \times 10^{-5} pT + 7.5887 \times 10^{-2} a_s^2 + 9.2690 \times 10^{-6} T^2 - \\
& 4.1327 \times 10^{-4} p^2 + 6.3298 \times 10^{-2} \mu^2.
\end{aligned} \tag{2.11}$$

The rms errors for the fits are 7.58 and 4.66  $\text{W m}^{-2}$ , respectively, when scaled by the planetary-average incident solar flux ( $q_0/4$ ).

One should note that there is a discrepancy between Eqns. 2.10 and 2.11 above and their analog equation, Eqn. 5, of Caldeira and Kasting (1992). An analysis of these formulae reveals that TOA albedo increases with  $Z$  in Eqns. 2.10 and 2.11, as it should, but decreases with  $Z$  in the older Eqn. 5. The inconsistency originated with differences in the way the radiative-convective model, which was used to make both sets of fits, was used to calculate stratospheric temperature,  $T_{\text{strat}}$ . Caldeira and Kasting calculated  $T_{\text{strat}}$  using Eqn. 1 of Kasting (1991),

$$T_{\text{strat}} = \frac{1}{2^{1/4}} \left[ \frac{S}{4\sigma} (1 - A) \right]^{1/4}, \tag{2.12}$$

where  $S$  is incident solar flux, and  $\sigma$  is the Stefan-Boltzmann constant. This equation, however, is appropriate only for global average conditions (i.e., for  $Z = 60^\circ$ ) and, thus, was applied incorrectly in calculating  $T_{\text{strat}}$  and TOA albedo for latitudes having solar zenith angles different from this value. We circumvented this problem

by parameterizing  $T_{\text{strat}}$  as the following function of  $Z$ .

$$T_{\text{strat}}(Z) = T_{\text{strat}}(60^\circ) \left[ \frac{F_s(Z)}{F_s(60^\circ)} \right]^{1/4}. \quad (2.13)$$

Here, in the notation of Kasting (1991),  $F_s$  is the absorbed fraction of incident solar flux, which was calculated for a variety of zenith angles between  $0^\circ$  and  $90^\circ$  using the radiative-convective model, and  $T_{\text{strat}}(60^\circ)$  was obtained using Eqn. 2.12 as before.

#### 2.2.4 Surface Albedo ( $a_s$ )

All of the planets that we considered have Earth-like (30:70) land-sea ratios, and their geography was varied by adjusting the zonal ocean fractions for the three geographic cases given in Table 2.1.

Latitude	Ocean fraction		
	Present geog.	Equatorial geog.	Polar geog.
90—80N	0.934	1.000	1.000
80—70	0.713	1.000	1.000
70—60	0.294	1.000	1.000
60—50	0.428	1.000	1.000
50—40	0.475	1.000	1.000
40—30	0.572	1.000	1.000
30—20	0.624	1.000	1.000
20—10	0.736	0.250	1.000
10—0	0.772	0.000	1.000
0—10S	0.764	0.000	1.000
10—20	0.780	0.250	1.000
20—30	0.769	1.000	0.367
30—40	0.888	1.000	0.000
40—50	0.970	1.000	0.000
50—60	0.992	1.000	0.000
60—70	0.896	1.000	0.000
70—80	0.246	1.000	0.000
80—90	0.000	1.000	0.000

Table 2.1: Latitudinal land-sea fractions for three model geographies.

Zonal ocean fractions for the present Earth were obtained from Sellers (1965). Surface albedo depends on temperature through its effect on the extent and reflectance properties of snow and ice cover. We assigned albedos to land and oceanic surfaces for three different temperature regimes.

For  $T > 273$  K, land was assigned an albedo of 0.20, which is characteristic of many terrestrial surfaces (Kondrat'ev 1969). The albedo of unfrozen ocean depends on solar zenith angle through the Fresnel reflectance formulae for water and can range from 0% to 100%. The fraction of incident short-wave energy reflected from a smooth oceanic surface ( $n = 1.33$ ), for  $0^\circ < Z < 90^\circ$ , was read from a table prepared by Kondrat'ev (1969, p.439).

For  $263 \text{ K} < T < 273 \text{ K}$ , land was allowed an unstable snow cover having an albedo of 0.45, and sea ice with  $a_s = 0.55$  was permitted to form in the oceans. We used data from Table 1 of Thompson and Barron (1981) to parameterize the ocean fraction covered by sea ice,  $f_i$ , as a function of surface temperature,

$$f_i = 1 - \exp\left[\frac{(T - 273K)}{10}\right]. \quad (2.14)$$

For  $T < 263$  K, the continents and oceans were assigned an albedo of 0.7, which is appropriate for stable snow cover over an ice cap.

The contribution of  $\text{H}_2\text{O}$  clouds to the global albedo was treated simply by assuming that clouds cover 50% of the surface at all times, and that the albedo of the cloud cover depends linearly on solar zenith angle (Cess 1976),

$$a_s = \alpha + \beta Z. \quad (2.15)$$

The values of  $\alpha$  ( $-0.078$ ) and  $\beta$  ( $0.65$ ) were adjusted to allow the model to reproduce Earth's latitudinal albedo profile (Jacobowitz et al. 1979). If we delineate albedos and zonal surface fractions for ocean, land, and ice using subscripts  $o$ ,  $l$ , and  $i$  respectively,

the zonally-averaged surface albedo,  $a_s$ , may be expressed as

$$a_s = 0.5 \{(1 - f_o)a_l + f_o [f_i a_i + (1 - f_i)a_o]\} + 0.5(\alpha + \beta Z). \quad (2.16)$$

### 2.2.5 Effective Heat Capacity (C)

The thermal time scale,  $\tau$ , depends on the effective zonal heat capacity,  $C$ , through the equation

$$\tau = \frac{CT}{I}, \quad (2.17)$$

where  $I$  is the outgoing infrared flux and  $C = \rho c_p \Delta l$ . Over the continents,  $\rho$ ,  $c_p$ , and  $\Delta l$  are the density, specific heat, and depth of the atmosphere, giving  $\tau \sim 50$  days. We adopted the effective heat capacity of the atmosphere over land,  $C_l$ , used by North et al. (1983),  $5.25 \times 10^6 \text{ J m}^{-2} \text{ K}^{-1}$ . Oceanic areas have much longer thermal time scales ( $\tau \sim 5$  years) because the surface temperature is coupled to the slowly varying temperature of the wind-mixed ocean layer with  $\Delta l = 50$  to 100 meters. The effective heat capacity of the atmosphere over ocean  $C_o$  and sea ice  $C_i$  depends in an unpredictable way on atmospheric and oceanic dynamics and, hence, can be treated as free parameters in time-dependent EBCMs.

North et al. (1983) chose  $C_o = 60C_l$  and  $C_i = 9.2C_l$ , where the value of  $C_o$  corresponds to a wind-mixed ocean layer 75 meters deep, and the value of  $C_i$  was introduced and adjusted to raise the amplitudes of seasonal cycles in the high latitudes. We required a similar, albeit slightly more complicated, approach to reduce  $\tau$  over the poles. We introduced an additional frozen oceanic heat capacity to resolve expected thermal differences between surfaces of thin transient sea ice ( $263 \text{ K} < T < 273 \text{ K}$ ) and of a stable ice cap ( $T < 263 \text{ K}$ ). In the first temperature regime, we allowed  $C_i = 9.2C_l$ , and over the ice cap,  $C_i = 2.0C_l$ . We also reduced the depth of our

wind-mixed ocean layer to 50 meters, giving  $C_o = 40C_1$ , to better match the observed latitudinal distribution of seasonal cycle amplitudes (North and Coakley 1979). We obtained a zonally-averaged effective heat capacity using the equation,

$$C = (1 - f_o)C_1 + f_o\{(1 - f_i)C_o + f_iC_i\}. \quad (2.18)$$

To summarize, the values of surface albedo and effective heat capacity used in the model are given in Table 2.2.

Temperatures (K)	Ocean		Land	
	$a_s$	$C/C_1$	$a_s$	$C/C_1$
$T > 273$	0 - 0.99	40.0	0.2	1
$263 < T < 273$	0.55	9.2	0.45	.
$T < 263$	0.7	2.0	0.7	.

Table 2.2: Model surface albedo ( $a_s$ ) and heat capacity ( $C = C_1$  for land).

### 2.2.6 Outgoing Infrared Flux (I)

As was done for TOA albedo, we used the radiative-convective model developed by Kasting to parameterize long-wave energy losses to space as a function of  $T$  and  $p\text{CO}_2$  ( $p$ ). Surface temperature sets the humidity and, hence, the contribution of  $\text{H}_2\text{O}$  vapor to the greenhouse effect. The parameterized outgoing IR flux is a polynomial fit to output from  $\sim 300$  runs of the radiative-convective model.

Because we sought a numerical, rather than analytic, solution to the energy-balance equation, Eqn. 1, we did not require the form of  $I$  to be the simple linear function of  $T$  (e.g.,  $A + BT$ ) used in similar models (Caldeira and Kasting 1992, North et al. 1981). We thereby used a higher order polynomial in  $T$  to obtain a low rms error ( $4.56 \text{ W m}^{-2}$ ) over a larger temperature range ( $190 \text{ K} < T < 380 \text{ K}$ ) than was obtained by

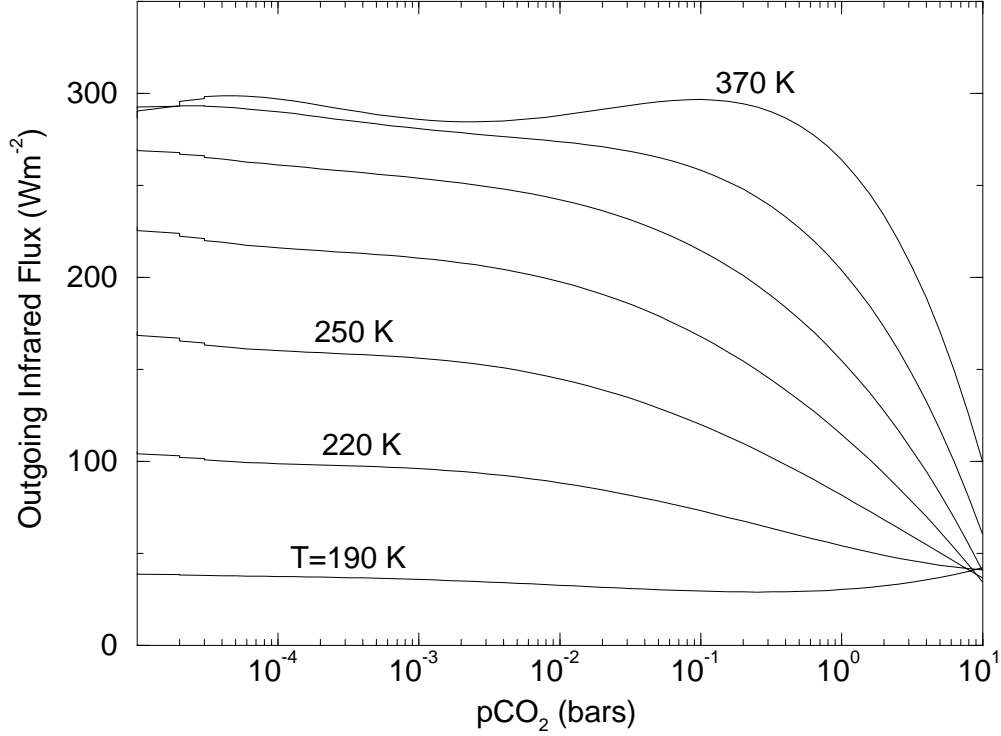


Figure 2.3: Model fits to outgoing infrared flux for different surface temperatures and CO<sub>2</sub> partial pressures. Surface temperatures are varied between 190 K and 370 K in steps of 30 K. The fits were calculated using Eqn. 2.19.

Caldeira and Kasting (their Eqns. 2-4). The polynomial given below may be applied in the range  $10^{-5} < p < 10$  bars. In units of  $\text{W m}^{-2}$ ,

$$\begin{aligned}
 I = & 9.468980 - 7.714727 \times 10^{-5} \phi - 2.794778T - 3.244753 \times 10^{-3} \phi T - \\
 & 3.547406 \times 10^{-4} \phi^2 + 2.212108 \times 10^{-2} T^2 + 2.229142 \times 10^{-3} \phi^2 T + \\
 & 3.088497 \times 10^{-5} \phi T^2 - 2.789815 \times 10^{-5} \phi^2 T^2 - 3.442973 \times 10^{-3} \phi^3 - \\
 & 3.361939 \times 10^{-5} T^3 + 9.173169 \times 10^{-3} \phi^3 T - 7.775195 \times 10^{-5} \phi^3 T^2 - \\
 & 1.679112 \times 10^{-7} \phi T^3 + 6.590999 \times 10^{-8} \phi^2 T^3 + 1.528125 \times 10^{-7} \phi^3 T^3 - \\
 & 3.367567 \times 10^{-2} \phi^4 - 1.631909 \times 10^{-4} \phi^4 T + 3.663871 \times 10^{-6} \phi^4 T^2 - \\
 & 9.255646 \times 10^{-9} \phi^4 T^3.
 \end{aligned} \tag{2.19}$$

Here,  $\phi = \log_e(p/3.3 \times 10^{-4})$ . A graphical representation of the above function is given in Fig. 2.3. As with the albedo fit, the troposphere was assumed to be fully

saturated with H<sub>2</sub>O and the stratosphere was isothermal. Reduction in the outgoing IR flux by H<sub>2</sub>O-cloud absorption was taken into account by subtracting 14.06 Wm<sup>-2</sup> from Eqn. 2.19. The value of the cloud correction was determined by requiring the model to obtain Earth's observed globally-averaged surface temperature (288 K) for the observed globally-averaged TOA albedo (0.31).

### 2.2.7 The Carbonate-Silicate Cycle

A key aspect of our attempt to simulate climate on planets with orbital characteristics and obliquities far removed from Earth's was to include the carbonate-silicate cycle, which controls the concentration of atmospheric CO<sub>2</sub> and, thus, the magnitude of the greenhouse effect. In this cycle, CO<sub>2</sub> released from volcanos is consumed by weathering of silicate minerals and precipitation of carbonate sediments on the sea floor. The rates of these processes on Earth must balance on time scales in excess of a half million years (see Holland 1978; Berner et al. 1983). The negative feedback that keeps the cycle in balance involves the dependence of silicate weathering rate on temperature (Walker et al. 1981). If surface temperatures become too low, silicate weathering slows down, and volcanic CO<sub>2</sub> accumulates in the atmosphere until the surface warms up. Conversely, if the surface temperature is too high, silicate weathering speeds up, CO<sub>2</sub> is removed from the atmosphere, the greenhouse effect diminishes, and the surface cools down.

Weathering was parameterized in the model as a function of zonal temperature and the available weathering surface, which is the zonal land fraction with  $T > 273K$ . We adopted the weathering dependence on temperature suggested by Berner et al. (1983):

$$W(T) = [1 + 0.087(T - T_0) + 1.86 \times 10^{-3}(T - T_0)^2]W_0, \quad (2.20)$$

where  $T$  is the zonally-averaged surface temperature,  $T_0$  is taken to be the planet average temperature (288 K) of present Earth, and  $W_0$  is the present rate of  $\text{CO}_2$  consumption by silicate weathering,  $3.3 \times 10^{14} \text{ g yr}^{-1}$  (Holland 1978). Averaged over all latitude belts and over the seasonal cycle, the mean weathering rate,  $\overline{W}$ , must equal the estimated global  $\text{CO}_2$  production by volcanos, which is assumed to be equal to  $W_0$ . This balance may be written as

$$\frac{\overline{W}}{W_0} = \frac{C_w \int_0^\tau dt \sum_{n=1}^{n_{\text{belts}}} A_n [1 + 0.087(T_n - T_0) + 1.86 \times 10^{-3}(T_n - T_0)^2]}{\int_0^\tau dt} \quad (2.21)$$

where  $A_n$  is the fractional zonal area available for weathering,  $\tau = 1 \text{ yr}$ , and  $C_w = 2.88$  is a constant which we adjusted to balance global weathering and outgassing for present Earth. The additional constant is required because our seasonally- and spatially-varying weathering rate does not equal the weathering rate calculated at a fixed global-mean surface temperature.

In our parameterization, the globally- and annually-averaged silicate weathering rate is always assumed to be equal to the volcanic outgassing rate of  $\text{CO}_2$  on the present Earth. This implies that a planet that receives less sunlight than does Earth must have a higher atmospheric  $\text{CO}_2$  concentration. Thus, planets farther out in the HZ tend to accumulate dense,  $\text{CO}_2$ -rich atmospheres. [The terrestrial planets do not follow this pattern, but that is because Venus is inside the inner edge of the HZ (Kasting 1988), while Mars is too small to recycle  $\text{CO}_2$  effectively (Pollack et al. 1987).] Atmospheric  $\text{CO}_2$  levels can also change in our model if the planetary obliquity is varied or if the surface geography is changed, because both of these factors affect the weathering rates calculated by Eqn. 2.21.

Note that our model assumes that atmospheric  $\text{CO}_2$  levels respond instantly to changes in planetary obliquity. This is a reasonable assumption for a planet with

Earth's CO<sub>2</sub> concentration, because the time scale for the carbonate-silicate cycle to equilibrate ( $\sim 0.5$  Myr) is shorter than the 10-Myr time scale for large, chaotic obliquity fluctuations (Laskar and Robutel 1993). However, atmospheric CO<sub>2</sub> would not have time to equilibrate over the 41,000-year period of Earth's current obliquity variation, or over the shorter (120,000-year) of the two dominant periods over which Mars' obliquity varies. So, the obliquities assumed in our climate simulations may be thought of as the average over one of these short-term cycles.

### 2.2.8 Dynamic Heat Transport

Transport of heat by advection is critical to the zonal energy balance of planets with high obliquities because their atmospheres develop large temperature gradients which should drive the winds. Traditional treatment of dynamic heat transport in EBCMs has been to average the velocity field over a scale height and around the planet and to model the heat flow as diffusion using the transport term of Eqn. 2.1. The diffusion coefficient,  $D$ , is commonly adjusted until models comfortably reproduce Earth's present latitudinal temperature gradient (see North 1981). Some investigators (Lindzen and Farrell 1977) have attempted a more realistic representation of transport by parameterizing  $D$  as a function of latitude, allowing for the differences in transport efficiency between the symmetric Hadley regime below 30° latitude to a baroclinic eddy transport regime at mid-latitudes. Here we have employed a methodology similar to that of Hoffert et al. (1981) who parameterized transport efficiency as a function of dynamic factors which may vary greatly from one atmosphere to another.

The case of Venus suggests that atmospheric pressure and planetary rotation rate are important transport parameters. Venus' atmosphere is  $\sim 100$  times more massive than Earth's and exhibits an extensive Hadley circulation that heats the poles to

within a few degrees of the equatorial temperature (Schubert 1983). A measure of the efficiency and poleward extent of the Hadley circulation is the Rossby number,  $R$ , expressed by Farrell (1990) as

$$R = gH\delta_h/\Omega^2r^2, \quad (2.22)$$

where  $g$  is gravitational acceleration,  $r$  is planet radius,  $H$  is pressure scale height,  $\Omega$  is planet rotation rate, and  $\delta_h$  is latitudinal temperature gradient.

The Rossby number for Earth is  $\sim 0.2$ , which corresponds to a Hadley cutoff latitude of  $\sim 30^\circ$  (Farrell 1990). The Rossby parameter for Venus is  $\sim 10^4$  times that of Earth, allowing its Hadley circulation to reach the pole. An examination of the Rossby number form, however, reveals no explicit atmospheric pressure dependence, indicating that the strength of Hadley transport on Venus derives not so much from its dense atmosphere as it does from its slow rotation ( $2\pi/\Omega = 243$  days). Hadley circulation is truncated at mid-latitudes on rapidly rotating planets (e.g., Earth) by large Coriolis forces that deflect air masses azimuthally and disrupt the symmetry of the north-south flow.

Neither Venus nor Earth rotates at its primordial rotation rate, as they have been affected by tidal interactions with the Sun and Moon, respectively (Laskar and Robutel 1993). However, the 24-hour rotation rate of Mars suggests that terrestrial planets born and evolving in relative tidal isolation will have rotation periods of many hours rather than many days. For want of a better choice, the planets we consider here are assumed to have 24-hour rotation periods, which implies that the extent of their Hadley circulations should be similar to Earth's.

Changes to scale height,  $H = RT/mg$ , will also affect Hadley heat transport. Temperatures do not vary much in the model atmospheres considered here, but the mean molecular weight,  $m$ , increases as the atmospheres become more CO<sub>2</sub>-rich. All

else being equal, larger mean molecular weights for atmospheres of planets in the outer HZ (assuming  $N_2$  is the other dominant gas) will cause the extent of their Hadley circulations to be slightly smaller.

The above discussion implies that dynamic heat transport on rapidly rotating, Earth-like planets will be accomplished most effectively by baroclinic eddies. The dynamical heat flux,  $Q_d$ , caused by eddy circulation is expressed by Gierasch and Toon (1973) as the following proportionality,

$$Q_d \propto \int_0^\infty \rho c_p \overline{vT} dz. \quad (2.23)$$

The velocity,  $v$ , and temperature,  $T$ , of the flow are averaged over longitude and time,  $\rho$  is the density,  $c_p$  is the specific heat of the atmosphere, and the integral is carried over height,  $z$ . Using the hydrostatic law and assuming  $\overline{vT}$  varies little with height, Eqn. 2.23 may be written

$$Q_d \propto p c_p \overline{vT}, \quad (2.24)$$

giving the desired transport dependence on atmospheric pressure  $p$ . Additional dependences can be inferred by examining the form of  $\overline{vT}$  given by Stone (1972),

$$\overline{vT} \propto \frac{1}{m^2 f^2}, \quad (2.25)$$

where  $f$  is the Coriolis parameter,  $\propto \Omega$ . It is comforting to recognize that these variables are components of the Rossby number considered previously, and additionally that the dominant rotation dependence ( $\Omega^{-2}$ ) is common to both forms. A notable difference is the  $m^{-2}$  dependence here compared to the  $m^{-1}$  dependence in the Rossby number. For consistency, we have included the dependence of transport on specific heat,  $c_p$ , which is slightly lower (by 14%) for  $CO_2$  than for  $N_2$ . Combining Eqns. 2.24 and 2.25, we obtain

$$Q_d \propto p c_p m^{-2} \Omega^{-2}. \quad (2.26)$$

The above proportionality may be expressed as an equation using the diffusion coefficient,  $D$ , which may be expressed in terms of normalized variables (with the subscript  $\circ$  referring to present Earth) as

$$\left(\frac{D}{D_0}\right) = \left(\frac{p}{p_0}\right) \left(\frac{c_p}{c_{p_0}}\right) \left(\frac{m_0}{m}\right)^2 \left(\frac{\Omega_0}{\Omega}\right)^2. \quad (2.27)$$

We adjusted  $D_0 = 0.58 \text{ W m}^{-2} \text{ K}^{-1}$  to match Earth's present latitudinal temperature gradient, and the latitude ( $\sim 72^\circ$ ) of the 263 K seasonal-mean ice line. Thus, the value of  $D_0$  includes to first approximation the effect of heat transport by ocean currents, which is an important driver of climate on Earth. We took  $c_{p_0} = 0.2401 \text{ cal g}^{-1}\text{K}^{-1}$  (CRC Handbook of Chemistry and Physics 1985-86 ed.),  $m_\circ = 28.0 \text{ amu}$ , and  $\Omega = \Omega_0 = 2\pi/24\text{hrs}$ .

### 2.2.9 CO<sub>2</sub> Clouds

The HZ outer edge has been suggested by KWR to be the distance at which CO<sub>2</sub> first condenses to form clouds within a planet's atmosphere. This is clearly a conservative assumption, as CO<sub>2</sub> clouds should not noticeably affect climate until they begin forming over large portions of the planet, and because high-altitude CO<sub>2</sub> clouds may warm, rather than cool (as do cirrus clouds on Earth) [see Forget and Pierrehumbert 1997]. KWR could not look at the spatial and temporal distribution of CO<sub>2</sub> clouds because their model was one-dimensional and time-independent. We revisited this problem with the energy-balance model to determine where and when clouds form, and to provide a revised estimate for the HZ outer edge. As in KWR, CO<sub>2</sub> clouds were not included explicitly in the planetary radiation balance. Only their effect on the tropospheric lapse rate was taken into account. The troposphere in each latitude zone was searched seasonally for clouds by comparing the saturation vapor pressure of CO<sub>2</sub> to its ambient pressure using the following method.

First, the depth of the troposphere was determined by our assumptions regarding stratospheric temperature. We parameterized  $T_{\text{strat}}$  as a function of  $p\text{CO}_2$  and  $T$  in the same way we performed the fit to  $I$  to obtain Eqn. 2.19. We obtained

$$T_{\text{strat}} = -188.1 - 1.955\phi + 3.810\phi^2 + 2.328T + 3.733 \times 10^{-4}\phi T - 2.856 \times 10^{-2}\phi^2 T - 3.329 \times 10^{-3}T^2 + 2.214 \times 10^{-5}\phi T^2 + 4.605 \times 10^{-5}\phi^2 T^2, \quad (2.28)$$

where  $\phi$  is the same as before. The fit was performed with  $Z = 60^\circ$  using Eqn. 2.12, which means that we slightly overestimated  $T_{\text{strat}}$ , and hence tropospheric depth, at the poles while underestimating their values at the equator. This suggests that clouds in reality are less likely to form at the poles and more likely to form at the equator than the model indicates. The effect of this error on our results, however, is expected to be small because a counterbalancing error is introduced in approximating tropospheric lapse rate, as will be discussed below.

Once  $T_{\text{strat}}$  was found, the troposphere was divided into 20 layers of equal thickness. The model stepped from the surface to the tropopause by assuming a constant lapse rate  $c = 6.5 \text{ K km}^{-1}$  and the barometric law for  $\text{CO}_2$ ,

$$p(h) = p(0) \left( \frac{T(h)}{T(0)} \right)^{mg/kc}. \quad (2.29)$$

Here,  $g$  is the gravitational constant,  $k$  is the Boltzmann constant,  $h$  is physical height and, here,  $m$  is the mean molecular weight of the atmosphere. Our assumed lapse rate for this calculation is slightly smaller than over the poles ( $\sim 10 \text{ K km}^{-1}$ ) and slightly larger than over the tropics ( $3\text{--}4 \text{ K km}^{-1}$ ) in reality and so, here, we underestimated polar cloud cover while overestimating clouds in the tropics. Thus, we err in the opposite sense of our previous error introduced in approximating  $T_{\text{strat}}$ , which should mitigate the effects of both approximations for this calculation. Clouds form at a height at which  $p > p_{\text{sat}}$ , the saturation vapor pressure, which we calculated using

Eqns. A5 and A6 of Kasting (1991). Finally, we determined the fraction of the globe that is covered with CO<sub>2</sub> clouds by summing over the latitudes in which clouds form and weighting them by zonal area and insolation.

### 2.2.10. Solving the Model

We obtained latitudinal temperature profiles by finding numerical solutions to the zonal energy-balance equation, Eqn. 2.1, with the constraint that the profiles also be solutions to the CO<sub>2</sub> weathering-balance equation, Eqn. 2.21. We integrated both equations simultaneously using the following method. We began with an isothermal planet (e.g.,  $T = 288K$ ) at the vernal equinox ( $L_s = 0$ ), and stepped the planet in its orbit by incrementing the time and orbit longitude using Eqn. 2.4.

For each  $\Delta t$ , we performed a spatial integration over all latitude zones. Orbital longitude set the solar declination according to Eqn. 2.3 and, hence, the diurnally-averaged insolation for each zone using Eqn. 2.9. The TOA albedo, outgoing IR flux, and weathering rate, which all depend on surface temperature, followed from Eqns. 2.10-2.11, 2.19 and 2.21, respectively. The dynamic heat transport term of Eqn. 2.1 was spatially differenced to 2nd-order in  $x$ , and operated on the global latitudinal temperature profile. The pressure-dependent transport coefficient  $D$  was calculated using Eqn. 2.27. Once the climate parameters for each zone were computed, the first term of Eqn. 2.1. was temporally differenced according to our assumptions made concerning effective heat capacity, and the surface temperatures were updated.

Every five orbits, we compared the seasonal-global mean weathering rate to the rate of CO<sub>2</sub> production by volcanos, and if the ratio of weathering to outgassing was less than unity, we increased pCO<sub>2</sub>. Conversely, we decreased pCO<sub>2</sub> for ratios greater than unity. The size of the adjustment was proportional to the size of the rate imbalance. We staggered the adjustments to pCO<sub>2</sub> by five orbital periods to allow

the slowly varying temperature of the oceans time to respond. We iterated on this procedure until the weathering rate converged to within  $10^{-3}$  of the outgassing rate.

The rate of convergence was predominantly affected by orbital semi-major axis, which set the orbital period, by the step-size  $\Delta t$ , and by the initial choice for  $p\text{CO}_2$ . For  $a = 1.0$  AU,  $\Delta t = 1$  day, and  $p_0 = 330$  ppm, the model calculations required 38 seconds of CPU time on a CRAY supercomputer. By contrast, convergence took 59 seconds for the same time step, but with  $a = 1.4$  AU, and  $p_0 = 2.0$  bars.

## 2.3 Results

### 2.3.1 Earth's Present Climate

First, we adjusted the model's free parameters to obtain a reasonable approximation of Earth's climate at  $23.5^\circ$  obliquity. We paid particularly close attention to reproducing the seasonal- and global-mean albedo (0.31) and surface temperature (288 K), the latitude of the permanent ice line ( $72^\circ$ ), and the amplitudes of zonal seasonal cycles. Results of the modeling are given in Table 2.3 and in Fig. 2.4a, where we illustrate how zonal temperatures vary over a 1-year seasonal cycle.

Focusing our attention on the zone centered on  $+45^\circ$ , we find that the temperature varies from 271.3 K ( $-1.8^\circ\text{C}$ ) to 285.8 K ( $12.7^\circ\text{C}$ ) with a seasonal cycle amplitude of 7.3 K, which is substantially smaller than the observed amplitude ( $\sim 16^\circ\text{C}$ ) for continental interiors at this latitude on Earth. Thus, our model amplitudes in zones containing substantial amounts of water are less than half the size of observed amplitudes over continents in the same zone, in good agreement with seasonal cycle amplitude differences found using a more sophisticated 2-D model (North et al. 1983) that resolved the continents and oceans.

geography	obl. ( $^{\circ}$ )	$T_{av}$ (K)	$A_{av}$	$pCO_2$ (ppm)	$T_{max}$ (K)		$T_{min}$ (K)	
present	23.5	288.1	0.311	330.	304.5	( $-5^{\circ}$ )	241.3	( $85^{\circ}$ )
equatorial	.	276.6	0.351	44.0	293.3	( $-5^{\circ}$ )	234.6	( $-85^{\circ}$ )
polar	.	282.4	0.323	38.7	325.9	( $-85^{\circ}$ )	217.0	( $-85^{\circ}$ )
polar	35.0	250.0	0.510	11.8	364.0	( $-85^{\circ}$ )	195.7	( $-85^{\circ}$ )
present	90.0	282.3	0.312	19.4	352.2	( $-85^{\circ}$ )	266.4	( $15^{\circ}$ )
equatorial	.	300.2	0.269	1670	339.4	( $-85^{\circ}$ )	274.1	( $-5^{\circ}$ )

Table 2.3: Model output with Earth at 1.0 AU. *obl* is obliquity,  $T_{av}$  is the seasonal- and global-mean temperature,  $A_{av}$  is the seasonal- and global-mean albedo, and  $pCO_2$  is carbon dioxide partial pressure, given in parts per million. Global temperature extremes,  $T_{max}$  and  $T_{min}$ , are listed left of the latitudes at which they occur.

Our simpler model averages the heat capacities for land and ocean within a zone around the entire globe. This presents the following problem: Because the model heat capacity for unfrozen ocean is 40 times that of the atmosphere over land, a simple weighting of the heat capacities by the respective zonal surface fractions yields a heat capacity characteristic of an oceanic zone rather than a continental zone. For zones with comparable amounts of land and sea (e.g.,  $+45^{\circ}$ ), the zonally-averaged heat capacity and, hence, thermal time scale are over 20 times that over a continent. Thus, the magnitudes of temperature extremes returned by the model are substantially smaller than those which would occur over a continental interior.

### 2.3.2 Earth at $90^{\circ}$ Obliquity

Our second climate simulation was performed with Earth's obliquity set equal to  $90^{\circ}$ . Results for the run are given in Table 2.3, and Fig. 2.4b illustrates the remarkable changes to Earth's climate that would follow. First, the tropics would become cold enough to sustain permanent snow cover because at high obliquity the Sun spends comparatively little time near the zenith at low latitudes. Also, each pole would be heated for 6 months, as they are at  $23.5^{\circ}$  obliquity, but with the Sun spending over 40 days within  $20^{\circ}$  of polar zenith. Because the opposite period of cooling would be

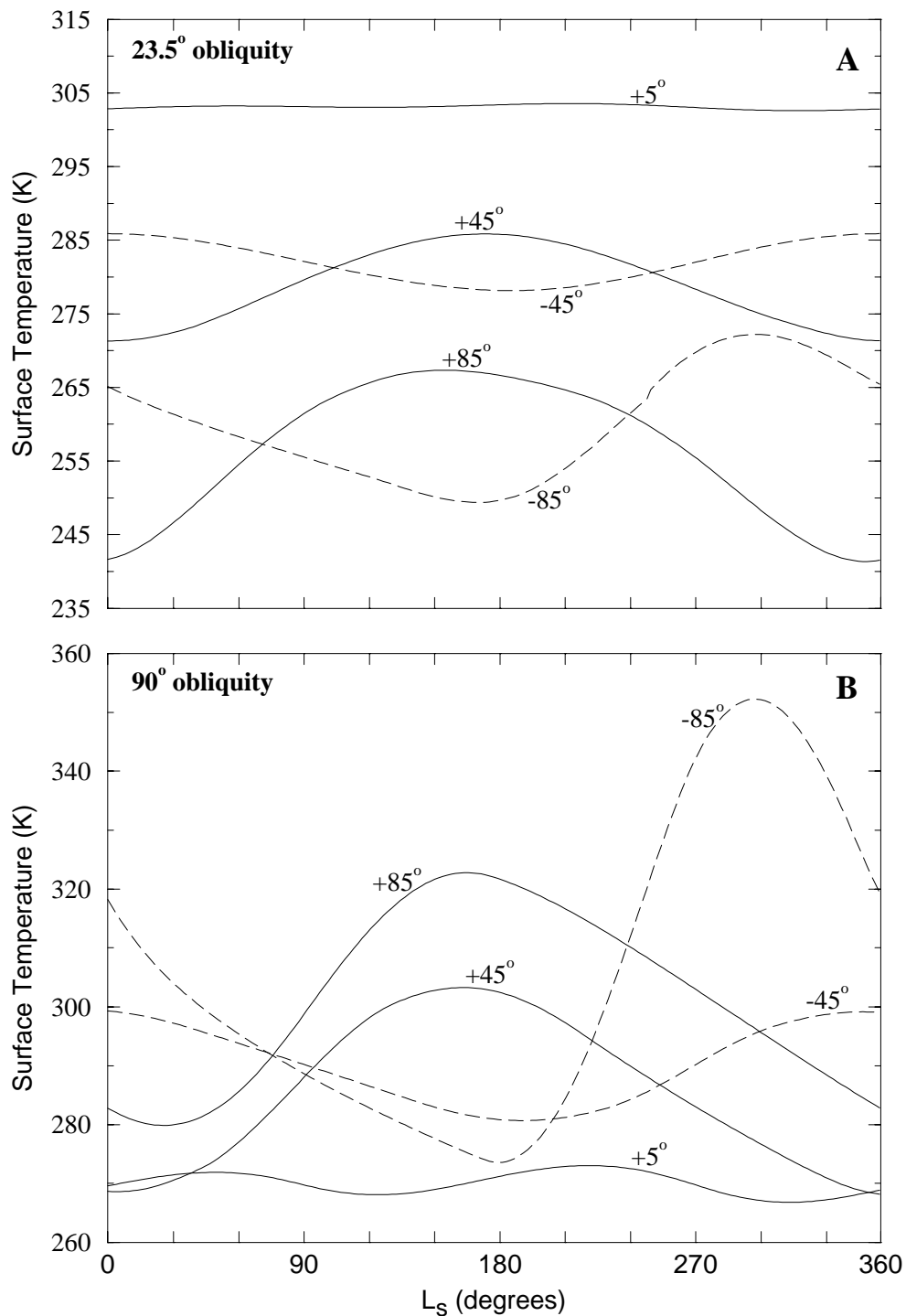


Figure 2.4: Representative seasonal temperature cycles for Earth at (a)  $23.5^\circ$  obliquity and at (b)  $90^\circ$  obliquity.  $L_s$  is the orbital longitude of the planet with respect to the vernal equinox ( $L_s = 0^\circ$ ). Solstices occur at  $L_s = 90^\circ$  and  $270^\circ$ . Temperatures are shown for 5 latitude zones, each  $10^\circ$  wide and centered on the latitude labeling the curves. Northern latitudes are indicated by solid lines, and southern latitudes are indicated by dashed lines.

equivalent to the length of darkness experienced by the pole at any obliquity, the net change to polar climate would be a warming, which would cause the ice to melt.

Under these circumstances, Earth's oceanic (northern) and continental (southern) poles would demonstrate markedly different seasonal cycle amplitudes because of their different thermal inertias. Despite the relatively high thermal inertia of the northern pole, the intensity and duration of sunlight experienced there at high obliquity doubles the amplitude of its temperature cycle (see Fig. 2.4), bringing summer temperatures over the Arctic ocean above 320 K. The seasonal variation in temperature over the southern pole is even more dramatic, with summer temperatures reaching 353 K, slightly lower than the survivable high-temperature limit (383 K) for thermophilic bacteria (Seeger et al. 1993) but higher than the maximum temperatures at which more advanced life forms survive today ( $\sim 330$  K). The seasonal minimum temperatures still dip below the freezing point of water.

Large seasonal temperature variations might also present a problem for life at lower latitudes. At  $+45^\circ$ , for example, model temperatures are found to vary between 268 K and 304 K. Over the continents at this latitude, the temperature variation could be twice this large, which would allow summertime temperatures to exceed 322 K and wintertime temperatures to fall below 250 K. Even more remarkable is that this variation, which exceeds the present range of temperatures observed on Earth today, would take place in only 6 months time. Whether any of Earth's dominant species could survive these rapid and large variations in temperature is an interesting biologic question. Photosynthetic life might be substantially challenged by long ( $\sim 90$ -day) periods of darkness during the winter at this latitude. Areas nearer the equator would have smaller seasonal temperature variations and shorter periods of darkness, so at least some areas of the planet might still be suitable for life at  $90^\circ$  obliquity.

Earth's  $\text{CO}_2$  level would also be affected by its obliquity because the weathering

rate depends on surface temperatures through Eqn. 2.21. Figure 2.5a compares the seasonally-varying global weathering rate for Earth at  $23.5^\circ$  and  $90^\circ$  obliquity. We find, in both cases, that the greatest weathering takes place during northern hemisphere summer, when the bulk of Earth's continents is warmest. Also, the weathering cycle amplitude is greater at high obliquity because the seasonal temperature variations are exaggerated. A second peak in the  $90^\circ$ -obliquity weathering cycle results from weathering of continents in the southern hemisphere around the northern winter solstice. Earth's equilibrium  $\text{CO}_2$  level at  $90^\circ$  obliquity is 19.4 ppm (Table 2.3), significantly lower than at present (330 ppm). This is because for a given  $\text{CO}_2$  level, the continents weather more rapidly, on average, at  $90^\circ$  obliquity than at  $23.5^\circ$ . Thus,  $\text{pCO}_2$  must equilibrate at a lower value for the high-obliquity planet than it does for the present Earth.

### 2.3.3 Effects of Changing the Geography

The difference in seasonal cycle amplitude over the northern and southern poles in Fig. 2.4b shows the model to be very sensitive to the location of continents. The difference would be even more pronounced if the Antarctic continent were larger because it would be able to sustain an even greater temperature gradient.

To examine the effects of continental size and position on climate for planets with different obliquities, we imitated Marshall et al. (1988) by performing simulations with all of Earth's continents clustered together to form a supercontinent, which we chose to center either on the equator or over the southern pole. Results of our simulations are given in Table 2.3 and in Fig. 2.5b. At  $23.5^\circ$  obliquity, an equatorial supercontinent would experience substantial weathering at the equinoxes. This would, in turn, draw down atmospheric  $\text{CO}_2$  from 330 ppm to 44 ppm, where the surface could cool enough to weather more slowly. A similar result was obtained by Marshall

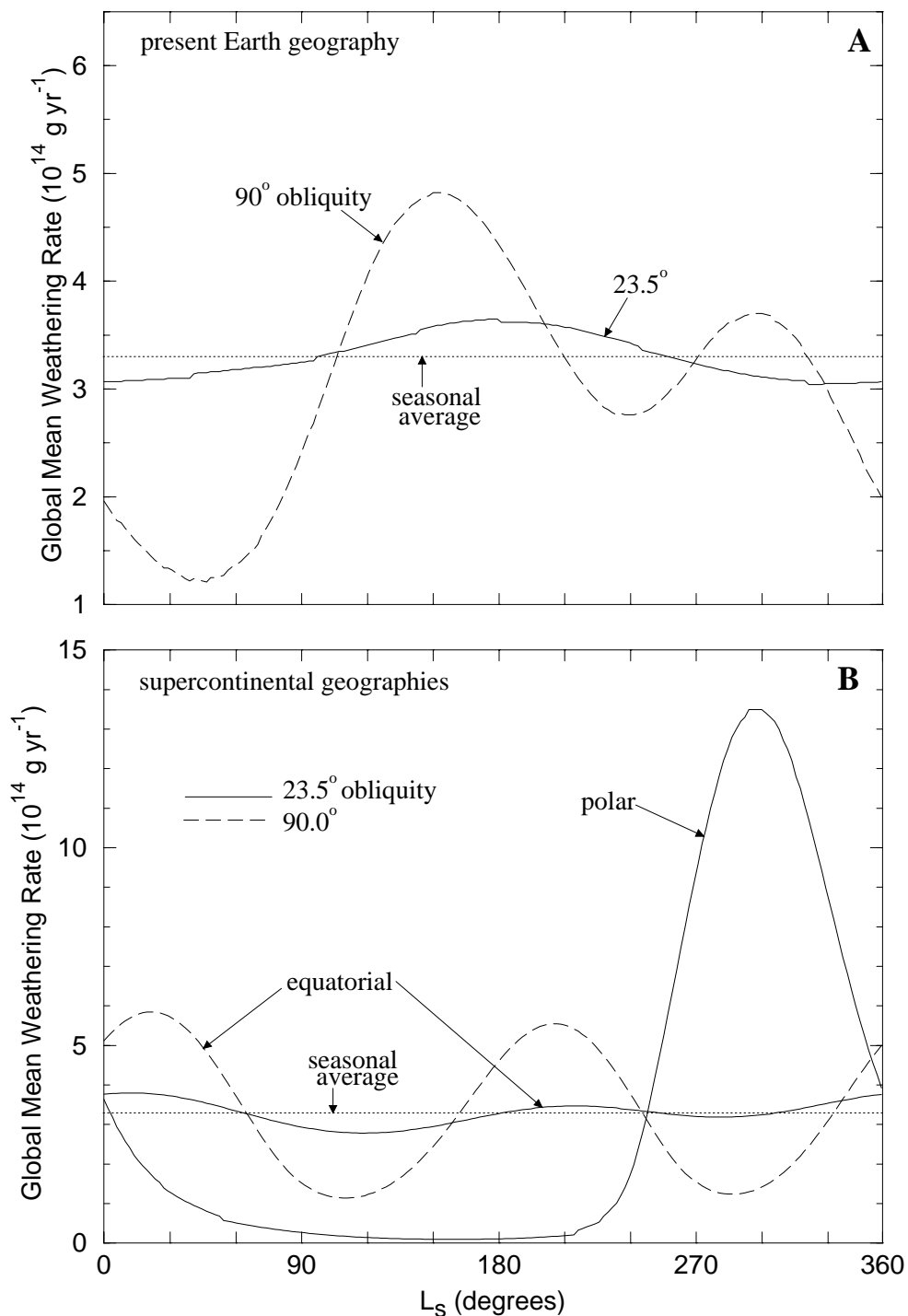


Figure 2.5: Variations in the global-mean weathering rate over a seasonal cycle for Earth at 1.0 AU, and with a  $23.5^\circ$  (solid lines) and  $90^\circ$  (dashed lines) obliquity. Cycles are shown for Earth with (a) present geography, and (b) two alternate geographies: a supercontinent covering 30% of Earth's surface centered on the equator, and a supercontinent centered on the south pole. The model forces the seasonal-average weathering rate to equal the  $\text{CO}_2$  volcanic outgassing rate =  $3.3 \times 10^{14} \text{ g yr}^{-1}$  (dotted line).

et al. (1988). Thus, the lower CO<sub>2</sub> level would safeguard the equatorial supercontinent from temperatures that might otherwise be warmer than Earth's tropics today. While permanent sea-ice caps would cover both poles poleward of  $\pm 52^\circ$ , continental temperatures would range from 286 K to a mild 293 K, which would provide optimal conditions for terrestrial-type life.

At high obliquity, the equatorial supercontinent would cool initially, which would cause weathering to slow or even cease, and CO<sub>2</sub> would accumulate in the atmosphere. We find that 1670 ppm of CO<sub>2</sub> is needed to thaw the continent and raise the weathering rate. As at low obliquity, the greatest weathering takes place near the equinoxes when the continent is warmest. Even in this extreme case, the supercontinent would remain unfrozen with temperatures never falling below 274 K.

The case of the polar supercontinent is more problematic because, even at  $23.5^\circ$  obliquity, areas near the southern pole would alternate between superheated (326 K) and subpolar (217 K) states every 6 months. Only a narrow region near the coast of the supercontinent ( $-26^\circ$  latitude) would demonstrate a seasonal cycle amplitude smaller than 30 K. Although the solar zenith angle would remain small during the sunlit summer months the prolonged illumination would be enough to warm the supercontinent and cause it to weather rapidly, as shown in Fig. 2.5b. Table 2.3 shows that the CO<sub>2</sub> level needed to balance the carbonate-silicate cycle (38.7 ppm) is even lower than for the case of the equatorial supercontinent. A slightly higher obliquity ( $35^\circ$ ) yields an even larger seasonal cycle, and temperature extremes near the confidence limits (360 K and 190 K) of the model, set by the fits to top-of-atmosphere albedo (Eqns. 2.10 and 2.11). For this case, an ice cap would cover the entire hemisphere opposite the continent, while the temperature extremes on the supercontinent would be everywhere damaging to life. These problems would be even more pronounced for planets having higher obliquities, or for planets with smaller

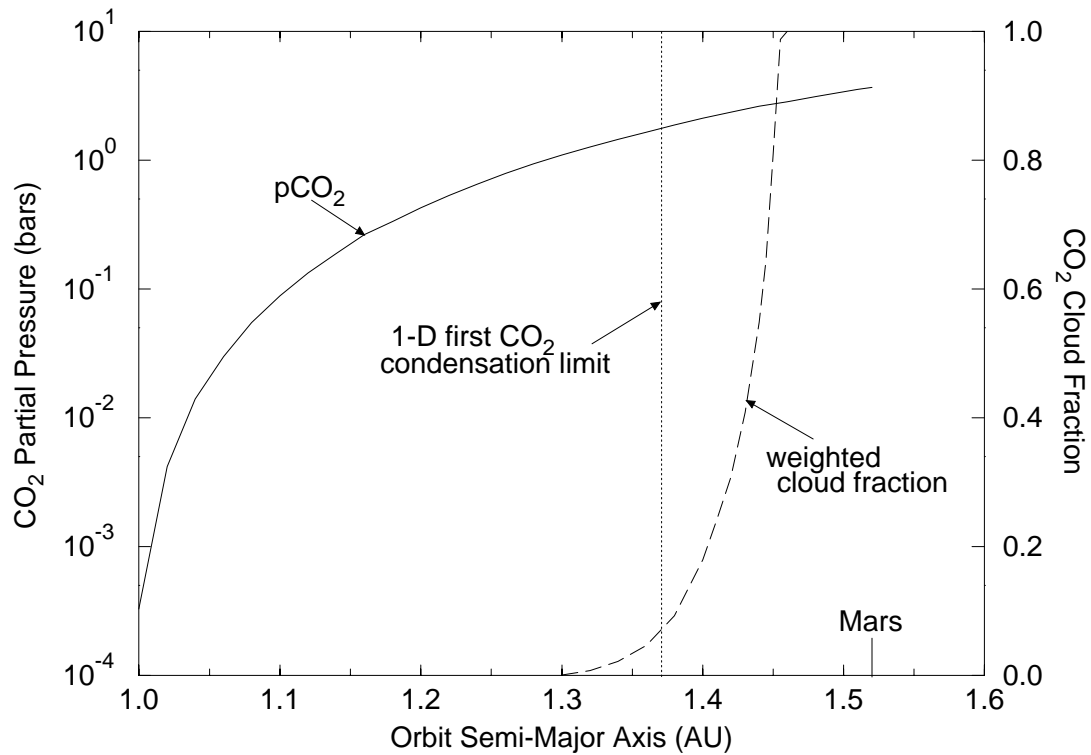


Figure 2.6: Carbonate-silicate cycle equilibrium CO<sub>2</sub> levels (solid line) for Earth at a variety of positions within the HZ. The 1-D first-CO<sub>2</sub>-condensation limit at 1.37 AU (dotted line) was found by KWR. CO<sub>2</sub> cloud fraction (dashed line) is an area- and insolation-weighted sum of the latitude zones in which clouds form somewhere within the troposphere.

endowments of water and larger continents. Clearly, high-obliquity planets with polar supercontinents are not very attractive candidates for harboring land-based life.

### 2.3.4 Dense CO<sub>2</sub> Atmospheres and the HZ Outer Edge

Earth could circumvent the problems it would face at high obliquity, or with a polar supercontinent, if it were farther from the Sun, where its atmosphere might contain larger amounts of CO<sub>2</sub>. A CO<sub>2</sub>-rich atmosphere would have a long radiative time constant because CO<sub>2</sub> is highly opaque to infrared radiation leaving the planet. The increase in Earth's global thermal inertia would decrease the amplitude of its seasonal cycle and cause the climate to be only weakly sensitive to continental topography.

To determine how dense an atmosphere one might expect to form, we performed

simulations with Earth at several orbital positions between 1.0 and 1.5 AU, while holding its obliquity and geography constant at present values. The object was to determine the level of CO<sub>2</sub> required to balance the carbonate-silicate cycle at these distances. The results of these calculations are shown in Fig. 2.6. Steady-state atmospheric CO<sub>2</sub> partial pressures range from  $3.3 \times 10^{-4}$  bar for Earth in its present orbit to nearly 4.0 bars at 1.50 AU. The CO<sub>2</sub> partial pressure asymptotically approaches 5 bars at the “maximum greenhouse” limit of 1.67 AU, beyond which a planet cannot be warmed by further addition of CO<sub>2</sub> (KWR). Here, the increased albedo caused by CO<sub>2</sub> outweighs its contribution to greenhouse warming.

A planet might not remain habitable out to this distance, however, because the planet would be covered by CO<sub>2</sub> clouds that possibly cool the surface. The results of Forget and Pierrehumbert (1997), however, suggest that such clouds might contribute to surface warming by increasing atmospheric opacity at infrared wavelengths. This issue is far from being resolved, so we are still justified in adopting the conservative assumption that the formation of CO<sub>2</sub> clouds is the limiting factor in defining the HZ outer edge. The distance at which CO<sub>2</sub> first condenses in a 1-D atmosphere was determined by KWR to be 1.37 AU (Fig. 2.6). This served as their conservative estimate of the HZ outer edge. Our model demonstrates that, in a two-dimensional model, clouds first appear at the poles around 1.30 AU, and that they become widespread between 1.40 and 1.45 AU. Thus, a conservative choice for the the outer edge of the Sun’s present HZ is  $\sim 1.40$  AU, not far from the 1-D estimate.

geography	obl. (°)	T <sub>av</sub> (K)	A <sub>av</sub>	pCO <sub>2</sub> (bars)	T <sub>max</sub> (K)	T <sub>min</sub> (K)	
present	23.5	290.6	0.337	2.12	296.4	(-15°)	274.5 (85°)
equatorial	.	285.5	0.346	1.89	291.5	(-5°)	272.4 (-85°)
polar	.	289.6	0.334	2.04	309.3	(-85°)	257.1 (-85°)
polar	65.0	246.2	0.488	1.15	362.8	(-85°)	189.9 (-85°)
present	90.0	287.9	0.324	1.87	319.1	(-85°)	275.5 (65°)
equatorial	.	293.3	0.319	2.15	313.3	(-85°)	282.9 (-5°)

Table 2.4: Model output with Earth at 1.4 AU.

### 2.3.5 Temperature Gradients and Seasonal Cycles at 1.4 AU

Planets near the outer edge of the HZ have dense CO<sub>2</sub> atmospheres as a result of the carbonate silicate cycle. One consequence of this is a reduction in the equator-to-pole temperature gradient. The reason for this reduction is two-fold. First, the poles are not able to cool as rapidly in winter as they do beneath a relatively IR-transparent atmosphere at 1.0 AU. This results in a warming of the poles relative to the equator, and a flattening of the latitudinal temperature profile (Fig. 2.7). The tropics are also warmed initially, but under these circumstances, the globally-averaged surface temperature is too high to maintain the present global weathering rate. To compensate, the model adjusts (lowers) the concentration of CO<sub>2</sub> until temperatures are globally reduced (i.e., the temperature profile in Fig. 2.7 is lowered) and the global weathering rate is re-equilibrated with the rate of CO<sub>2</sub> production by outgassing for the new latitudinal distribution of surface temperatures. Thus, despite its possessing a dense CO<sub>2</sub>-rich atmosphere, Earth at 1.4 AU is shown to be cooler in the tropics than it is at present, although the average temperature of the planet increases to 290.6 K (Table 2.4).

A second reduction in latitudinal temperature gradient derives from more efficient dynamic heat transport as the total atmospheric pressure,  $P$ , is raised. At 1.4 AU,  $p\text{CO}_2 = 2.12$  bars,  $P = 3.12$  bars,  $c_p = 0.91c_{p_0}$ ,  $m = 1.35m_0$  so, from Eqn. 2.27,  $D = 1.56D_0 = 0.91 \text{ W m}^{-2} \text{ K}^{-1}$ . Figure 2.7 contrasts the effects of raising the IR opacity of the atmosphere and of enhancing heat transport. The dotted-line profile for Earth at 1.4 AU shows the effect of opacity alone, whereas the solid-line profile for 1.4 AU illustrates the combined influence. Nearly 70% of the reduction in the

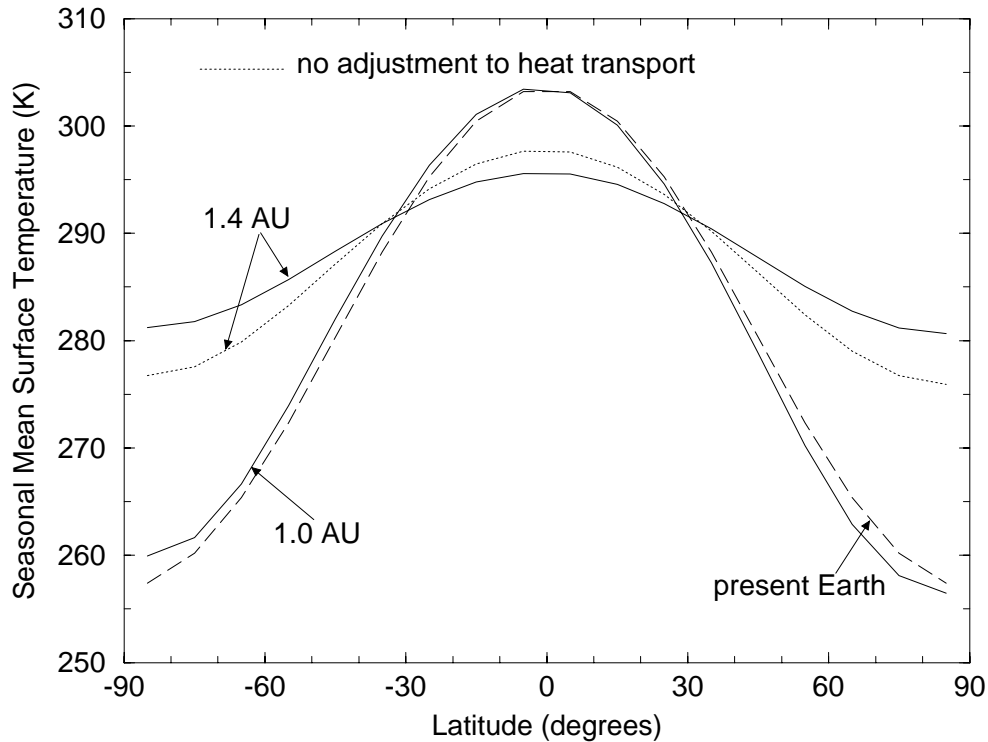


Figure 2.7: Latitudinal temperature profiles for Earth at 1.0 AU and 1.4 AU (both marked with solid lines). The profile indicated by a dotted line is for Earth at 1.4 AU with the heat transport parameter held constant ( $D = 0.58 \text{ W m}^{-2} \text{ K}^{-1}$ ). Observations (dashed line) are taken from North and Coakley (1979) and parameterized as  $T(x) = 14.2 - 30.2P_2(x)$ , where  $T$  is the seasonal-average surface temperature ( $^{\circ}\text{C}$ ),  $x$  is the sine of latitude, and  $P_2(x)$  is the second Legendre polynomial  $(3x^2 - 1)/2$ .

equator-to-pole temperature gradient between 1.0 AU (47 K) and 1.4 AU (15 K) is caused by the radiative properties of  $\text{CO}_2$ , while the remainder is caused by dynamics. This is significant because it implies that our results are only weakly sensitive to our uncertain assumptions concerning heat transport in atmospheres vastly different from Earth's.

We next experimented with Earth at 1.4 AU and with a  $90^{\circ}$  obliquity to illustrate how elevated  $\text{CO}_2$  levels affect seasonal temperature cycles. Figure 2.8 shows that the amplitudes of temperature cycles would be greatly reduced. The reason for this is the same as before: as more  $\text{CO}_2$  accumulates in the atmosphere, the global thermal time constant and, hence, global thermal inertia grow. Thus, zonal temperatures respond

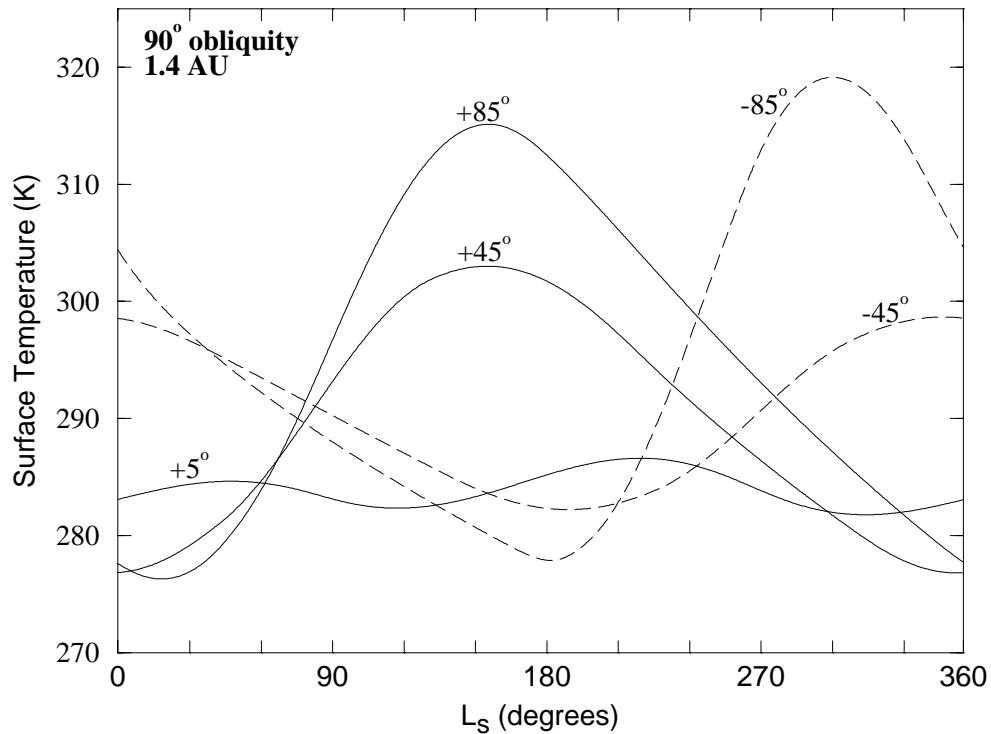


Figure 2.8: Seasonal temperature cycles for Earth at 1.4 AU, and with  $90^\circ$  obliquity.

slowly to changes in insolation, and the magnitudes of the seasonal temperature extremes are reduced.

A comparison of Figs. 2.8 and 2.4b shows that the amplitude of the seasonal cycle at  $+45^\circ$  latitude is reduced by 30% in moving from 1.0 AU to 1.4 AU. The  $90^\circ$  obliquity seasonal cycle at 1.4 AU is only slightly greater (2 K) than the observed amplitude for the same latitude on Earth today. Differences in heat capacity and, hence, temperature extremum (315 K and 319 K) for the northern and southern poles are shown to be essentially eliminated. We note that Earth would be ice-free under these circumstances and, with the exception of the summertime poles, would be able to support life over an even greater fraction of its surface than it does at present.

Finally, we repeated the geographic variation experiments described in Sec. 2.3.3 with Earth at 1.4 AU to determine if an Earth with a dense  $\text{CO}_2$  atmosphere and a supercontinent would be equally habitable. Results from these runs are given in Table

2.4. The promising result is that such a planet would be able to sustain temperatures over a polar supercontinent within the limits of the model to a much higher obliquity ( $65^\circ$ ) than at 1.0 AU. At  $23.5^\circ$  obliquity, the polar supercontinent would demonstrate a seasonal temperature range comparable to the equator-to-pole gradient for present Earth. This suggests that a wide variety of planets with  $\text{CO}_2$ -rich atmospheres would be immune to the climatic problems caused by high obliquity.

## 2.4 Discussion

An obvious weakness of our model is the averaging of heat capacity, surface albedo, and temperature over  $10^\circ$ -wide latitudinal zones extending around the planet. This causes us to underestimate the amplitude of the seasonal cycle over the continents (except in the supercontinent scenarios, where an entire latitude band may be devoid of water). Also, by averaging the climate parameters around the planet, we have ignored meridional land-sea temperature gradients which affect dynamic heat transport and weather.

Perhaps the most severe limitation of the model is its gross oversimplification of the effects of weather on the global climate. As explained in Sec. 2.2.8, we modeled latitudinal heat transport as diffusion, whereas in reality, wind patterns and energy transport are much more complicated. This simplification afforded us speed in computation, but we are not really able to predict how latitudinal energy transport would differ on planets with higher obliquities, or with denser atmospheres. Some first-order changes were predicted by adjusting the diffusion coefficient,  $D$  (Eqn. 2.27), to account for changes to atmospheric pressure. Large latitudinal temperature gradients in atmospheres of planets at high obliquity (Fig. 2.4b) may tend to increase heat

transport to a greater extent than we predict by driving vigorous Hadley circulation cells and causing increased baroclinic wave activity. We suspect, but cannot prove, that temperature gradients in more realistic dynamic atmospheres would be smaller than predicted here.

A third area of uncertainty is the model's treatment of H<sub>2</sub>O-clouds, which we assumed to cover exactly half of the planet's surface at all times, as is approximately true on Earth. If H<sub>2</sub>O-cloud cover increases as the surface temperature warms, as seems likely, then surface temperature extremes may be further buffered by cloud feedback. This is particularly important over polar oceans where the temperatures predicted by our model exceed 320 K at high obliquity. Negative cloud feedback might significantly reduce these summertime extremes, rendering the polar regions much more habitable. A three-dimensional atmospheric circulation model with predictive clouds is needed to investigate this possibility.

Given the limitations of the present climate model, a natural question is: Why even attempt to study this problem at this crude level of approximation? The answer is that many of our conclusions depend more strongly on atmospheric CO<sub>2</sub> levels and the carbonate-silicate cycle feedback than they do on the details of the atmospheric climate model. The problem deserves to be examined with a 3-D general circulation model, but the results of any such study will be of dubious utility unless it includes the types of feedback processes studied here. Using a 2-D, azimuthally symmetric model (e.g., Farrell 1990) would make the calculation considerably more difficult without improving significantly on such factors as high-latitude heat transport or the spatial distribution of clouds. Even with a more rigorous treatment of climate, we suspect that our basic conclusion of this chapter would remain unchanged: that many planets (i.e., those with dense atmospheres) would still be climatically suitable for life at high

obliquity.

## Chapter 3

# THE EQUATIONS OF PRECESSION

### 3.1 Preface

The equations of precession and their manipulations appear many places within the astrophysics and geophysics literature (e.g., Goldreich 1966; Colombo 1966; Kinoshita 1975, 1977; Ward 1974, 1991; Laskar et al. 1993a, 1993b, and Laskar and Robutel 1993; Williams 1994; Touma and Wisdom 1994), but many (not all) of these works suffer from either brevity and incompleteness or, on the other extreme, from the inclusion of burdensome detail. Of the more useful resources are the books by Roy (1988), Danby (1988), and Stacy (1992). Indeed, much of what is shared below has been obtained from these works, as well as from the papers by Laskar, Ward, and Colombo referenced above.

The equations of precession may be obtained with minimal effort by formulating a Hamiltonian for the rigid body motion of the Earth in the presence of the Sun and the Moon (e.g., Laskar et al. 1993a, Touma and Wisdom 1994b); however, little intuition is gained by doing this. Here, the equations are derived from the basic laws of mechanics; that is, by calculating the changes to Earth's spin-angular momentum that result from torques exerted by the Sun and the Moon on Earth's equatorial bulge. The main goal of this chapter is to take these very simple principles and to derive, with sufficient and comprehensible detail, the equations of precession as written by Ward (1974) and Laskar et al. (1993a, 1993b).

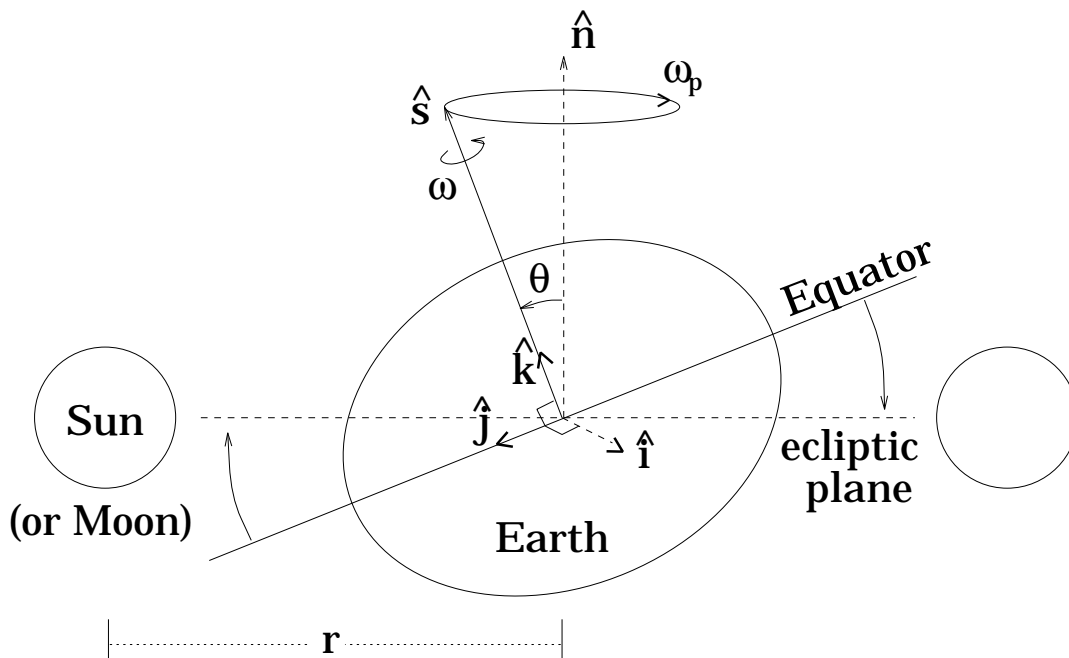


Figure 3.1: The Earth-Sun (or Earth-Moon) configuration of maximum precessional torque. The torque results from Earth's asymmetric gravitational potential (i.e., its equatorial bulge), and is directed perpendicular to the spin axis,  $\hat{s}$ , and into the page. The sign of the torque is the same for both halves of the orbit, which causes the spin axis to precess about the ecliptic normal,  $\hat{n}$ , with a frequency  $\omega_p$ . Maximum torque is applied when the Sun or the Moon is farthest from Earth's equatorial plane. Thus, the solar contribution is zero at an equinox and greatest at a solstice. Adapted from (Stacey 1992).

### 3.2 Torques on Earth's Equatorial Bulge

Fundamentally, Earth precesses because it is made oblate by its rotation. The gravitational potential,  $V$ , of the oblate Earth at a distance  $r$  from its center of mass is given by MacCullagh's formula (Danby 1988),

$$V = -\frac{GM}{r} - \frac{G}{2r^3}(A + B + C - 3I). \quad (3.1)$$

Here,  $G$  is the gravitational constant,  $M$  is Earth's mass, and  $A$ ,  $B$ , and  $C$  are Earth's inertial moments along the three Cartesian coordinate axes,  $x$ ,  $y$ , and  $z$ , respectively.

The  $x$  and  $y$  axes lie in the plane of Earth's equator, and the  $z$  axis is parallel to the spin axis. The center of mass is the coordinate origin. Thus,  $C$  is the principal inertial moment, and  $A$  and  $B$  are the secondary inertial moments. The variable  $I$  is Earth's moment of inertia about a line parallel to  $\vec{r} = x\hat{i} + y\hat{j} + z\hat{k}$ , and extending to the distant position  $r = (x^2 + y^2 + z^2)^{1/2}$ , and may be written

$$I = \frac{Ax^2 + By^2 + Cz^2}{r^2}. \quad (3.2)$$

Inserting Eqn. 3.2 into 3.1 gives

$$V = -\frac{GM}{r} - \frac{G}{2r^3} \left[ A + B + C - \frac{3(Ax^2 + By^2 + Cz^2)}{r^2} \right]. \quad (3.3)$$

Terms of the form  $f(r)$  that are a function of  $r$  only will not contribute a gravitational torque  $\vec{\Gamma}$  since  $\vec{r} \times -\vec{\nabla}f(r) = 0$ . This leaves

$$V = \frac{3G}{2r^5} (Ax^2 + By^2 + Cz^2). \quad (3.4)$$

The potential *energy* is then  $U = mV$ , where  $m$  is the mass located at  $r$ . Thus,  $\vec{r} \times -\vec{\nabla}U$  gives

$$\vec{\Gamma} = -\frac{3Gm}{r^5} [(C - B)yz\hat{i} + (A - C)zx\hat{j} + (B - A)xy\hat{k}]. \quad (3.5)$$

This is the torque exerted by the oblate Earth on mass  $m$ , which is simply the negative of the torque exerted *by* mass  $m$  on the Earth. Reversing the sign in Eqn. 3.5 and assuming symmetry about the spin axis, so that  $A = B$ , yields

$$\vec{\Gamma} = \frac{3Gm(C - A)z(y\hat{i} - x\hat{j})}{r^5}, \quad (3.6)$$

with  $\Gamma_z = 0$ . With the relations

$$\begin{aligned} z &= \vec{r} \cdot \hat{k} = r(\hat{r} \cdot \hat{k}) \\ y\hat{i} - x\hat{j} &= \vec{r} \times \hat{k} = r(\hat{r} \times \hat{k}), \end{aligned} \quad (3.7)$$

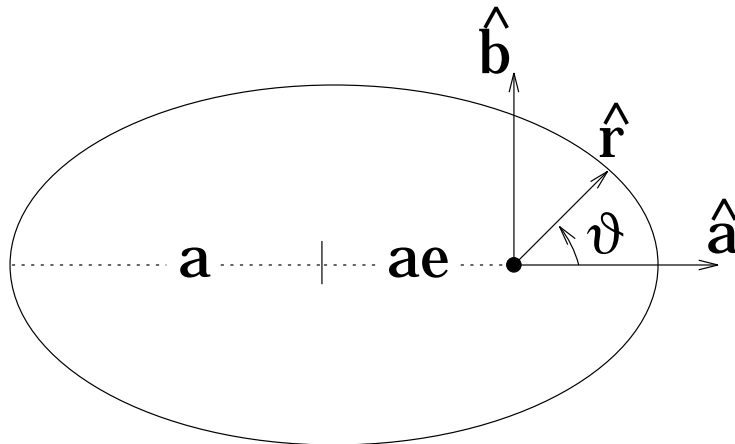


Figure 3.2: Variables used in averaging the precessional torques over an orbit. The solar perturbations are averaged over the orbit of the Earth.

Eqn. 3.6 may be written

$$\vec{\Gamma} = \frac{3Gm(C - A)(\hat{r} \cdot \hat{k})(\hat{r} \times \hat{k})}{r^3}, \quad (3.8)$$

### 3.3 Averaging the Torques Over an Orbit

What follows is a procedure borrowed from Colombo (1966). Equation 3.8 may be alternatively expressed as a change to Earth's angular momentum,  $d\vec{L}/dt$ , resulting in a reorientation of the spin axis. The momentum variation may then be averaged over the orbital period of the perturbing body ( $P = 1$  year for the Sun) by writing

$$\overline{\frac{d\vec{L}}{dt}} = 3Gm(C - A) \frac{\int_0^P \frac{(\hat{r} \cdot \hat{k})(\hat{r} \times \hat{k}) dt}{r^3}}{\int_0^P dt}. \quad (3.9)$$

The integration may be performed over orbital longitude,  $\vartheta$ , by making the substitu-

tion  $dt = d\vartheta/\dot{\vartheta}$ . Thus, Eqn. 3.9 becomes

$$\overline{\frac{d\vec{L}}{dt}} = \frac{3Gm(C-A)}{P} \int_0^{2\pi} \frac{(\hat{r} \cdot \hat{k})(\hat{r} \times \hat{k})d\vartheta}{r^3\dot{\vartheta}}. \quad (3.10)$$

Now, it can be shown using Kepler's second law that

$$r^2\dot{\vartheta} = \frac{2\pi a^2(1-e^2)^{1/2}}{P}, \quad (3.11)$$

where  $a$  and  $e$  are the orbital semi-major axis and eccentricity, respectively. Also, the equation of an ellipse

$$r = \frac{a(1-e^2)}{1+e\cos\vartheta} \quad (3.12)$$

may now be used to substitute  $\vartheta$  for  $r$ . Equation 3.10 then becomes

$$\overline{\frac{d\vec{L}}{dt}} = \frac{3Gm(C-A)}{2\pi a^3(1-e^2)^{3/2}} \int_0^{2\pi} (1+e\cos\vartheta)(\hat{r} \cdot \hat{k})(\hat{r} \times \hat{k})d\vartheta \quad (3.13)$$

The unit vectors  $\hat{a}$  and  $\hat{b}$ , defined in Fig. 3.2, lie in the orbit plane and are perpendicular to each other. A third unit vector  $\hat{n}$  is normal to orbit plane and points away the page. This vector is the normal to the ecliptic plane if the perturbing body is the Sun. Thus,

$$\begin{aligned} \hat{r} &= \hat{a} \cos \vartheta + \hat{b} \sin \vartheta \\ \hat{b} &= \hat{n} \times \hat{a}. \end{aligned} \quad (3.14)$$

The vectors  $\hat{a}$ ,  $\hat{b}$ , and  $\hat{n}$  define the coordinate axes for the orbital plane. Recalling that  $\hat{i}$ ,  $\hat{j}$ , and  $\hat{k}$  are the coordinate axes fixed to the spin axis of the Earth,  $\hat{k}$  may be written in terms of components  $k_a$ ,  $k_b$ , and  $k_n$  defined with respect to the orbit coordinate axes. Hence,

$$\hat{k} = k_a\hat{a} + k_b\hat{b} + k_n\hat{n}, \quad (3.15)$$

and

$$\begin{aligned}\hat{r} \cdot \hat{k} &= k_a \cos \vartheta + k_b \cos \vartheta \\ \hat{r} \times \hat{k} &= k_n (\sin \vartheta \hat{a} - \cos \vartheta \hat{b}) + (\cos \vartheta k_b - \sin \vartheta k_a) \hat{n}.\end{aligned}\quad (3.16)$$

Inserting these relations into Equation 3.13 gives

$$\begin{aligned}\frac{d\vec{L}}{dt} &= \frac{3Gm(C-A)}{2\pi a^3(1-e^2)^{3/2}} \int_0^{2\pi} (1+e \cos \vartheta)(k_a \cos \vartheta + k_b \cos \vartheta) \left[ k_n (\sin \vartheta \hat{a} - \cos \vartheta \hat{b}) \right. \\ &\quad \left. + (\cos \vartheta k_b - \sin \vartheta k_a) \hat{n} \right] d\vartheta,\end{aligned}\quad (3.17)$$

which, after considerable algebraic manipulation, may be easily integrated to obtain

$$\frac{d\vec{L}}{dt} = \frac{3Gm(C-A)k_n(k_b \hat{a} - k_a \hat{b})}{2a^3(1-e^2)^{3/2}}.\quad (3.18)$$

Now, it may be recognized that

$$\begin{aligned}k_n &= \hat{k} \cdot \hat{n} \\ k_b \hat{a} - k_a \hat{b} &= \hat{k} \times \hat{n}.\end{aligned}\quad (3.19)$$

Also, the spin-angular momentum,  $\vec{L}$ , may be written

$$\vec{L} = A\omega_x \hat{i} + B\omega_y \hat{j} + C\omega_z \hat{k},\quad (3.20)$$

where  $\omega$  is the angular velocity of the rotating Earth. It is also true that

$$A\omega_x \hat{i} \approx B\omega_y \hat{j} \ll C\omega_z \hat{k},\quad (3.21)$$

so that

$$\vec{L} \cong C\omega_z \hat{k}.\quad (3.22)$$

Dropping the subscript on  $\omega$ , and writing

$$\frac{d\vec{L}}{dt} = C\omega \frac{d\hat{k}}{dt},\quad (3.23)$$

leads to the expression for the precession rate of Earth's spin axis

$$\frac{d\hat{k}}{dt} = \frac{3Gm(C - A)(\hat{k} \cdot \hat{n})(\hat{k} \times \hat{n})}{2a^3(1 - e^2)^{3/2}C\omega}. \quad (3.24)$$

Now, it helps to recognize that

$$\begin{aligned} \hat{k} \cdot \hat{n} &= \cos \theta \\ \hat{k} \times \hat{n} &= \sin \theta \hat{p} \end{aligned} \quad (3.25)$$

where  $\theta$  is Earth's obliquity (Fig. 3.1) and  $\hat{p}$  is the direction of precession, which is perpendicular to both  $\hat{k}$  and  $\hat{n}$  (i.e., into the page in Fig. 3.1). Also,

$$\left| \frac{d\hat{k}}{dt} \right| \propto \cos \theta \sin \theta, \quad (3.26)$$

so that the precession rate is maximum when  $\theta = 45^\circ$ . The total precession rate is found by summing the influences of the Sun ( $\odot$ ) and the Moon (m). Hence,

$$\frac{d\hat{k}}{dt} = \frac{3G(C - A)(\hat{k} \cdot \hat{n})(\hat{k} \times \hat{n})}{C\omega} \left[ \frac{M_\odot}{a^3(1 - e^2)^{3/2}} + \frac{M_m}{a_m^3(1 - e_m^2)^{3/2}} \right]. \quad (3.27)$$

In addition, the lunar contribution contains a small correction factor  $1 - \frac{3}{2} \sin^2 i_m$  to account for the slight  $5^\circ$ -inclination of the lunar orbit with respect to the ecliptic plane. Writing Kepler's third law  $n^2 = GM_\odot/a$ , where  $n$  is Earth's mean angular velocity about the Sun, Eqn. 3.27 may be expressed (using  $\hat{s}$  now in place of  $\hat{k}$ )

$$\frac{d\hat{s}}{dt} = \alpha(\hat{s} \cdot \hat{n})(\hat{s} \times \hat{n}), \quad (3.28)$$

where

$$\alpha = \frac{3n^2 C - A}{2\omega C} \left[ (1 - e^2)^{-3/2} + \frac{M_m}{M_\odot} \left( \frac{a}{a_m} \right)^3 (1 - e_m^2)^{-3/2} \left( 1 - \frac{3}{2} \sin^2 i_m \right) \right] \quad (3.29)$$

is known as the precession constant. Together, Eqns. 3.28 and 3.29 are the fundamental equations of precession that apply when the plane of Earth's orbit is stationary.

The case in which the ecliptic plane is also moving will be considered in the next section.

### 3.4 The Moving Ecliptic Plane

Earth's orbit is in constant motion as a result of gravitational interactions with the other planets. The orbit is thereby made to precess about the normal to the invariable plane of the Solar System. The invariable plane is an inertial plane of reference and has a normal vector  $\hat{k}$  (see Fig. 3.3). The moving ecliptic plane defines the noninertial plane of reference. The goal of this section is to obtain the equations of precession in the noninertial reference frame. What follows is an expanded form of a similar exposition by Ward (1974).

First, the unit vector  $\hat{s}$  in the inertial reference frame is related to the vector  $\hat{s}^*$  in the noninertial (orbit) frame by the transformation

$$\hat{s}^* = \mathbf{A}\hat{s}, \quad (3.30)$$

where  $\mathbf{A}$  is an Euler transformation matrix relating the invariable plane to the ecliptic plane through an inclination and a rotation. After the plane is inclined by an angle  $I$ , the rotation is about the normal to the ecliptic plane  $\hat{n}$  and by an amount  $\Omega$ , which is the longitude of ascending node (Fig. 3.3). Thus, the transformation may be considered in two parts, with  $I$  and  $\Omega$  as the Euler angles, and using the matrices  $\mathbf{B}$  and  $\mathbf{C}$  written by Goldstein (1980) as

$$\mathbf{B} = \begin{pmatrix} \cos \Omega & \sin \Omega & 0 \\ -\sin \Omega & \cos \Omega & 0 \\ 0 & 0 & 1 \end{pmatrix}, \quad (3.31)$$

and

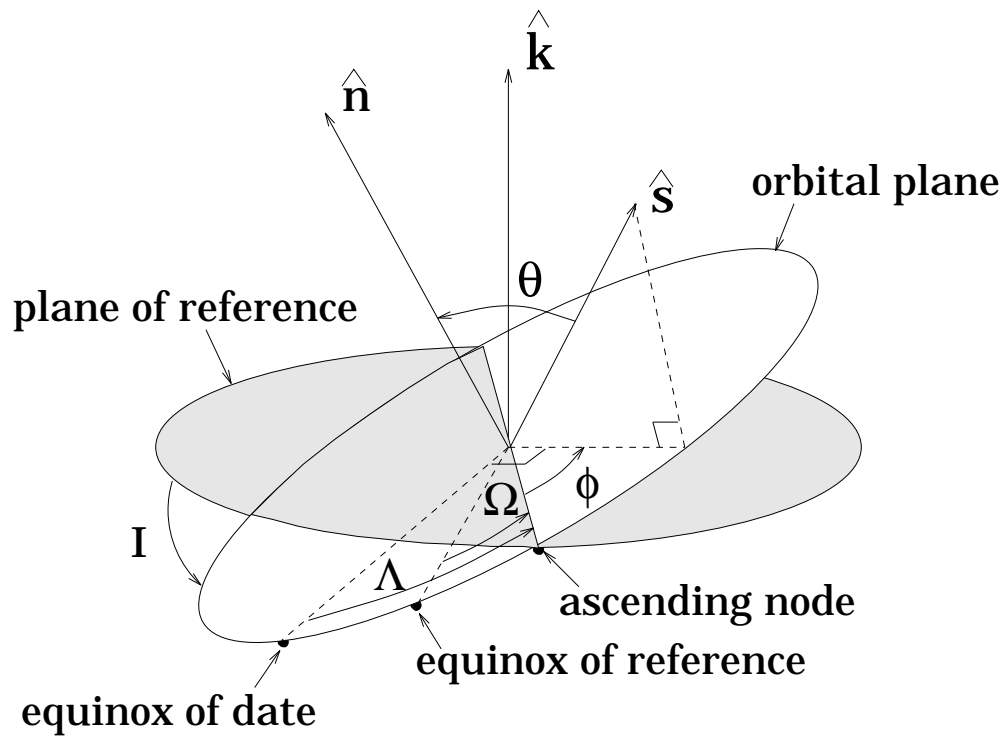


Figure 3.3: Planes and variables of precession. The plane of reference is either the invariable plane of the Solar System (Ward 1974) or the J2000 ecliptic plane (Laskar et al. 1993b).

$$\mathbf{C} = \begin{pmatrix} 1 & 0 & 0 \\ 0 & \cos I & \sin I \\ 0 & -\sin I & \cos I \end{pmatrix}. \quad (3.32)$$

Now,  $\mathbf{A}=\mathbf{BC}$ , or

$$\mathbf{A} = \begin{pmatrix} \cos \Omega & \sin \Omega & 0 \\ -\cos I \sin \Omega & \cos I \cos \Omega & \sin I \\ \sin I \sin \Omega & -\sin I \cos \Omega & \cos I \end{pmatrix}. \quad (3.33)$$

Differentiating Eqn. 3.30 with respect to time gives

$$\frac{d\hat{s}^*}{dt} = \frac{d\mathbf{A}}{dt}\hat{s} + \mathbf{A}\frac{d\hat{s}}{dt}. \quad (3.34)$$

Now, replacing  $\hat{s}$  with  $\mathbf{A}\hat{s}^*$  and using Eqn. 3.28 to substitute for  $d\hat{s}/dt$  allows Eqn. 3.34 to be written

$$\frac{d\hat{s}^*}{dt} = \frac{d\mathbf{A}}{dt}\mathbf{A}^{-1}\hat{s}^* + \alpha(\hat{s}^* \cdot \hat{n}^*)(\hat{s}^* \times \hat{n}^*). \quad (3.35)$$

The inverse transformation matrix  $\mathbf{A}^{-1}$  is equal to the transpose matrix  $\tilde{\mathbf{A}}$  given by

$$\tilde{\mathbf{A}} = \begin{pmatrix} \cos \Omega & -\cos I \sin \Omega & \sin I \sin \Omega \\ \sin I & \cos I \cos \Omega & -\sin I \cos \Omega \\ 0 & \sin I & \cos I \end{pmatrix}. \quad (3.36)$$

Forming the time derivative  $d\mathbf{A}/dt$  (by employing the raised  $\dot{\cdot}$  notation), and multiplying with  $\tilde{\mathbf{A}}$  yields

$$\frac{d\mathbf{A}}{dt}\tilde{\mathbf{A}} = \begin{pmatrix} 0 & \cos I\dot{\Omega} & -\sin I\dot{\Omega} \\ -\cos I\dot{\Omega} & 0 & \dot{I} \\ \sin I\dot{\Omega} & \dot{I} & 0 \end{pmatrix}. \quad (3.37)$$

Now, multiplying by the unit vector  $\hat{s}^* = s_x^*\hat{x}^* + s_y^*\hat{y}^* + s_z^*\hat{z}^*$ , where  $\hat{x}^*$  is along the line of nodes and  $\hat{z}^*$  is parallel to  $\hat{n}$  (see Fig. 3.3), gives

$$\begin{aligned} \frac{d\mathbf{A}}{dt}\tilde{\mathbf{A}}\hat{s}^* &= \begin{pmatrix} 0 & \cos I\dot{\Omega} & -\sin I\dot{\Omega} \\ -\cos I\dot{\Omega} & 0 & \dot{I} \\ \sin I\dot{\Omega} & \dot{I} & 0 \end{pmatrix} \begin{pmatrix} s_x^* \\ s_y^* \\ s_z^* \end{pmatrix} \\ &= \begin{pmatrix} s_y^* \cos I\dot{\Omega} - s_z^* \sin I\dot{\Omega} \\ -s_x^* \cos I\dot{\Omega} + s_z^* \dot{I} \\ s_x^* \sin I\dot{\Omega} + s_y^* \dot{I} \end{pmatrix}. \end{aligned} \quad (3.38)$$

This is the desired substitution for the first term on the right-hand side of Eqn. 3.35.

The second term on the right-hand side of Eqn 3.35 may be rewritten using

$$\alpha(\hat{s}^* \cdot \hat{n}^*)(\hat{s}^* \times \hat{n}^*) = \alpha s_z^*(s_y^*\hat{x}^* - s_x^*\hat{y}^*). \quad (3.39)$$

Equation 3.35 now yields three expressions for the rate of change of the spin vector in the noninertial frame.

$$\begin{aligned}
ds_x^*/dt &= s_y^* \cos I\dot{\Omega} - s_z^* \sin I\dot{\Omega} + \alpha s_z^* s_y^* \\
ds_y^*/dt &= -s_x^* \cos I\dot{\Omega} + s_z^* \dot{I} - \alpha s_z^* s_x^* \\
ds_z^*/dt &= s_x^* \sin I\dot{\Omega} - s_y^* \dot{I}.
\end{aligned} \tag{3.40}$$

Finally, the vector  $\hat{s}^*$  may be expressed in terms of the spherical coordinates  $\phi$  and  $\theta$  shown in Fig. 3.3 using the relations

$$\begin{aligned}
s_x^* &= \cos \phi \sin \theta \\
s_y^* &= \sin \phi \sin \theta \\
s_z^* &= \cos \theta,
\end{aligned} \tag{3.41}$$

where  $\theta$  is the obliquity. Taking the time derivative of Eqns. 3.41 gives

$$\begin{aligned}
ds_x^*/dt &= -\sin \phi \sin \theta \dot{\phi} + \cos \phi \cos \theta \dot{\theta} \\
ds_y^*/dt &= \cos \phi \sin \theta \dot{\phi} + \sin \phi \cos \theta \dot{\theta} \\
ds_z^*/dt &= -\sin \theta \dot{\theta}.
\end{aligned} \tag{3.42}$$

Then, solving for the quantities  $\dot{\phi}$  and  $\dot{\theta}$  yields

$$\dot{\phi} = (\dot{s}_y^* + \dot{s}_z^* \sin \phi \cot \theta) \csc \theta \sec \phi, \tag{3.43}$$

and

$$\dot{\theta} = -\dot{s}_z^* \csc \theta. \tag{3.44}$$

Finally, using Eqns 3.40 and 3.41 to eliminate all components of the spin vector  $\hat{s}^*$ , and converting the raised  $\cdot$  notation back to standard form, we obtain

$$\frac{d\theta}{dt} = -\sin I \cos \phi \frac{d\Omega}{dt} + \sin \phi \frac{dI}{dt}, \tag{3.45}$$

and

$$\frac{d\phi}{dt} = -\alpha \cos \theta - (\cos I - \sin I \cot \theta \sin \phi) \frac{d\Omega}{dt} + \cot \theta \cos \phi \frac{dI}{dt}. \quad (3.46)$$

These equations describe the motion of the spin vector as viewed from a reference frame co-moving with the orbital plane, and are the fundamental equations of luni-solar precession as written by Ward (1974). It is important to note that if the ecliptic were stationary (i.e.,  $\dot{I} = \dot{\Omega} = 0$ ), then the spin axis would precess at a constant rate  $d\phi/dt = -\alpha \cos \theta$  about  $\hat{n}$  with a constant obliquity. [The spin axis would also “nod”, or *nutate*, slightly (by  $< 10''$ ) over the lunar month and over the year from torques directed perpendicular to the precessional torques.]

### 3.5 Converting to the Notation of Laskar

The goal of this section is to obtain the equations of precession as written by Laskar et al. (1993a and 1993b) from Ward’s Eqns. 3.45 and 3.46. This will be accomplished by defining a new parameter

$$p_A = \Lambda - \Omega, \quad (3.47)$$

where  $\Lambda$  is the angle on the ecliptic plane from the equinox of date to the ascending node, and  $\Omega$  is the angle between the equinox of reference and the ascending node (see Fig. 3.3). And, by definition, the angle between the spin axis and the equinox of date is  $90^\circ$ . Thus,

$$\Lambda = 90^\circ - \phi, \quad (3.48)$$

so that

$$\phi = 90^\circ - p_A - \Omega. \quad (3.49)$$

Now, Eqn. 3.49 may be used to substitute for the variable  $\phi$  in Eqns. 3.45 and 3.46.

Hence, these equations become

$$\frac{d\theta}{dt} = -\sin I \cos(90^\circ - p_A - \Omega) \frac{d\Omega}{dt} + \sin(90^\circ - p_A - \Omega) \frac{dI}{dt} \quad (3.50)$$

$$\begin{aligned} -\frac{dp_A}{dt} - \frac{d\Omega}{dt} &= -\alpha \cos \theta - [\cos I - \sin I \cot \theta \sin(90^\circ - p_A - \Omega)] \frac{d\Omega}{dt} + \\ &\quad \cot \theta \cos(90^\circ - p_A - \Omega) \frac{dI}{dt}. \end{aligned} \quad (3.51)$$

Using trigonometric identities, it is easy to show that

$$\begin{aligned} \cos(90^\circ - p_A - \Omega) &= \sin(p_A + \Omega) = \sin p_A \cos \Omega + \cos p_A \sin \Omega, \\ \sin(90^\circ - p_A - \Omega) &= \cos(p_A + \Omega) = \cos p_A \cos \Omega - \sin p_A \sin \Omega. \end{aligned} \quad (3.52)$$

Inserting these relations into Eqns. 3.50, and grouping all the terms containing  $p_A$  yields

$$\begin{aligned} \frac{d\theta}{dt} &= \left( -\sin I \cos \Omega \frac{d\Omega}{dt} - \sin \Omega \frac{dI}{dt} \right) \sin p_A + \\ &\quad \left( -\sin I \sin \Omega \frac{d\Omega}{dt} + \cos \Omega \frac{dI}{dt} \right) \cos p_A \end{aligned} \quad (3.53)$$

$$\begin{aligned} -\frac{dp_A}{dt} - \frac{d\Omega}{dt} &= -\alpha \cos \theta - \cos I \frac{d\Omega}{dt} + \cot \theta \left[ \left( \sin I \cos \Omega \frac{d\Omega}{dt} + \sin \Omega \frac{dI}{dt} \right) \cos p_A + \right. \\ &\quad \left. \left( -\sin I \sin \Omega \frac{d\Omega}{dt} + \cos \Omega \frac{dI}{dt} \right) \sin p_A \right]. \end{aligned} \quad (3.54)$$

The analytic symmetries in Eqns. 3.53 and 3.54 enable them to be simplified by defining new variables:

$$\begin{aligned} \mathcal{A} &= \cos \Omega \frac{dI}{dt} - \sin I \sin \Omega \frac{d\Omega}{dt} \\ \mathcal{B} &= \sin \Omega \frac{dI}{dt} + \sin I \cos \Omega \frac{d\Omega}{dt}. \end{aligned} \quad (3.55)$$

Also,

$$\mathcal{C} = \frac{(1 - \cos I) d\Omega}{2 dt}. \quad (3.56)$$

Equations 3.53 and 3.54 may now be expressed

$$\frac{d\theta}{dt} = -\mathcal{B} \sin p_A + \mathcal{A} \cos p_A \quad (3.57)$$

$$-\frac{dp_A}{dt} - \frac{d\Omega}{dt} = -\alpha \cos \theta + 2\mathcal{C} - \frac{d\Omega}{dt} + \cot \theta (\mathcal{A} \cos p_A + \mathcal{B} \sin p_A) \quad (3.58)$$

Equation 3.58 may be simplified further to read

$$\frac{dp_A}{dt} = \alpha \cos \theta - 2\mathcal{C} + \cot \theta (\mathcal{A} \cos p_A + \mathcal{B} \sin p_A). \quad (3.59)$$

To account for the effects of space-time curvature in the vicinity of the Earth, a small correction  $p_g \approx 0.02''\text{yr}^{-1}$ , known as the *geodetic precession*, is subtracted from Eqn. 3.59 to give

$$\frac{dp_A}{dt} = \alpha \cos \theta - 2\mathcal{C} + \cot \theta (\mathcal{A} \cos p_A + \mathcal{B} \sin p_A) - p_g. \quad (3.60)$$

Together, Eqns. 3.60 and 3.57 are the equations of precession as written by Laskar et al. (1993a, 1993b).

### 3.6 The Laplace-Lagrange Variables $h$ , $k$ , $p$ , and $q$

Secular changes to a planet's orbital elements are traditionally calculated from six perturbative equations (one for each element) first developed by Laplace and Lagrange, and later refined by Brouwer and van Woerkom (1950) and Brouwer and Clemence (1961). Today the equations appear in many introductory textbooks on orbital mechanics, including Roy (1988) and Danby (1988). In these works (and many others), it is pointed out that a useful simplification may be made if the eccentricity  $e$  and the inclination  $i$  are small quantities; the six perturbative equations may be reduced to four by expressing them in terms of the variables (called Laplace-Lagrange variables)

$$\begin{aligned}
\mathbf{h} &= e \sin \varpi \\
\mathbf{k} &= e \cos \varpi \\
\mathbf{p} &= \sin(i/2) \cos \Omega \\
\mathbf{q} &= \sin(i/2) \sin \Omega.
\end{aligned} \tag{3.61}$$

Here,  $i$  is the inclination of the orbit relative the plane of reference,  $\varpi$  is the argument of perihelion, which is related to longitude of perihelion,  $\omega = \Omega + \varpi$ , and the other variables are as explained earlier. There are a couple of important differences between the notation of Laskar and Ward. First, the plane of reference used by Laskar is the J2000 ecliptic plane, whereas Ward uses the invariable plane. Here I have referred to the inclination of the ecliptic plane relative the invariable plane as  $I$ . To convert to the notation of Laskar,  $I$  is simply exchanged with  $i$ , and while  $I$  is different from  $i$ ,  $dI/dt$  does equal  $di/dt$ . Also, the longitude of the ascending node as measured with respect to the J2000 ecliptic plane will not equal the same quantity measured with respect to the invariable plane. However,  $d\Omega/dt$  is the same for both, and since this is the only form in which  $\Omega$  appears in the equations, no adjustments are necessary.

In the works by Laskar, the precession equations are often written in terms of the Laplace-Lagrange variables  $\mathbf{p}$  and  $\mathbf{q}$ , rather than  $i$  and  $\Omega$ , using the variables  $\mathcal{A}$ ,  $\mathcal{B}$ , and  $\mathcal{C}$  that were employed earlier. In terms of  $\mathbf{p}$  and  $\mathbf{q}$ , these variables are (Laskar et al. 1993a, 1993b)

$$\begin{aligned}
\mathcal{A} &= \frac{2}{(1 - \mathbf{p}^2 - \mathbf{q}^2)^{1/2}} (\dot{\mathbf{q}} + \mathbf{p}(\mathbf{q}\dot{\mathbf{p}} - \mathbf{p}\dot{\mathbf{q}})) \\
\mathcal{B} &= \frac{2}{(1 - \mathbf{p}^2 - \mathbf{q}^2)^{1/2}} (\dot{\mathbf{p}} - \mathbf{q}(\mathbf{q}\dot{\mathbf{p}} - \mathbf{p}\dot{\mathbf{q}})) \\
\mathcal{C} &= (\mathbf{q}\dot{\mathbf{p}} - \mathbf{p}\dot{\mathbf{q}})
\end{aligned} \tag{3.62}$$

Equations 3.55 and 3.56 may be expanded using Eqns. 3.61 and their derivative equations

$$\begin{aligned}\dot{\mathbf{p}} &= \frac{\cos(i/2) \sin \Omega}{2} \frac{dI}{dt} + \sin(i/2) \cos \Omega \frac{d\Omega}{dt} \\ \dot{\mathbf{q}} &= \frac{\cos(i/2) \cos \Omega}{2} \frac{dI}{dt} - \sin(i/2) \sin \Omega \frac{d\Omega}{dt}.\end{aligned}\quad (3.63)$$

Thus,

$$\begin{aligned}\mathcal{C} &= (\mathbf{q}\dot{\mathbf{p}} - \mathbf{p}\dot{\mathbf{q}}) \\ &= \frac{\sin(i/2) \cos(i/2) \cos \Omega \sin \Omega}{2} \frac{dI}{dt} + \sin^2(i/2) \cos^2 \Omega \frac{d\Omega}{dt} \\ &\quad - \frac{\sin(i/2) \cos(i/2) \cos \Omega \sin \Omega}{2} \frac{dI}{dt} + \sin^2(i/2) \sin^2 \Omega \frac{d\Omega}{dt} \\ &= \sin^2(i/2) \frac{d\Omega}{dt} \\ &= \frac{(1 - \cos i)}{2} \frac{d\Omega}{dt},\end{aligned}\quad (3.64)$$

$$\begin{aligned}\mathcal{A} &= \frac{2}{(1 - \mathbf{p}^2 - \mathbf{q}^2)^{1/2}} (\dot{\mathbf{q}} + \mathbf{p}(\mathbf{q}\dot{\mathbf{p}} - \mathbf{p}\dot{\mathbf{q}})) \\ &= \frac{2}{\cos(i/2)} \left[ \frac{\cos(i/2) \cos \Omega}{2} \frac{dI}{dt} - \sin(i/2) \sin \Omega \frac{d\Omega}{dt} + \sin^3(i/2) \sin \Omega \frac{d\Omega}{dt} \right] \\ &= \cos \Omega \frac{dI}{dt} - \frac{2 \sin(i/2) \sin \Omega}{\cos(i/2)} \frac{d\Omega}{dt} + \frac{2 \sin^3(i/2) \sin \Omega}{\cos(i/2)} \frac{d\Omega}{dt} \\ &= \cos \Omega \frac{dI}{dt} - \frac{2 \sin(i/2) \sin \Omega}{\cos(i/2)} \frac{d\Omega}{dt} (1 - \sin^2(i/2)) \\ &= \cos \Omega \frac{dI}{dt} - 2 \sin(i/2) \cos(i/2) \sin \Omega \frac{d\Omega}{dt} \\ &= \cos \Omega \frac{dI}{dt} - \sin i \sin \Omega \frac{d\Omega}{dt},\end{aligned}\quad (3.65)$$

$$\begin{aligned}
\mathcal{B} &= \frac{2}{(1 - \mathbf{p}^2 - \mathbf{q}^2)^{1/2}} (\dot{\mathbf{p}} - \mathbf{q}(\mathbf{q}\dot{\mathbf{p}} - \mathbf{p}\dot{\mathbf{q}})) \\
&= \frac{2}{\cos(i/2)} \left[ \frac{\cos(i/2) \sin \Omega}{2} \frac{dI}{dt} + \sin(i/2) \cos \Omega \frac{d\Omega}{dt} - \sin^3(i/2) \cos \Omega \frac{d\Omega}{dt} \right] \\
&= \sin \Omega \frac{dI}{dt} + \frac{2 \sin(i/2) \cos \Omega}{\cos(i/2)} \frac{d\Omega}{dt} - \frac{2 \sin^3(i/2) \cos \Omega}{\cos(i/2)} \frac{d\Omega}{dt} \\
&= \sin \Omega \frac{dI}{dt} + \frac{2 \sin(i/2) \cos \Omega}{\cos(i/2)} \frac{d\Omega}{dt} (1 - \sin^2(i/2)) \\
&= \sin \Omega \frac{dI}{dt} + 2 \sin(i/2) \cos(i/2) \cos \Omega \frac{d\Omega}{dt} \\
&= \sin \Omega \frac{dI}{dt} + \sin i \cos \Omega \frac{d\Omega}{dt}. \tag{3.66}
\end{aligned}$$

Thus, we have arrived at the Eqns. 3.55-3.56 from another direction.

### 3.7 Solving the Precession Equations

For this work, solutions to the equations of precession (Eqns. 3.57 and 3.60) were obtained using an extremely accurate Fortran code borrowed from Jacques Laskar of the Bureau de Longitudes in Paris, France. The integration scheme has been thoroughly described by Laskar in the readily available literature (Laskar et al. 1993b). Here I will summarize the main points concerning the workings of Laskar's code.

Because the motion of Earth's spin axis depends on the secular changes to its orbital plane that arise from the gravitational influences of other planets, the first step in integrating the precession equations is to obtain an accurate solution of the positions of all the planets in the Solar System. Traditionally, the orbital solution (e.g., Bretagnon 1974, Applegate 1986, Sussman and Wisdom 1988, Laskar 1988, 1989) has been obtained first and, then, used as input to code used to integrate the precession equations. [For the integrations performed in Chapters 5 and 6, I

used a self-generated orbital solution obtained using the code of Levison and Duncan (1994).] The motion of Earth's spin axis was obtained in this way by Berger (1976), Berger et al. (1992), and more recently by Laskar and Robutel (1993), and Laskar et al. (1993a, 1993b). Quinn et al. (1991) integrated the equations of motion for the complete Solar System and the spin axis simultaneously over 3 Myr. This solution was successfully compared to the DE 102 ephemeris obtained by Newhall et al. 1983 and employed by the Jet Propulsion Laboratory. The error in ecliptic pole position over 3 Myr, which results mainly from computational roundoff, is estimated to be  $< 0.03$  radians. Laskar et al. (1993b) later showed that his latest orbital solution (La90) and precession solution was a close match to the solution of Quinn et al., with differences of  $< 0.002$  in eccentricity and  $< 0.001$  radians in obliquity. Thus, these two solutions may be viewed as equivalent and standard for testing the accuracy of all subsequent solutions.

The code employed by Laskar to integrate the precession equations uses the orbital solution La90 (a file listing the Laplace-Lagrange variables  $\mathbf{h}$ ,  $\mathbf{k}$ ,  $\mathbf{p}$ , and  $\mathbf{q}$  from -20 Myr to 10 Myr) as input. The form of Eqns. 3.57 and 3.60 requires one to first calculate  $\dot{\mathbf{p}}$  and  $\dot{\mathbf{q}}$  from the input data. Once completed, the actual integration is performed using an Adams multi-step method with a step size of 200 years ( $< 1\%$  Earth's present 26 Kyr precession period) and a Runge Kutta routine of order 8 to create the starting table. With this step size, the integration is rapid; a 10 Myr integration takes  $< 25$  seconds using a Sun Ultra 1 computer.

Apart from roundoff error, the second significant source of error in the precession integration arises from uncertainty in the variables comprising the precession rate parameter  $\alpha$  in Eqn. 3.57. Variables such as the spin rate of Earth ( $\omega$ ) are known with considerable precision and, thus, are not suspect. However, the dynamic ellipticity  $(C - A)/C \approx 0.00327379(3)$  (where the digit in parentheses is the  $1\sigma$ -uncertainty in

the last digit) is less constrained by available data. If the dynamic ellipticity is in error by only 1 part in  $10^8$ , the error in obliquity over 10 Myr is  $\sim 10^{-4}$  radians, which is still far less than the 0.03-radian error attributed to roundoff over 3 Myr. To see how the magnitude of roundoff error is affected by the choice of step size, I compared the results of two integrations performed over 10 Myr using step sizes of 200 and 400 years. The difference in obliquity at the end of the runs was  $\sim 10^{-11}$  radians, which suggests that the 200-year step size was more than appropriate for these calculations.

It should be pointed out that even with the most accurate code available, one should not expect to be able to model accurately the motion of the spin axis for more than  $\sim 10 - 20$  Myr because even the smallest numerical imprecisions in input will result in exponential divergence of solutions on a time scale of  $\sim 5$  Myr (Laskar 1989). Thus, over 5 Myr, the 0.03-radian roundoff error (compounded over 3 Myr) would become 0.05 radians =  $2.9^\circ$ , which is approximately equal to the range in obliquity that Earth's spin axis moves through over a precessional cycle. Therefore, after 5 Myr, one cannot know anything about the position of spin axis except for that it is somewhere within its  $3^\circ$ -range of motion. Beyond 5 Myr, one does not even know this much with absolute confidence. Some of the integrations performed for this thesis were done for periods longer than 100 Myr. Such integrations do not yield exact positions of the spin axis over the period of the integration, but they do constrain the dynamical evolution that is possible.

## Chapter 4

# THE SYMPLECTIC ORBIT INTEGRATOR *SWIFT*

### 4.1 Symplectic Integration

Symplectic integration schemes have the advantage over traditional orbit integration methods (e.g., Burlisch-Stoer multi-step, or high-order Runge-Kutta) of conserving energy and momentum to within machine precision. This is because symplectic integration operates on the N-body Hamiltonian (Wisdom and Holman 1991),

$$H = \sum_{i=0}^{n-1} \frac{p_i^2}{2m_i} - \sum_{i<j} \frac{Gm_i m_j}{r_{ij}}, \quad (4.1)$$

rather than on the Newtonian equations of motion (Quinn et al. 1991),

$$\frac{d^2 \mathbf{r}_i}{dt^2} = \frac{G(M_\odot + m_i)}{r_i^3} \mathbf{r}_i + \sum_{j=1 \neq i}^n \frac{Gm_j}{|\mathbf{r}_i - \mathbf{r}_j|^3} (\mathbf{r}_j - \mathbf{r}_i) - \sum_{j=1 \neq i}^n \frac{Gm_j}{r_j^3} \mathbf{r}_j, \quad (4.2)$$

which do not map the energy of the system with infinite precision (Gladman et al. 1991). Thus, truncation error in the integrals of motion for ordinary differential equation (ODE) integrations accumulates over time, whereas the same error for the symplectic scheme does not. Indeed, the dominant source of error in symplectic integrations is from computational round-off ( $O 10^{-14} - 10^{-16}$ ). The practical advantage, then, is that symplectic integrators can achieve numerical precision comparable to the ODE integrators but with a significantly greater ( $\sim 10\times$ ) time step. Thus, the symplectic schemes are particularly useful for long billion-year integrations such as have been attempted by Wisdom and Holman (1991,1992).

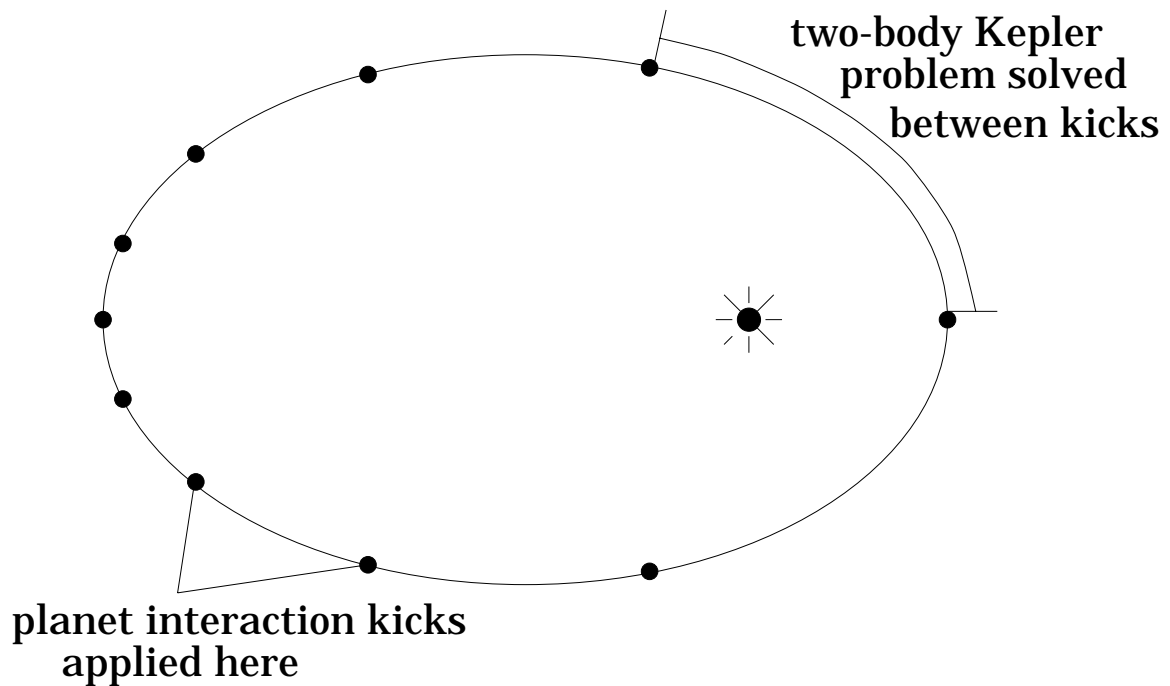


Figure 4.1: The principle of the symplectic orbit integrator *SWIFT*

## 4.2 Phase Error

A weakness of the symplectic scheme is that an integrator can conserve energy and momentum without retaining any information regarding the position, or *phase*, of a planet in its orbit. Thus, phase error tends to accumulate over time so that after many orbits, the investigator knows nothing about the specific whereabouts of a planet in its orbit. This feature of the symplectic algorithm is particularly troublesome for low-order calculations. Gladman et al. (1991) find phase-error growths of  $O 10^{-6}$  per 1000 orbits using a symplectic integrator of order 4 and doing 200 calculations per orbit, which translates into a cumulative phase error of  $2\pi$  radians in only 1 Myr. Higher-order routines have been found to reduce the phase-error growth rate by several orders of magnitude, but the number of steps required per orbit to achieve adequate precision over long time scales is still too large to give symplectic algorithms an

advantage over traditional schemes. Thus, the symplectic algorithm is not especially useful for making long-range projections of planetary position.

### 4.3 *SWIFT*

The symplectic integrator employed for this thesis was coded by Hal Levison and Martin Duncan using the mapping method described by Wisdom and Holman (1991,1992). The code, known as *SWIFT*, has been tested and successfully applied to problems of far-reaching importance ranging from the orbital evolution of comets (Levison and Duncan 1994) to the orbital stability of closely-spaced planets (Chambers et al. 1996). Here, I have applied *SWIFT* to the problem of reducing a possible high obliquity of early Earth with ice sheets (Chapter 5), and to simulate the orbits of hypothetical terrestrial planets in extrasolar planetary systems (Chapter 6). The method of Wisdom and Holman is to allow each planet to orbit for a time about the Sun subject to no external perturbations. This is the *2-body Kepler* problem, which can be solved exactly (see Danby 1988). Planet interaction kicks are then applied every time step (Fig. 4.1) by calculating an interaction Hamiltonian in the barycentric (Jacobi) rest frame. The Jacobi coordinates are specified relative the barycenter of the system interior to the orbit of the planet in question. Thus, the Jacobi coordinate origin of Venus is the barycenter of Mercury and the Sun, and for Mars is the barycenter of the Sun, Mercury, Earth, and Venus. Use of the Jacobi coordinates is necessary to enable the planet interaction to be expressed in terms of a separable, 2-body Hamiltonian, which can be solved exactly.

### 4.4 Numerical Precision and Choice of Time Step

The precision of the mapping method depends critically on the number of interaction kicks applied per orbit. If the points per orbit (PPO) is too small, a numerical truncation error will accumulate rapidly. The goal, then, is to choose a small enough step size so that truncation error is comparable to that introduced by machine imprecision for the desired length of integration. Gladman et al. (1991) show that error in momentum from round-off is  $\sim 10^{-13}$  after  $10^5$  years using a symplectic integrator of order six and 200 PPO. Using *SWIFT* to calculate 100 PPO, I obtain a positional error of  $7 \times 10^{-13}$  over  $2 \times 10^5$  years. (The error was found by integrating the equations of motion forwards and backwards by the same amount and comparing the initial position to the final position.) Reducing the number of PPO to 10 increases the error by approximately one order of magnitude. Thus, if the error in position over  $10^5$  years is  $10^{-12}$  AU, the error over 100 Myr is  $\sim 10^{-9}$  AU, or 100 meters. This level of precision is more than acceptable for the qualitative studies to which *SWIFT* is applied here. Hence, a step size was chosen to ensure that the PPO for the innermost planet was always greater than 10, and typically between 20 and 50. A 10-Myr integration of the entire Solar System with 20 points on Mercury's orbit required  $\sim 6$  hrs CPU time using a Sun Ultra 1 computer.

## Chapter 5

# HIGH OBLIQUITY AS AN EXPLANATION FOR LOW-LATITUDE GLACIAL CLIMATES OF THE EARLY EARTH

### 5.1 Overview

Was Earth's own obliquity ever much different from its present value? Geologic and climatic indicators suggest that the answer to this question may be “yes”, even though Earth's current  $23.5^\circ$ -obliquity is very stable (Laskar et al. 1993a). Paleomagnetic data suggest that Earth was glaciated at low latitudes during the Paleoproterozoic [ $\sim 2.4 - 2.2$  Ga] (Evans et al. 1997, Williams and Schmidt *in press*) and during the Neoproterozoic [ $\sim 820$ -550 Ma] (Frakes 1979, Embleton and Williams 1986, Zhang and Zhang 1985, Schmidt and Williams 1995, Park 1997, Kirschvink 1992), although some of the Neoproterozoic data are disputed (Meert and Van der Voo 1994, Williams et al. 1995). If Earth's magnetic field was aligned more or less with its spin axis, as today, then either the polar ice caps must have extended well down into the tropics – the “snowball Earth” hypothesis (Kirschvink 1992) – or the present zonation of climate with respect to latitude must have been reversed. The simplest explanation for the low-latitude Precambrian glaciations is that the climate was very cold in the past as a consequence of reduced solar luminosity, uncompensated by high levels of greenhouse gases. The expected 6.5% decrease in solar luminosity at 0.8 Ga (Gough 1981) would have caused at least a  $10^\circ$  drop in global surface temperatures, had atmospheric  $\text{CO}_2$

levels remained constant (Kasting 1992), and the  $\sim 17\%$  luminosity decrease at  $\sim 2.3$  Ga would have had an even larger cooling effect.

It is difficult to explain, however, how the ice caps could have extended to low latitudes without causing the extinction of most or all surface life. Energy-balance climate models (Marshall et al. 1988, Caldeira and Kasting 1992, Crowley and Baum 1993) suggest that runaway glaciation should occur if the ice line extends equatorward of  $25\text{-}30^\circ$  latitude. At least some of the ancient glaciations appear to have occurred at latitudes much lower than this (Kirschvink 1992). Had the ice line moved down below the critical latitude for stability, the Earth should have transitioned into a globally-glaciated state in which even the oceans would have frozen down to a depth of  $\sim 1$  km (Bada 1994). If this had occurred during the Neoproterozoic, Earth could eventually have escaped from this state by atmospheric buildup of volcanically-released  $\text{CO}_2$ . However, this process would have required  $\sim 10^4 - 10^5$  years, during which time the ocean would have been deprived of sunlight. No evidence for a corresponding mass extinction of marine life is seen in the geologic record. Runaway glaciation during earlier periods of Earth history has been suggested to have been effectively irreversible (Caldeira and Kasting 1992), although this may not be true if  $\text{CO}_2$  ice clouds are strongly warming (Forget and Pierrehumbert 1997).

An alternative explanation for low-latitude glacial climate during the Precambrian (Williams 1975, 1993) is that Earth's obliquity was  $> 54^\circ$  during its early history, which would have made the equator the coldest part of the planet (Ward 1974). The obliquity of the early Earth is unconstrained by the giant impact thought to have formed the Moon (Hartmann et al. 1986). Williams (1993) has argued that the Moon-forming collision between the Earth and a Mars-sized object could have tilted the terrestrial spin axis by as much as  $70^\circ$ , although the obliquity need not have been this high to glaciare the lower latitudes preferentially.

However, for this theory to be viable, one needs to identify a mechanism that could have caused Earth’s obliquity to decrease by several tens of degrees between  $\sim 600$  Ma – the age of the youngest low-latitude glacial deposits (Frakes 1979, Embleton and Williams 1986, Zhang and Zhang 1985) – and 430 Ma, when paleo-tidal data suggest that the obliquity was close to its present value (Williams 1993). Williams himself suggested that core-mantle dissipation could have caused the obliquity to decrease. However, this appears to be unlikely because the viscosity of the outer core is too low (Rochester 1976, Néron de Surgy and Laskar 1997). Furthermore, even if it could be shown to work, this mechanism should have operated throughout Earth’s history, making it difficult to explain how the obliquity could have remained high as late as 600 Ma.

## 5.2 Climate Friction

To make Williams’ hypothesis work, one needs a mechanism for reducing the obliquity that might have operated preferentially during the Late Proterozoic. We suggest that obliquity-oblateness feedback (Rubincam 1990), sometimes termed “climate friction”, could have done the job. A secular obliquity drift can occur as a result of the time delay between a planet’s oscillating obliquity and cyclic variations in oblateness resulting from changes in continental ice volume and sea level. To understand the analytic origin of the obliquity drift, we will first obtain a simplified solution of the equations of precession (Eqns. 3.45 and 3.46). The variables in the following discussion are taken from Chapter 3. In the limit where the orbital inclination  $I$  is small,  $dI/dt = 0$ , and  $d\Omega/dt = \text{constant}$  [actually a sum of many time-varying sinusoids (Ward 1974)], Eqns. 3.45 and 3.46 may be approximately written

$$\frac{d\theta}{dt} \approx -\sin I \cos \phi \frac{d\Omega}{dt} \quad (5.1)$$

$$\frac{d\phi}{dt} \approx -\alpha \cos \theta - \cos I \frac{d\Omega}{dt}. \quad (5.2)$$

A lesser third term containing  $\sin \phi$  was eliminated from Eqn. 5.2 because it contributed only a small correction. Also,  $\cos \theta$  in Eqn. 5.2 is reasonably approximated by  $\cos \bar{\theta}$ , where  $\bar{\theta}$  is the mean obliquity, since  $\theta$  varies little over an obliquity cycle. As  $d\theta/dt \propto \cos \phi$ , and the right-hand side of Eqn. 5.2 is approximately constant, it is easy to see that, to first order, the obliquity executes a sinusoidal variation of amplitude  $\sin I d\Omega/dt$  and frequency

$$\omega = (-\alpha \cos \bar{\theta} - \cos I d\Omega/dt). \quad (5.3)$$

We are interested in the case when the right-hand side of Eqn. 5.2 is not constant, but variable as a result of an ice age. The growth and decay of continental glaciers, and subsequent isostatic response of Earth's upper mantle changes the oblateness of Earth (hence, the dynamic ellipticity and the precession constant  $\alpha$ ) slightly over an obliquity cycle. Thus,

$$\alpha = \alpha_0 + \Delta\alpha, \quad (5.4)$$

where the subscript zero denotes the value of an ice-free planet in hydrostatic equilibrium. Dividing Eqn. 5.1 by 5.2 yields

$$\frac{d\theta}{d\phi} \approx \frac{\sin I \cos \phi d\Omega/dt}{\alpha \cos \bar{\theta} + \cos I d\Omega/dt}. \quad (5.5)$$

Using Eqns. 5.3 and 5.4, this may be written

$$\frac{d\theta}{d\phi} \approx \frac{-\sin I \cos \phi d\Omega/dt}{\omega[1 - (\Delta\alpha \cos \bar{\theta}/\omega)]}, \quad (5.6)$$

which after first order Taylor expansion becomes

$$\frac{d\theta}{d\phi} \approx \frac{-\sin I \cos \phi d\Omega/dt}{\omega} \left( 1 + \frac{\Delta\alpha \cos \bar{\theta}}{\omega} \right). \quad (5.7)$$

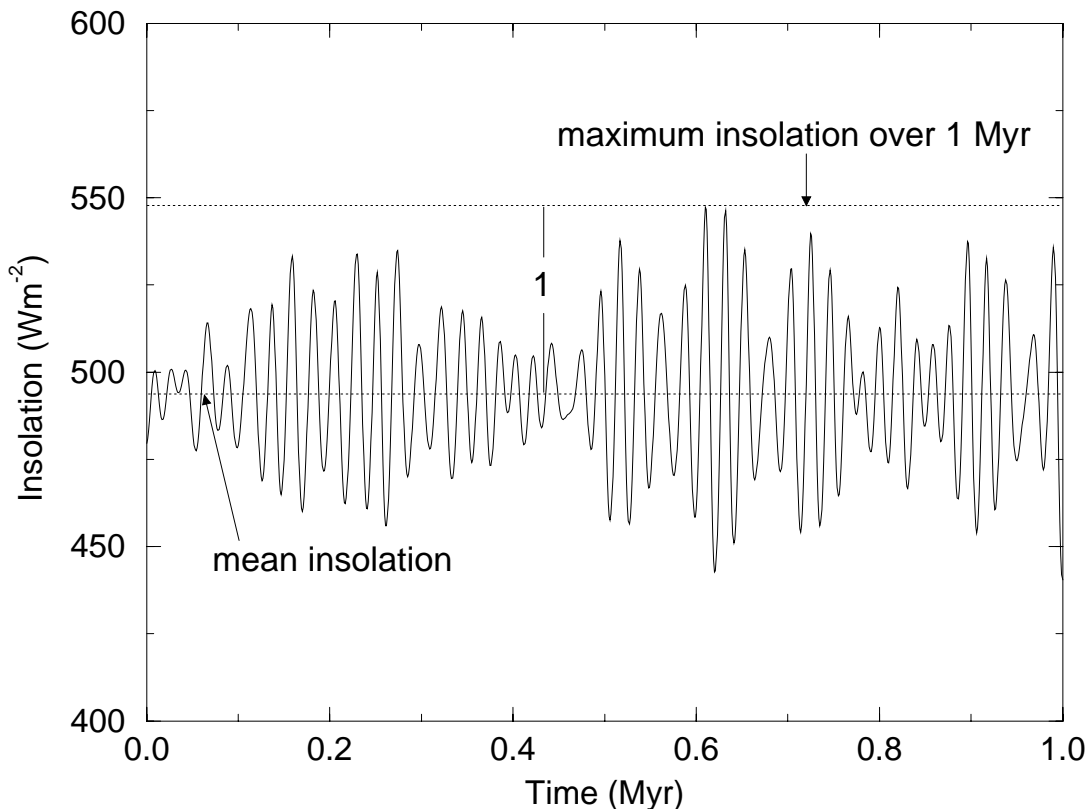


Figure 5.1: Diurnally-averaged, summer-solstice insolation received at  $45^\circ\text{N}$  latitude ( $S_{45}$ ). The solar constant is  $1350 \text{ Wm}^{-2}$ . The mean insolation (marked by the lower-horizontal dotted line) and maximum insolation-cycle amplitude (normalized to 1) are updated every 1 Myr.

The variable  $\Delta\alpha$  depends on obliquity-induced changes to insolation through its effect on glacial mass, ocean depth, and the deformation of the solid Earth. The area of a large, pole-centered glacier is assumed to be limited by the maximum diurnally-averaged insolation received at  $45^\circ$  latitude,  $S_{45}$  (see Fig. 5.1). Milankovitch employed  $S_{65}$  to model glaciers of the Pleistocene, but the glaciers modeled here extend to much lower latitudes. Equation 2.9 may be used to write

$$S_{45} = \frac{q_0}{\pi} (H \sin(45^\circ) \sin \theta + \cos(45^\circ) \cos \theta \sin H), \quad (5.8)$$

where  $q_0$  is the solar constant and

$$\cos H = -\tan(45^\circ) \tan \theta. \quad (5.9)$$

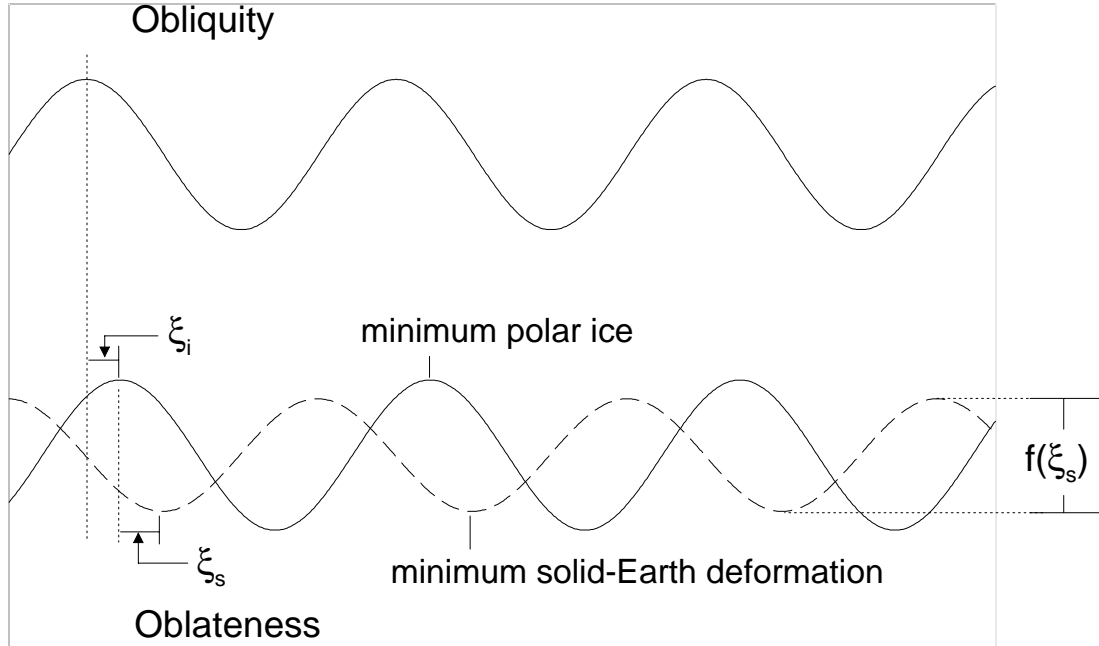


Figure 5.2: Oblateness response to a hypothetical, sinusoidal obliquity cycle. The contribution from ice sheets (indicated by a solid line) is shown to lag the obliquity by an angle  $\xi_i$ . The solid-Earth response (indicated by a dashed line) has a relative amplitude of  $f(\xi_s)$  and lags ice volume by an angle  $\xi_s$ .

Now, following Ito et al. (1995),

$$\Delta\alpha = \frac{3n^2\chi}{2\nu} \frac{(C-A)}{C} \frac{\Delta J_2}{J_2} \left[ f(\xi_s) S_{45}(\phi - \xi_i - \xi_s) - S_{45}(\phi - \xi_i) \right], \quad (5.10)$$

where  $\chi$  is the portion of Eqn. 3.29 in [ ] brackets,  $\Delta J_2/J_2 = (\Delta C - \Delta A)/(C - A)$  is the change to Earth's oblateness resulting from the ice sheets, and lagging the phase of the insolation cycle by  $\xi_i$ ,

$$f(\xi_s) \approx 0.8 - 0.8 \left( \frac{\xi_s}{90^\circ} \right) \quad (5.11)$$

is the normalized amplitude of the oblateness changes resulting from isostatic adjustment of the solid earth, which is assumed to lag the phase of the periodic ice-volume variation (see Fig. 5.2) by

$$\xi_s = (0.033P + 2570\text{years}) \frac{360^\circ}{P} \quad (5.12)$$

(see Ito et al. 1995). Here,  $P = 2\pi/\omega$  is the main period of the obliquity oscillation which may be estimated using Eqn. 5.3. In the actual computation,  $S_{45}$  was normalized (see Fig. 5.1) so that the oblateness variation from ice loading was never greater than the largest possible value of  $\Delta J_2/J_2$  for maximum glacial coverage (as will be estimated in Sec. 5.3). A useful analytic simplification is enabled by the approximation of  $S_{45}(\omega t)$  with  $\sin(\omega t)$ . Inserting Eqn. 5.10 into Eqn. 5.7 gives

$$\frac{d\theta}{d\phi} \approx \frac{-\sin I \cos \phi d\Omega/dt}{\omega} - \frac{3n^2 \chi \sin I d\Omega/dt \cos \bar{\theta}}{2\nu\omega^2} \frac{(C-A)\Delta J_2}{C J_2} \times \left[ f(\xi_s) \left( \cos(\xi_s + \xi_i) \sin \phi \cos \phi + \sin(\xi_s + \xi_i) \cos^2 \phi \right) - \left( \cos(\xi_i) \sin \phi \cos \phi + \sin(\xi_i) \cos^2 \phi \right) \right]. \quad (5.13)$$

Averaging Eqn. 5.13 over a precession cycle eliminates terms containing  $\cos \phi$  and  $\cos \phi \sin \phi$ . This may be recast using  $\phi = \omega t$  to give the secular drift of obliquity over time,

$$\frac{d\theta}{dt} \approx \frac{3n^2 \chi \sin I d\Omega/dt \cos \bar{\theta}}{4\nu\omega} \frac{(C-A)\Delta J_2}{C J_2} \left[ \sin(\xi_i) - f(\xi_s) \sin(\xi_s + \xi_i) \right]. \quad (5.14)$$

### 5.3 Changes to Oblateness During an Ice Age

Rubincam (1993) demonstrated that such “climate friction” could account for a  $10^\circ$  drift in the Martian obliquity over 4.5 Gyr. Bills (1994) later calculated that a much larger drift ( $+60^\circ$  in 100 Myr) was possible for Earth, assuming a glacial-interglacial variation in oblateness of 1% based on oxygen isotope data for the Pleistocene glaciations. This estimate was later revised downward (see Rubincam 1995) after it was pointed out (Peltier and Jiang 1994) that the original calculation had neglected ice-induced compression of the solid Earth. The long response time ( $\sim 10^4$  years) of the viscous upper mantle to changes in ice volume allows the solid-earth variation to can-

cel only a fraction,  $f(\xi_s)\Delta J_2/J_2$ , of the water-ice variation. Subsequent calculations (Peltier and Jiang 1994, Mitrovica and Forte 1995) that included this effect lowered the estimate of the net change in oblateness to  $\sim 0.4\%$ . Constrained by this result, subsequent authors (Ito et al. 1995, Rubincam 1995) have concluded that the change to Earth's obliquity cannot have been more than  $10\text{-}20^\circ$  over Earth's entire ( $\sim 450$  Myr) glacial history.

These calculations, however, assume that all ice ages were of comparable severity to those in the Pleistocene, which is not necessarily true. Different continental configurations, and possibly lower global-average temperatures, could have resulted in larger  $\Delta J_2/J_2$  values for earlier glaciations. If the continents were at one time clustered around one of the poles, as may have occurred during the Late Proterozoic (Hecht and Scotese 1997) the change to oblateness from ice loading and lowering of sea level would have been maximized. The maximum oblateness variation that was possible may be estimated by first expressing the oblateness of Earth

$$J_2 = \frac{C - A}{Ma^2}, \quad (5.15)$$

with  $C$  and  $A$  being Earth's principal and secondary inertial moments, respectively ( $M$  and  $a$  are Earth's mass and mean radius). This enables one to write

$$\frac{\Delta J_2}{J_2} = \frac{\Delta C - \Delta A}{C - A}. \quad (5.16)$$

The problem is to calculate  $\Delta C$  and  $\Delta A$  for the ice-age redistribution of ocean water. This is done by assuming that in an ice age, Earth's continents are covered completely by water ice of uniform thickness, and that the water used to form the continental glaciers is uniformly subtracted from the global ocean. The changes to the inertial moments as a consequence of ice loading may be calculated independently of the changes resulting from the lowering of sea level. Hence,

$$\Delta C = \Delta C_{\text{ice}} + \Delta C_{\text{ocean}}, \quad (5.17)$$

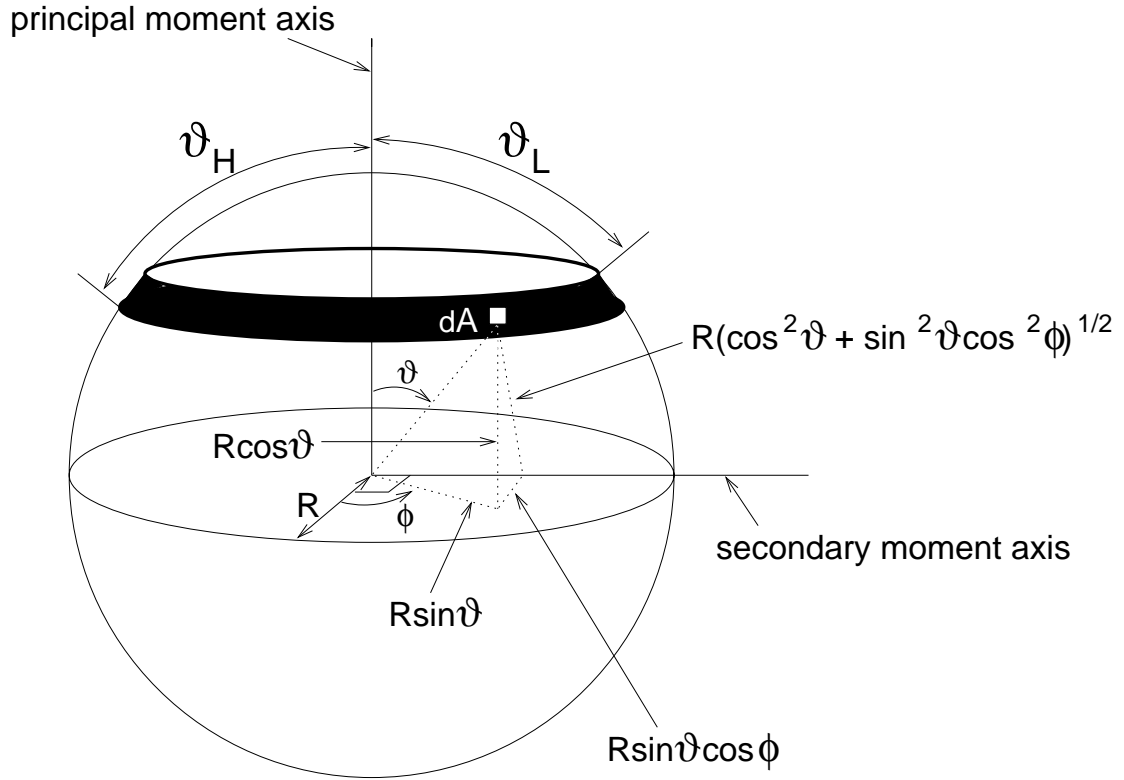


Figure 5.3: Geometry for the calculation of the ice-age change to oblateness.

and

$$\Delta A = \Delta A_{\text{ice}} + \Delta A_{\text{ocean}}. \quad (5.18)$$

The geometry needed to solve these equations is illustrated in Fig. 5.3, where  $\vartheta$  and  $\varphi$  are the polar and azimuthal angles, respectively ( $\vartheta_L$  short for  $\vartheta_{\text{Low}}$  and  $\vartheta_H$  short for  $\vartheta_{\text{High}}$ ), and  $R$  is Earth's radius.

The continental area is indicated in Fig. 5.3 as a darkened band lying between the latitudes  $\vartheta_L$  and  $\vartheta_H$ . The principal moment axis is used to calculate changes to  $C$ , and the secondary moment axis is used to calculate changes to  $A$ . Adding ice to the solid Earth increases both  $C$  and  $A$ ; hence,  $\Delta C_{\text{ice}}$  and  $\Delta A_{\text{ice}}$  are positive quantities. The change to the principle moment may be written

$$\Delta C_{\text{ice}} = \int dM_{\text{ice}} r^2, \quad (5.19)$$

where  $r = R \sin \vartheta$  is the distance between the ice and the principal moment axis and  $dM_{\text{ice}} = \rho_i l_i dA$  is the mass of ice ( $\rho_i$  and  $l_i$  are the density and thickness of the ice sheets) sitting over the infinitesimal area element  $dA = R^2 \sin \vartheta d\vartheta d\varphi$ . The integral then becomes

$$\Delta C_{\text{ice}} = \int_0^{2\pi} d\varphi \int_{\vartheta_L}^{\vartheta_H} \rho_i l_i R^4 \sin^3 \vartheta d\vartheta, \quad (5.20)$$

which may be integrated to obtain

$$\Delta C_{\text{ice}} = 2\pi R^4 \rho_i l_i \left( \frac{\cos(3\vartheta_H) - \cos(3\vartheta_L) + 9 \cos(\vartheta_L) - 9 \cos(\vartheta_H)}{12} \right). \quad (5.21)$$

The calculation of  $\Delta A_{\text{ice}}$  is performed in a similar way, but with  $r$  in Eqn. 5.19 being the distance between the ice sheets and the secondary moment axis, which from Fig. 5.3 is

$$r = R(\cos^2 \vartheta + \sin^2 \vartheta \cos^2 \varphi)^{1/2}. \quad (5.22)$$

Inserting this into Eqn. 5.19 gives

$$\begin{aligned} \Delta A_{\text{ice}} &= \int_0^{2\pi} d\varphi \int_{\vartheta_L}^{\vartheta_H} \rho_i l_i R^4 (\cos^2 \vartheta + \sin^2 \vartheta \cos^2 \varphi) \sin \vartheta d\vartheta, \\ &= \rho_i l_i R^4 \left( 2\pi \int_{\vartheta_L}^{\vartheta_H} \cos^2 \vartheta \sin \vartheta + \int_0^{2\pi} \cos^2 \varphi d\varphi \int_{\vartheta_L}^{\vartheta_H} \sin^3 \vartheta d\vartheta \right), \\ &= \pi \rho_i l_i R^4 \left( 2 \int_{\vartheta_L}^{\vartheta_H} \cos^2 \vartheta \sin \vartheta + \int_{\vartheta_L}^{\vartheta_H} \sin^3 \vartheta d\vartheta \right), \\ &= \pi \rho_i l_i R^4 \left( \frac{2 \cos^3 \vartheta_L - 2 \cos^3 \vartheta_H}{3} + \right. \\ &\quad \left. \frac{\cos(3\vartheta_H) - \cos(3\vartheta_L) + 9 \cos(\vartheta_L) - 9 \cos(\vartheta_H)}{12} \right). \quad (5.23) \end{aligned}$$

Subtracting water from the oceans acts in the opposite sense to adding ice to the continents;  $C$  and  $A$  are both reduced and, so,  $\Delta C_{\text{ocean}}$  and  $\Delta A_{\text{ocean}}$  are both negative. Starting as before, the change to the principal moment is written

$$\Delta C_{\text{ocean}} = - \int dM_{\text{ocean}} r^2, \quad (5.24)$$

where  $dM_{\text{ocean}} = \rho_o l_o dA$ . Here,  $\rho_o$  and  $l_o$  are the density and depth of water removed. Assuming sea level drops uniformly over the entire globe, the depth of the water that is removed may be found by requiring the total mass of water ( $M_{\text{ocean}}$ ) be equal to the total mass of ice formed ( $M_{\text{ice}}$ ). In the equations that follow,  $A$  is the global surface area of ocean and ice.

$$\begin{aligned} M_{\text{ocean}} &= M_{\text{ice}} \\ \rho_o l_o A_o &= \rho_i l_i A_i \\ l_o &= \frac{\rho_i l_i A_i}{\rho_o A_o} \end{aligned} \quad (5.25)$$

Performing the area integration over only the ocean portion of the globe, Eqn. 5.24 becomes

$$\Delta C_{\text{ocean}} = -2\pi\rho_o l_o R^4 \left( \int_0^{\vartheta_L} \sin^3 \vartheta d\vartheta + \int_{\vartheta_H}^{\pi} \sin^3 \vartheta d\vartheta \right), \quad (5.26)$$

which may be integrated as before to yield

$$\Delta C_{\text{ocean}} = -2\pi R^4 \rho_o l_o \left( \frac{\cos(3\vartheta_L) - \cos(3\vartheta_H) + 9 \cos(\vartheta_H) - 9 \cos(\vartheta_L) + 16}{12} \right) \quad (5.27)$$

Now using Eqn. 5.25 to substitute for  $l_o$ , Eqn. 5.24 becomes

$$\Delta C_{\text{ocean}} = \frac{-2\pi R^4 \rho_i l_i A_i}{A_o} \left( \frac{\cos(3\vartheta_L) - \cos(3\vartheta_H) + 9 \cos(\vartheta_H) - 9 \cos(\vartheta_L) + 16}{12} \right) \quad (5.28)$$

Since I have assumed that the continents are completely covered by ice, the ice surface area,  $A_i$ , is equal to the continental surface area, given by

$$\begin{aligned} A_i &= \int_0^{2\pi} d\varphi \int_{\vartheta_L}^{\vartheta_H} R^2 \sin \vartheta d\vartheta \\ &= 2\pi R^2 (\cos \vartheta_L - \cos \vartheta_H) \end{aligned} \quad (5.29)$$

The surface area of the oceans,  $A_o$ , is then simply

$$\begin{aligned}
A_o &= 4\pi R^2 - A_i \\
&= 4\pi R^2 - 2\pi R^2(\cos \vartheta_L - \cos \vartheta_H) \\
&= 2\pi R^2(2 - \cos \vartheta_L + \cos \vartheta_H),
\end{aligned} \tag{5.30}$$

which allows Eqn. 5.28 to be written

$$\Delta C_{\text{ocean}} = -2\pi R^4 \rho_i l_i \left( \frac{\cos \vartheta_L - \cos \vartheta_H}{2 - \cos \vartheta_L + \cos \vartheta_H} \right) \left( \frac{\cos(3\vartheta_L) - \cos(3\vartheta_H) + 9 \cos(\vartheta_H)}{12} \right. \\
\left. \frac{-9 \cos(\vartheta_L) + 16}{12} \right). \tag{5.31}$$

$\Delta A_{\text{ocean}}$  is found in a similar way. Thus,

$$\begin{aligned}
\Delta A_{\text{ocean}} &= - \int dM_{\text{ocean}} r^2, \\
&= - \left( \int_0^{2\pi} d\varphi \int_0^{\vartheta_L} dM_{\text{ocean}} r^2 d\vartheta + \int_0^{2\pi} d\varphi \int_{\vartheta_H}^{\pi} dM_{\text{ocean}} r^2 d\vartheta \right) \\
&= -\rho_o l_o R^4 \left( \int_0^{2\pi} d\varphi \int_0^{\vartheta_L} (\cos^2 \vartheta + \sin^2 \vartheta \cos^2 \varphi) \sin \vartheta d\vartheta + \right. \\
&\quad \left. \int_0^{2\pi} d\varphi \int_{\vartheta_H}^{\pi} (\cos^2 \vartheta + \sin^2 \vartheta \cos^2 \varphi) \sin \vartheta d\vartheta \right) \\
&= -\rho_o l_o R^4 \left( 2\pi \int_0^{\vartheta_L} \cos^2 \vartheta \sin \vartheta d\vartheta + \pi \int_0^{\vartheta_L} \sin^3 \vartheta d\vartheta + \right. \\
&\quad \left. 2\pi \int_{\vartheta_H}^{\pi} \cos^2 \vartheta \sin \vartheta d\vartheta + \pi \int_{\vartheta_H}^{\pi} \sin^3 \vartheta d\vartheta \right) \\
&= -\pi \rho_o l_o R^4 \left( \frac{2 \cos^3 \vartheta_L + 2 \cos^3 \vartheta_H}{3} + \right. \\
&\quad \left. \frac{\cos 3\vartheta_L - \cos 3\vartheta_H + 9 \cos \vartheta_H - 9 \cos \vartheta_L + 16}{12} \right) \tag{5.32}
\end{aligned}$$

and Eqn. 5.25 may be used to substitute  $l_o$  as before.

These equations may now be used to determine the maximum change to Earth's oblateness that is possible as a result of ice loading over a supercontinent. The supercontinent will be assumed to cover exactly 30% of Earth's surface, as is approximately

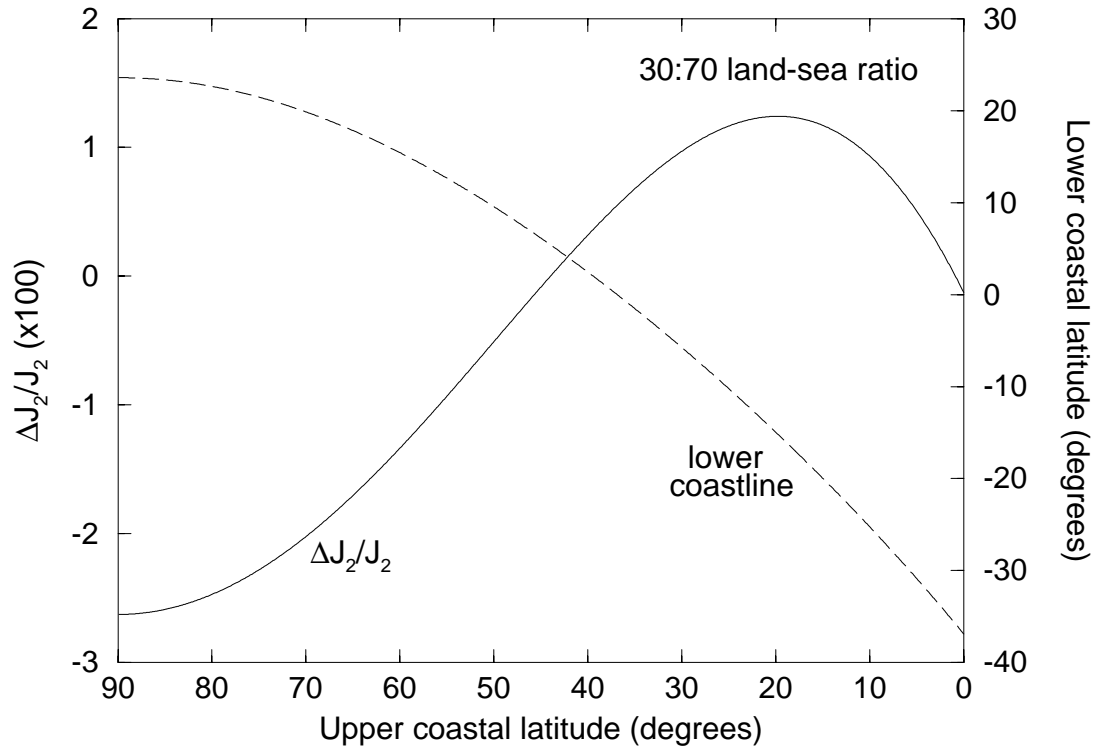


Figure 5.4: Change to Earth's oblateness ( $\Delta J_2/J_2$ ) from continental ice loading and a lowering of sea level. The supercontinent wraps completely around the planet and extends from the upper coastal latitude (x-coordinate) to the lower coastal latitude (rightmost y-coordinate). The continents are uniformly covered by 3.5 km of ice, and total continental surface area is fixed at 30%. The water that forms the glaciers is uniformly subtracted from the steep-walled ocean basins.

true if all of Earth's continents were clustered together today. It will also be assumed that the climate is cold enough for glaciers to cover all of the available continental surface area to a uniform depth of 3.5 km, comparable to the thickness of modern-day ice structures over Greenland and Antarctica. Using Eqns. 5.19, 5.21, 5.29, and 5.30, the change to Earth's oblateness ( $\Delta J_2/J_2$ ) may be calculated from Eqn. 5.14 for a variety of supercontinental positions between the pole and the equator. For this calculation,  $C - A$  was taken to be  $3.4197 \times 10^{42}$  g cm<sup>2</sup>. This value is  $\sim 1.3$  [or  $(24 \text{ hrs}/21 \text{ hrs})^2$ ] times the value for present Earth (Stacey 1992), which is rotating  $\sim 87\%$  as fast as it was during the late Precambrian (Walker and Zahnle 1987). The results are shown in Fig. 5.4. In the instance when the supercontinent is centered

on one pole (and the lower coastal latitude is  $\sim 26^\circ$ ), the change to Earth's oblateness is negative (Earth is made less oblate) and the amplitude of the adjustment is  $\sim 2.6\%$ . By comparison, ice loading over a supercontinent straddling the equator (between  $\pm 17.5^\circ$  latitude) increases Earth's oblateness, but the change to  $\Delta J_2/J_2$  is only  $\sim 1.5\%$ .

The calculations for this chapter were performed for the case when a supercontinent lay over one pole. Thus, the maximum oblateness variation that we assumed was  $\sim 2.6\%$ . Under these assumptions, we calculated that the net oblateness variation (with solid-Earth response included),

$$\frac{\Delta J_2}{J_2} \left[ S_{45}(\xi_i) - f(\xi_s) S_{45}(\xi_s + \xi_i) \right], \quad (5.33)$$

is only  $\sim 0.66\%$  on average, owing to differences in insolation cycle amplitude and, thus, maximum ice volume over time. This is still more than 1.5 times the maximum variation thought possible for the Pleistocene, which could have enabled a correspondingly high rate of secular obliquity drift for the Late Proterozoic.

## 5.4 Drift Dependence on the Ice-Sheet-Formation Phase Lag

The sign and magnitude of the obliquity-oblateness feedback depend on the location and areal extent of the continents, and on the phase lags between the solar forcing and ice volume,  $\xi_i$ , and between ice volume and solid earth depression,  $\xi_s$ . High-latitude ice sheets cause  $J_2$  to decrease because they cancel out part of the Earth's equatorial bulge. For  $25^\circ < \xi_i < 206^\circ$ , the resulting secular change in obliquity is positive (see Fig. 5.5). Low-latitude ice sheets, which might occur at times of high obliquity, produce an obliquity drift in the same direction because both the effect on  $J_2$  and the phasing with respect to the obliquity cycle are reversed. Previ-

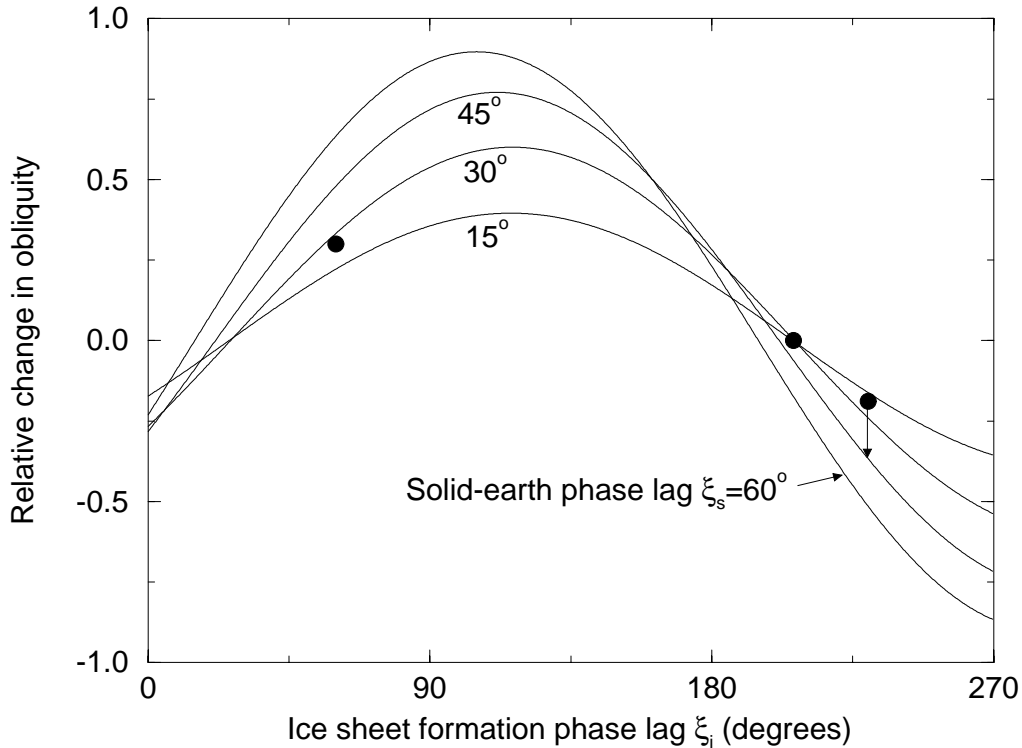


Figure 5.5: Rate and direction of obliquity drift for different values of the phase lag ( $\xi_i$ ) between the obliquity-insolation forcing and the ice sheet variation. The four curves show the effect of varying the phase lag ( $\xi_s$ ) between the glacial extremum and the resulting isostatic response of the solid Earth. Plotted on the vertical axis is the quantity  $[\sin \xi_i - f(\xi_s) \sin(\xi_i + \xi_s)]$  (see Eqn. 5.14). The filled circles mark the ice-sheet-formation phase lags ( $\xi_i$ ) used for the three calculations shown in Fig. 5.7. The solid-Earth phase lag,  $\xi_s$ , was  $28^\circ$  for each run, but with  $\xi_i = 230^\circ$ , the value  $\xi_s$  grows from  $28^\circ$  to  $45^\circ$  (see Ito et al. 1995) over 100 Myr (indicated by an arrow) as a result of an increase to the ice-loading frequency as the obliquity drifts downward.

ous studies of climate friction (Ito et al 1995; Rubincam 1993, 1995; Bills 1994) have assumed that the feedback would be in this direction, based on phase lag estimates for the Pleistocene glaciations. Imbrie et al. (1992) favor  $\xi_i \sim 80^\circ$  (or  $\sim 9$  Kyr) for the 41-Kyr obliquity cycle based on cross-spectral analysis of northern hemisphere, high-latitude, summer (NHHS) insolation and  $\delta^{18}\text{O}$  values in marine carbonates over the past 2 Ma. However, the actual ages of marine sediments are not known with great precision prior to  $\sim 30$  Ka, so such inferences are not very firm. A phase lag of  $< 90^\circ$  is also suggested by analogy with the seasonal cycle, in which the coldest win-

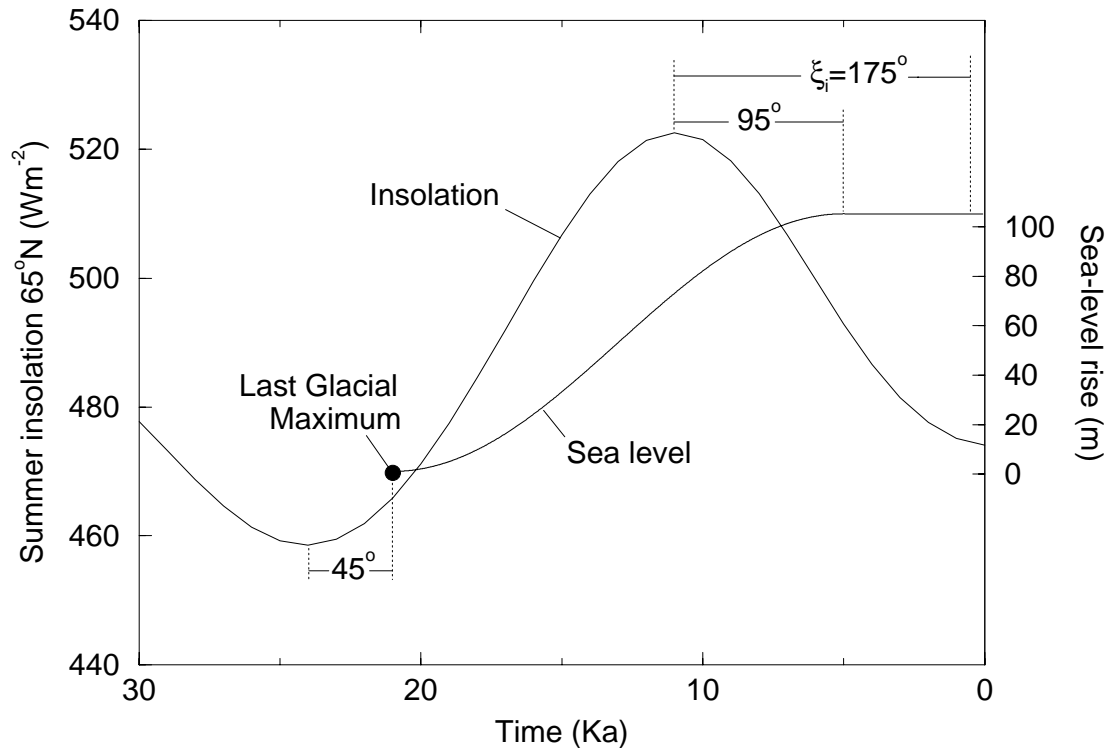


Figure 5.6: Insolation and relative sea level for the period defining the last deglaciation. The curve showing summer insolation at  $65^{\circ}\text{N}$  was obtained using the orbital solution La90 provided by Laskar et al. (1993b) with code to solve the equations of precession and insolation. Last glacial maximum took place at  $\sim 21$  Ka. The sea-level variation between 21 Ka and 5 Ka is a sinusoidal fit to model results of Peltier (1994). The slope in the sea-level variation indicates that the initial meltdown was very rapid, and that subsequent changes to the masses of the remaining (Antarctic and Greenland) ice structures have, since  $\sim 5$  Ka, been negligible. The value of  $\xi_i$  is ambiguous, as it could be defined either as the time between minimum insolation and glacial maximum or that between maximum insolation and glacial minimum (which itself is difficult to identify precisely).

ter temperatures and highest snow accumulation at mid-latitudes occur 1-2 months after winter solstice. Ice volume need not respond in the same manner, though, to the much slower (and weaker) changes in insolation caused by orbital variations. If deglaciation does not begin until NHHLS insolation reaches its peak, then ice volume would be more than  $180^{\circ}$  out of phase with the solar forcing.

Accurate age dates are available for the last deglaciation, which is thought to have been triggered by a precessionally-induced increase in NHHLS insolation. As Fig.

5.6 illustrates, the value of  $\xi_i$  for this one event could lie anywhere between  $45^\circ$  and  $175^\circ$ , depending on how one interprets the shape of the sea level (ice volume) curve. The response of ice volume to NHHLS insolation is not sinusoidal and presumably depends in a complicated manner on both climate and continental positions. With this in mind, it is quite conceivable that climate friction could act to decrease a planet's obliquity, as required to make Williams' hypothesis work.

## 5.5 Results

To determine what changes to Earth's obliquity might have been possible, we integrated the equations of motion for the planets in the Solar System over 100 Myr using a symplectic orbit integrator provided by Levison and Duncan (1994) and described in greater detail in Chapter 4. We used a step size of 0.01 years ( $\approx 21$  points on Mercury's orbit), which yielded positional errors of  $2.3 \times 10^{-9}$  AU ( $\sim 337$  meters) on Mercury's orbit over 100 Myr from numerical round-off. The equations of precession (Eqns. 3.57 and 3.60) were then integrated over 100 Myr using the integrator provided by Jacques Laskar (Laskar et al 1993b), which acted on the the orbital solution obtained earlier. Laskar's code was modified to adjust Earth's oblateness every  $10^3$  years according to Eqn. 5.10. The integrations were performed for several different values of  $\xi_i$ .

We assumed, somewhat arbitrarily, that Earth's obliquity was  $55^\circ$  at 600 Ma – the age of the youngest low-latitude glacial deposits (Frakes 1979, Embleton and Williams 1986, Zhang and Zhang 1985). Williams suggested that the obliquity must originally have been  $> 54^\circ$  because this is the critical latitude above which the poles receive more annually-averaged insolation than does the equator. Ice sheets respond to insolation in a nonlinear manner, though, so Earth's obliquity during the Precambrian need not

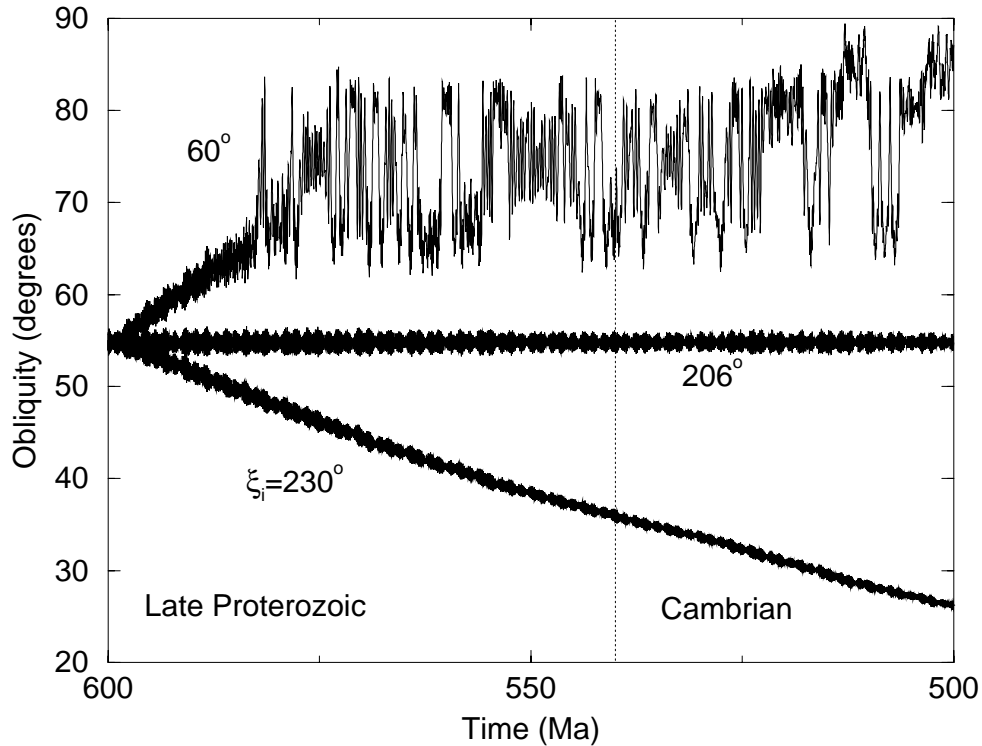


Figure 5.7: Secular drift in obliquity over 100 Myr spanning the Late Proterozoic-Cambrian boundary (indicated by a vertical dotted line) for three different values of the ice-sheet-formation phase lag  $\xi_i$ . For the three calculations,  $\Delta J_2/J_2 = 0.0262$  and the obliquity is started at  $55^\circ$ , which sets the initial period of the obliquity cycle  $P \sim 58.5$  Kyr and the phase lag of solid Earth deformation,  $\xi_s$ . The case of positive drift, with  $\xi_i = 60^\circ$ , shows the spin axis entering a spin-orbit resonance at an obliquity of  $\sim 65^\circ$  in under 20 Myr, where it then is able to vary chaotically upwards to  $90^\circ$ .

actually have been this high. We further assumed that  $\xi_s$  was  $\sim 45^\circ$  initially (see Ito et al. 1995) and that the maximum value of  $\Delta J_2/J_2$  caused by ice loading was 2.6%. Under these assumptions, Fig. 5.7 shows that Earth's obliquity could have been reduced to within  $3^\circ$  of its present value by 500 Ma if  $\xi_i = 230^\circ$ . This result is in good agreement with the geologic data referenced earlier (Williams 1993).

## 5.7 Explaining the Inclination of Lunar Orbit

Support for the hypothesis that Earth's obliquity has decreased comes from analyzing the lunar orbit. At present, the lunar orbit is inclined  $\sim 5^\circ$  to the ecliptic plane. Backwards integrations by Goldreich (1966) and others (Touma and Wisdom 1994a) predict that the lunar orbit was inclined by at least  $10^\circ$  to Earth's equatorial plane when it formed. [The lunar orbit precesses about the ecliptic plane normal now, but it would have precessed around Earth's spin axis when the Earth-Moon distance was  $< 10R_\oplus$ .] This result is in apparent conflict with the widely accepted giant-impact theory of lunar origin, in which the Moon accretes from an impact-generated debris disk aligned with Earth's equator (Ida et al. 1997). Had the Moon formed in Earth's equatorial plane, as predicted, its orbit should now lie in the ecliptic plane (Rubincam 1975). The present lunar inclination implies that either the Moon was never in the equatorial plane (i.e., that the giant-impact model is wrong) or that it was perturbed away from the equatorial plane early in its history. Orbital resonances between the Earth and Moon early in the system's history might be able to accomplish this (Rubincam 1975, Touma and Wisdom submitted), but this explanation depends critically on the details (e.g., terrestrial viscosity) of Earth-Moon tidal evolution, which are not well known. Thus, whether such resonances are responsible for the present lunar inclination is still an open question.

A second possibility is that the inclination of the lunar orbit was altered by a chance collision with a high-mass object. Such an impact must have occurred before 4.45 Ga when the Moon is thought to have already accreted  $> 99\%$  of its present mass (Ryder 1990). Applying momentum conservation and assuming a direct collision perpendicular to Earth's equatorial plane, the mass required to tilt the lunar orbit by an angle  $\Theta$  is  $M_{\text{imp}} \approx M_{\text{m}}(GM_\oplus)^{1/2}a_{\text{m}}^{1/2} \sin \Theta / V_{\text{imp}}a_{\text{imp}}$ , where  $M_{\text{m}}$  and  $M_\oplus$  are the mass of the Moon and Earth, respectively,  $G$  is the gravitational constant,  $V_{\text{imp}}$  is

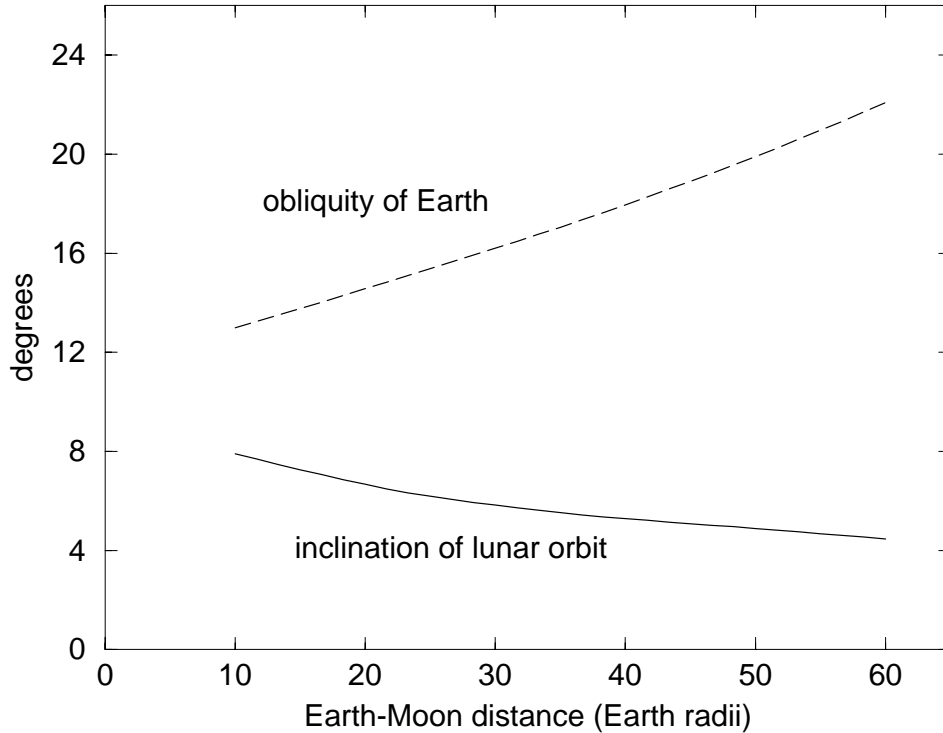


Figure 5.8: Momentum exchange between the Earth and Moon as a consequence of their tidal evolution. Adapted from Williams (1993).

the impactor velocity, and  $a_m = a_{\text{imp}}$  is the Earth-Moon separation when the impact occurred. Thus, if  $a_m = 10 R_\oplus$ ,  $\Theta = 10^\circ$  [as needed to explain the present  $5^\circ$  inclination (Rubincam 1975)], and  $V_{\text{imp}} = 13 \text{ km sec}^{-1}$ , then  $M_{\text{imp}} \sim 3.3\% M_m$  ( $\sim 600$  Imbrium impactors), which corresponds to impactor diameter of  $\sim 1100 \text{ km}$ . It is unlikely that such an impact ever occurred, as an object this size would have either fragmented the Moon or produced a crater of size comparable to the lunar diameter. No impact feature of this size is evident on the lunar surface.

Here, we suggest that the lunar orbit was tilted in gravitational response to the secular downward drift of Earth's obliquity discussed earlier. At present, Earth's mean obliquity is slowly increasing from tidal interactions with the Moon (Goldreich 1966). The lunar inclination is decreasing at the same time so that the angular momentum of the Earth-Moon system is approximately conserved (see Fig. 5.8).

Momentum conservation may be approximately written

$$L_{\oplus} \frac{d\hat{s}_{\oplus}}{dt} + L_{\text{m}} \frac{d\hat{s}_{\text{m}}}{dt} = 0, \quad (5.34)$$

where  $L_{\oplus} = C\omega$  is the spin-angular momentum of Earth,  $L_{\text{m}} = M_{\text{m}}(GM_{\oplus})^{1/2}a_{\text{m}}^{1/2}$  is the orbital angular momentum of the Moon, and the unit vectors  $\hat{s}_{\oplus}$  and  $\hat{s}_{\text{m}}$  are in the direction of Earth's spin axis and the lunar orbit normal, respectively. Here, we have assumed that  $|dL_{\oplus}/dt| \approx |dL_{\text{m}}/dt| \approx 0$ , because the time scale for secular obliquity drift is much shorter than the rate of tidal evolution of the Earth-moon system. This implies that the change to the lunar inclination is opposite the change to obliquity. Eqn. 5.34 may be approximately written

$$\left| \frac{d\hat{s}_{\text{m}}}{dt} \right| = \frac{L_{\oplus}}{L_{\text{m}}} \left| \frac{d\hat{s}_{\oplus}}{dt} \right| \quad \text{or} \quad |\Delta\hat{s}_{\text{m}}| = \frac{L_{\oplus}}{L_{\text{m}}} |\Delta\hat{s}_{\oplus}|, \quad (5.35)$$

where

$$|\Delta\hat{s}_{\text{m}}| = 2 \sin(\Theta_{\text{o}}/2) \quad |\Delta\hat{s}_{\oplus}| = 2 \sin(\Theta_{\text{i}}/2), \quad (5.36)$$

and  $\Theta_{\text{o}}$  and  $\Theta_{\text{i}}$  are the angular change to Earth's obliquity and lunar inclination, respectively. For the Late Proterozoic,  $a_{\text{m}} \sim 57R_{\oplus}$ , and  $\omega \sim 2\pi/(21 \text{ hrs})$  (Walker and Zahnle 1986). If we assume that the maximum change to the lunar inclination that occurred as a result of climate friction is  $\Theta_{\text{i}} = +6^{\circ}$  (allowing for a subsequent  $1^{\circ}$  reduction, to  $5^{\circ}$ , as a result of tidal friction since 500 Ma), then the required change to Earth's obliquity is  $\theta_{\text{o}} = -25.4^{\circ}$ . This implies that Earth's obliquity may have been  $23.5^{\circ} + 25.4^{\circ} \sim 49^{\circ}$  for much of the Precambrian, which is only slightly less than the  $54^{\circ}$  obliquity suggested by Williams. Given the uncertainty in the actual obliquity that would be required to cause low-latitude glaciation, we believe that the information obtained from the lunar orbit provides strong support for the idea that the low-latitude glaciations of the Precambrian were a consequence of high planetary obliquity.

## Chapter 6

# THE SUSCEPTIBILITY OF EARTH-LIKE PLANETS TO LARGE OBLIQUITY VARIATIONS

### 6.1 Motion of Earth's Spin Axis

The development of life on Earth has to some degree been enabled by its relatively stable obliquity and, hence, stable climate over most of its geologic history. Today the obliquity fluctuates by  $\sim 1.5^\circ$  about a  $23.3^\circ$  mean. Even these small changes in obliquity, however, can dramatically alter the amount of ice over the poles through their influence on insolation in these areas. It is interesting to speculate how climate might respond to much larger, and possibly chaotic, obliquity variations that could episodically tip Earth over onto its side. Indeed, it has been shown in Chapter 2 that climate at high obliquity might be biologically limiting on Earth-like planets with thin atmospheres and predominantly polar continents.

Earth's own obliquity variation is nearly sinusoidal with a main period of  $\sim 41$  Kyr (Fig. 6.1a), and arises from the concurrent precessional motions of the spin axis and the orbital plane (Chapter 3). The  $50''yr^{-1}$  spin-axis precession is a consequence of gravitational torques exerted by the Sun and the Moon on Earth's equatorial bulge. Earth's orbit plane also precesses about the normal to the Solar System's invariable plane in gravitational response to the other planets with a dominant frequency of  $-18.9''yr^{-1}$ . (The minus sign indicates that the direction of orbit precession is oppo-

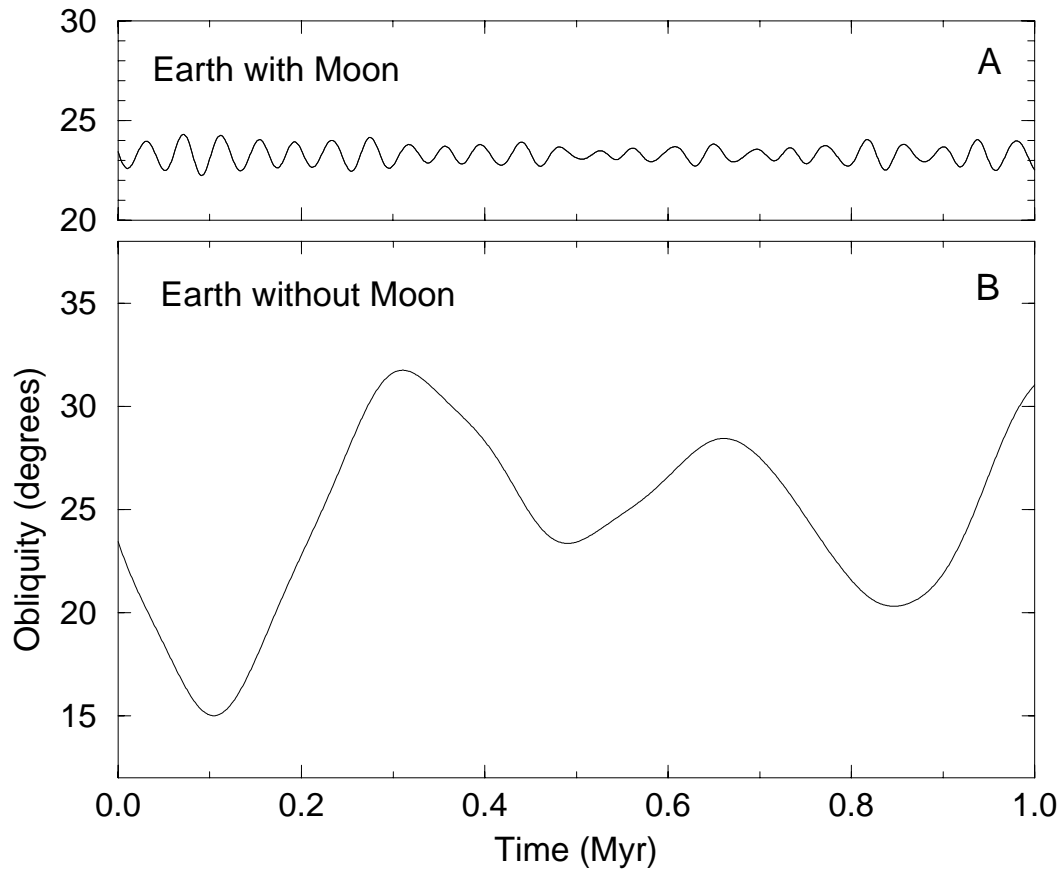


Figure 6.1: The obliquity of Earth over 1 Myr with the Moon (A) and without the Moon (B). The curves were obtained using code borrowed from Laskar.

site the motion of the spin axis). The nodal precession is different from the precession of perihelion, which is a reorientation of the orbit within the orbital plane, and which is also important in cases where orbits are eccentric. The inclination of the orbital plane also varies as a consequence of the same planet-planet interactions. The first-order obliquity response is, from Eqn. 5.3, simply the sum of the two precession velocities:  $50''yr^{-1} - 18.9''yr^{-1} = 31.1''yr^{-1}$ , which yields a period for the main variation of 41 Kyr. The amplitude of the variation is  $\sim \sin(I)d\Omega/dt$ , where  $I$  ( $1.58^\circ$ ) is the inclination of Earth's orbit relative to the invariable plane (Ward 1992). This yields an obliquity range of  $2.97^\circ$ .

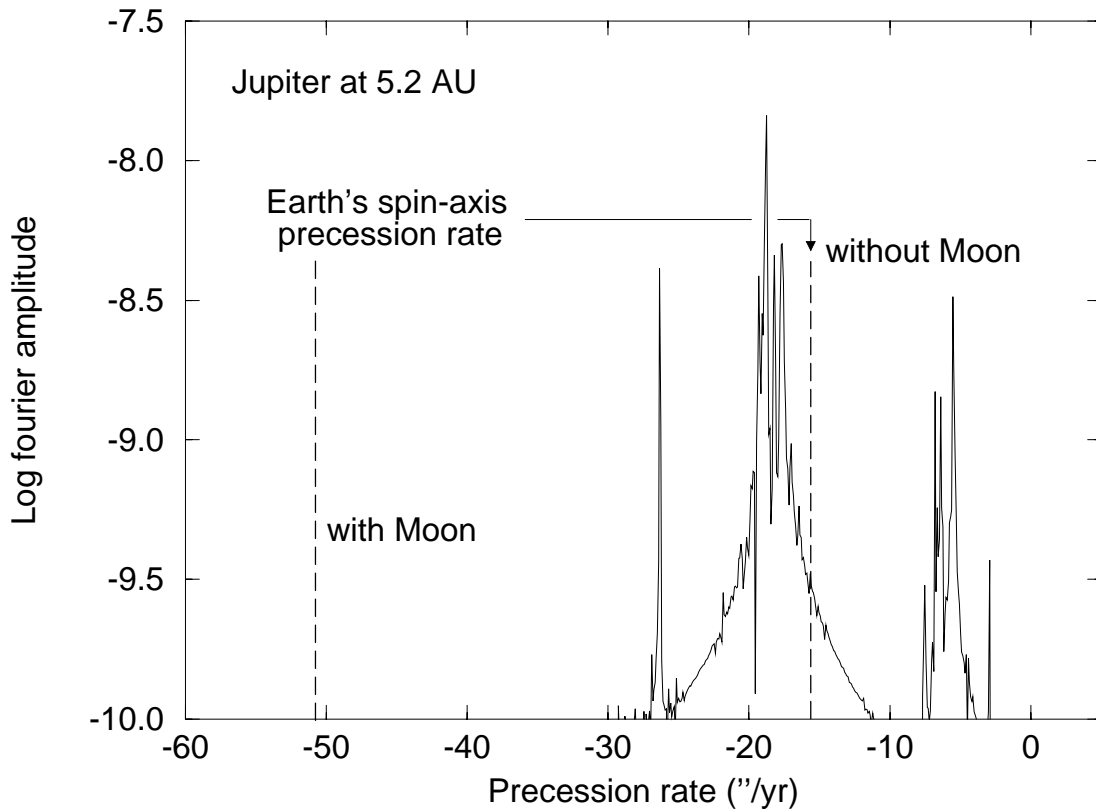


Figure 6.2: The leading orbit-precession frequencies for Earth in the present Solar System, with Jupiter at 5.2 AU. The rates of spin precession with and without the Moon are indicated by vertical dotted lines.

To better understand the source of the obliquity cycle, the orbits of the planets in the Solar System were followed for 17 Myr using a mixed-variable, symplectic orbital integrator (Levison and Duncan 1994), which has been described in Chapter 4. The orbital solution was then Fourier-analyzed to yield a power spectrum of the main frequencies of orbit precession (Fig. 6.2). The calculated spectrum in Fig. 6.2 is shown to be a close match to the finely-resolved spectrum of Laskar (Laskar et al. 1993b) given in Fig. 6.3. The obliquity integrator of Laskar (see Chapter 3) was then used to obtain the motion of Earth's spin axis over 1 Myr (Fig. 6.1a). Earth's present obliquity oscillation is small because the rates of spin- and orbit-precession are very different. However, if these two precessional motions ever happened to be resonance, Earth's obliquity would vary considerably, and possibly in chaotic fashion.

Figure 6.3: Fourier spectrum of Earth's orbit precession frequencies as calculated using the very accurate frequency-analysis method of Laskar. Borrowed from Laskar et al. (1993b).

## 6.2 Influence of the Moon on Precession

Clearly the condition for a stable obliquity will not be realized everywhere in nature. Other Earth-sized planets, for example, are unlikely to possess as large a satellite as the Moon and, therefore, may tend to precess more slowly than does Earth. A moon-less Earth would precess at a rate of  $\sim 16''yr^{-1}$  (assuming a present-day spin rate), which is comparable to the leading frequencies of orbital precession. The resulting obliquity variation (Fig. 6.1b) is considerably amplified and chaotic (non-periodic). Laskar and colleagues (Laskar et al. 1993a, Néron de Surgy and Laskar 1997) have demonstrated that Earth's obliquity might ultimately reach  $85^\circ$  under such circumstances.

Figure 6.4: Zone of chaotic behavior for the motion of Earth's spin axis (dark region). The precession constant is  $\alpha$  and the precession rate is  $\alpha \cos \theta$ , where  $\theta$  is the obliquity of the spin axis. Earth presently sits in a region of spin-axis stability (point marked  $\oplus$ ), but if Earth was situated within the dark region, its obliquity could wander horizontally between the limits of the chaotic zone. Borrowed and adapted from Laskar and Robutel (1993).

A similar fate would be rendered planets *with* moons if those moons were smaller than Earth's Moon or were farther away, as the spin-precession rate is  $\propto M_m/a_m^3$  (see Eqn. 3.29). According to Fig. 6.4, Earth would encounter the leading orbital precession frequencies if its precession constant  $\alpha$  were smaller than  $\sim 30''\text{yr}^{-1}$  – the limit for spin-axis stability. Ward (1982) demonstrated that this hypothetical destabilizing event will be realized in 1-2 Gyr when the Moon has receded from its present distance of  $60R_\oplus$  to  $\sim 66R_\oplus$  and Earth's obliquity has grown to  $30^\circ$  as a result of tidal evolution. It is interesting to note that the obliquity would vary chaotically *today* if the Moon were slightly less than half its present size, or  $0.47M_m$  (see Fig. 6.5); this serves to illuminate the fragility of our present situation.

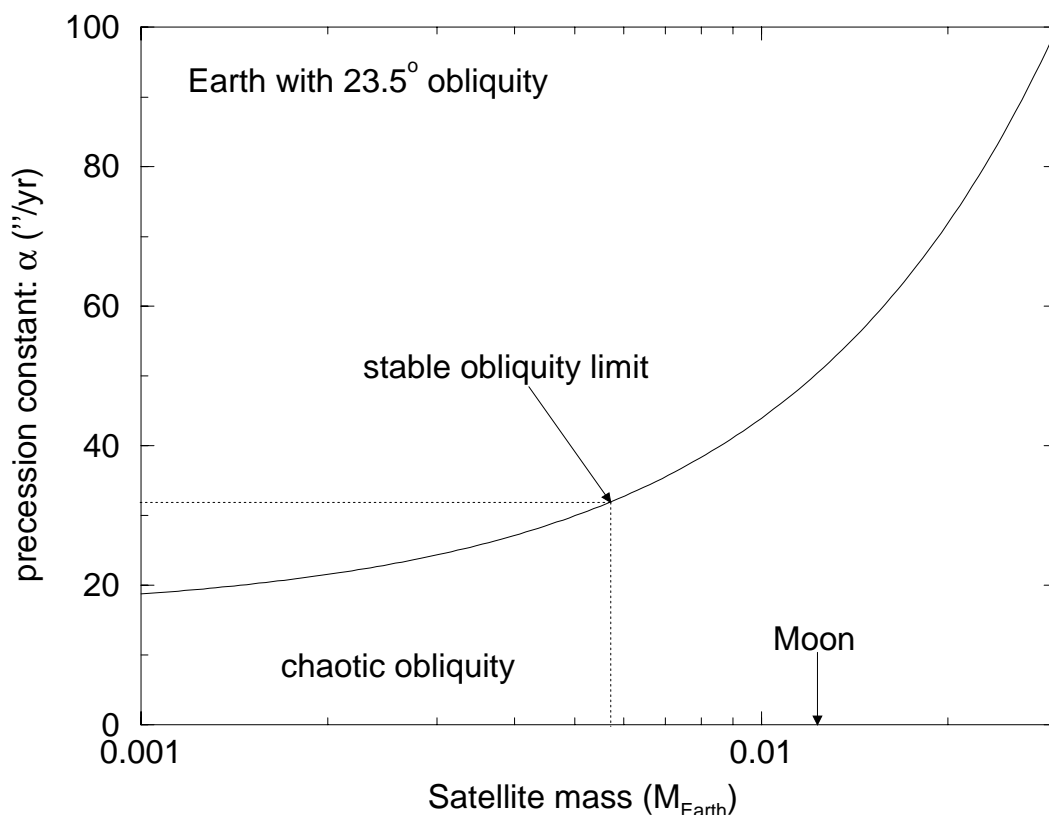


Figure 6.5: Dependence of the precession constant  $\alpha$  on satellite mass. The satellite orbital distance is  $60 R_{\oplus}$  and Earth's spin period is 24 hours. The dotted horizontal line marks the edge of the region of chaos shown in Fig. 6.4 for an obliquity of  $23.5^\circ$ . If the Moon were less than  $\sim 0.47$  its present mass, Earth's obliquity could vary chaotically between  $20^\circ$  and  $90^\circ$  in times less than 100 Myr.

### 6.3 Planet Spacing and Orbit Precession

Whether planets with moons have stable obliquities or not will depend on the precessional motion of their orbits and, hence, on the sizes and distances of neighboring planets. All of the newly discovered extrasolar planets are Jupiter-sized objects orbiting near or within what is the terrestrial-planet region of the Solar System. Any terrestrial planets in these systems will tend to have their orbits precess much more rapidly than Earth's because of strong planet-planet interactions.

To determine the rates of orbit precession that are possible in other planetary systems, I repeated the orbital integration of the complete Solar System, but with Jupiter at a variety of distances Sun-ward of 5.2 AU. By incrementally decreasing Jupiter's orbital radius and then integrating Earth's obliquity over 1 Myr, the orbital position of resonance, where the change to Earth's obliquity is the greatest, was found to be  $\sim 3.1$  AU (Fig. 6.6a). The exercise was then repeated for the case when Earth does not have a moon. In this instance, the condition of maximum spin-orbit resonance occurs with Jupiter at  $\sim 4.1$  AU (Fig. 6.6b) because Earth's rate of spin precession is smaller. It is interesting to note that without the Moon, the range of obliquity over 1 Myr with Jupiter at 2.0 AU is comparable to the range of obliquity that occurs with the Moon present and with Jupiter at 5.2 AU. So, Earth's spin axis without the Moon could be just as stable as it is today if the planets in the Solar System were more tightly spaced. What is not known is whether the orbit of Earth and Mars would be stable for billions of years with Jupiter sitting at 2.0 AU from the Sun.

As was done earlier, the orbital solutions of Earth with Jupiter at 4.1 AU and 3.1 AU were Fourier-analyzed to find the leading orbit precession frequencies. The increase in the rates of precession results in a shifting of the power spectrum in Fig. 6.2 to the left, although it is difficult to follow the changes to specific frequencies corresponding to nodal precession of each of the planets (i.e., the peaks labeled with  $s_n$  in Fig. 6.2) without a more rigorous analysis. The amplitude of the obliquity variation also increases as spin precession and orbit precession approach resonance. The Fourier spectrum of Earth's orbit precession frequencies with Jupiter at 4.1 AU is shown in Fig. 6.7, and the corresponding obliquity variations over 1 Myr are given in Fig. 6.8. For comparison, the frequency spectrum and obliquity variations with

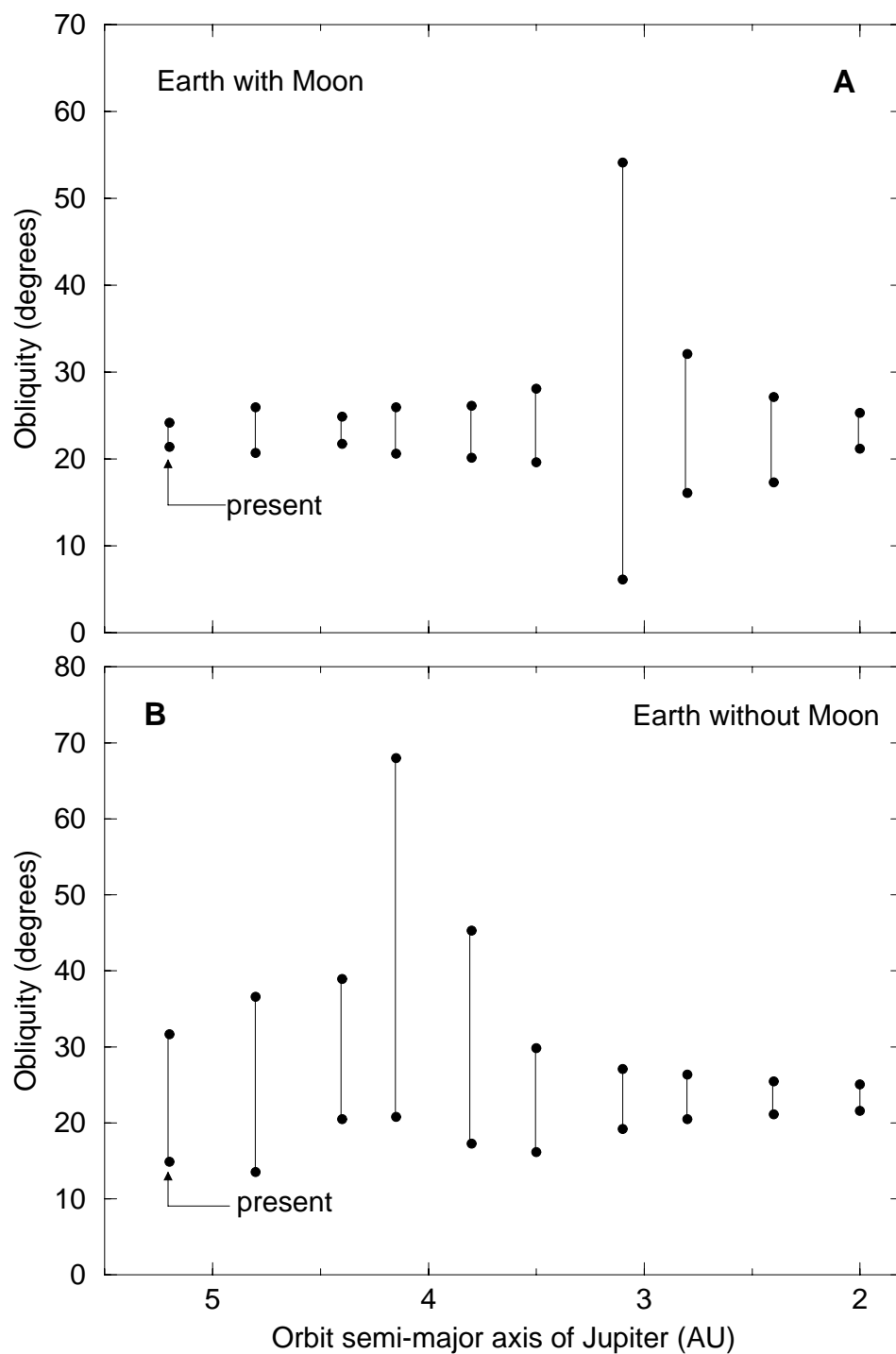


Figure 6.6: Variation in Earth's obliquity over 1 Myr as a function of Jupiter's orbital position. Vertical lines span the range in obliquity for the cases of Earth (A) with the Moon and (B) without the Moon. The longest lines mark the orbital positions of spin-orbit resonance.

Jupiter at 3.1 AU are given in Figs. 6.9 and 6.10, respectively. In the latter case, the spin precession of a moon-less Earth is now much smaller than the leading frequencies of orbit precession, and the obliquity of Earth is shown to be more stable than when the Moon is present. It is also interesting to note the presence of a prominent peak in the 3.1 AU-Fourier spectrum at a frequency of  $\sim 7''\text{yr}^{-1}$ . This peak is close to frequencies of nodal precessions of Mercury and Venus (labeled  $s_1$  and  $s_2$  in Fig. 6.2) in the present Solar System. Whether the common peak in the two spectra have the same dynamical origin (that is, from the motions of Mercury and Venus) is unclear.

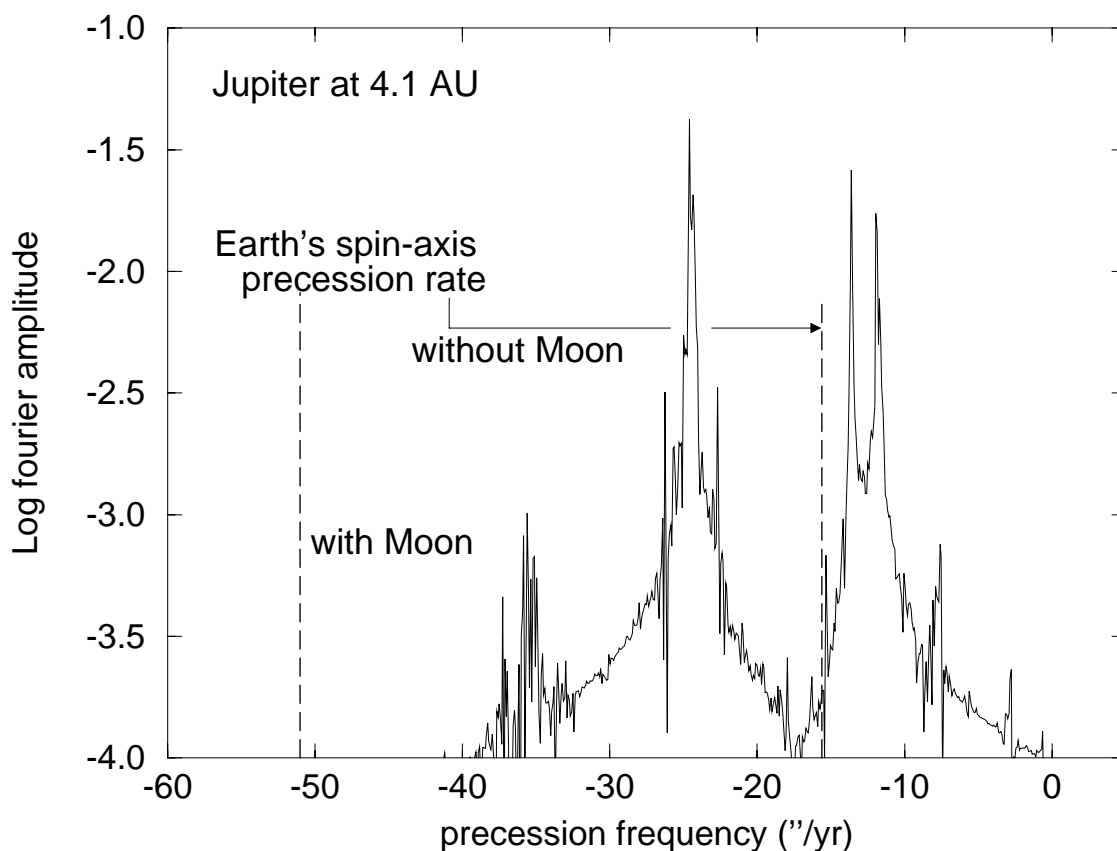


Figure 6.7: Fourier spectrum of Earth's orbital precession frequencies with Jupiter at 4.1 AU. The spin precession rates of Earth with and without the Moon are indicated with vertical dashed lines.

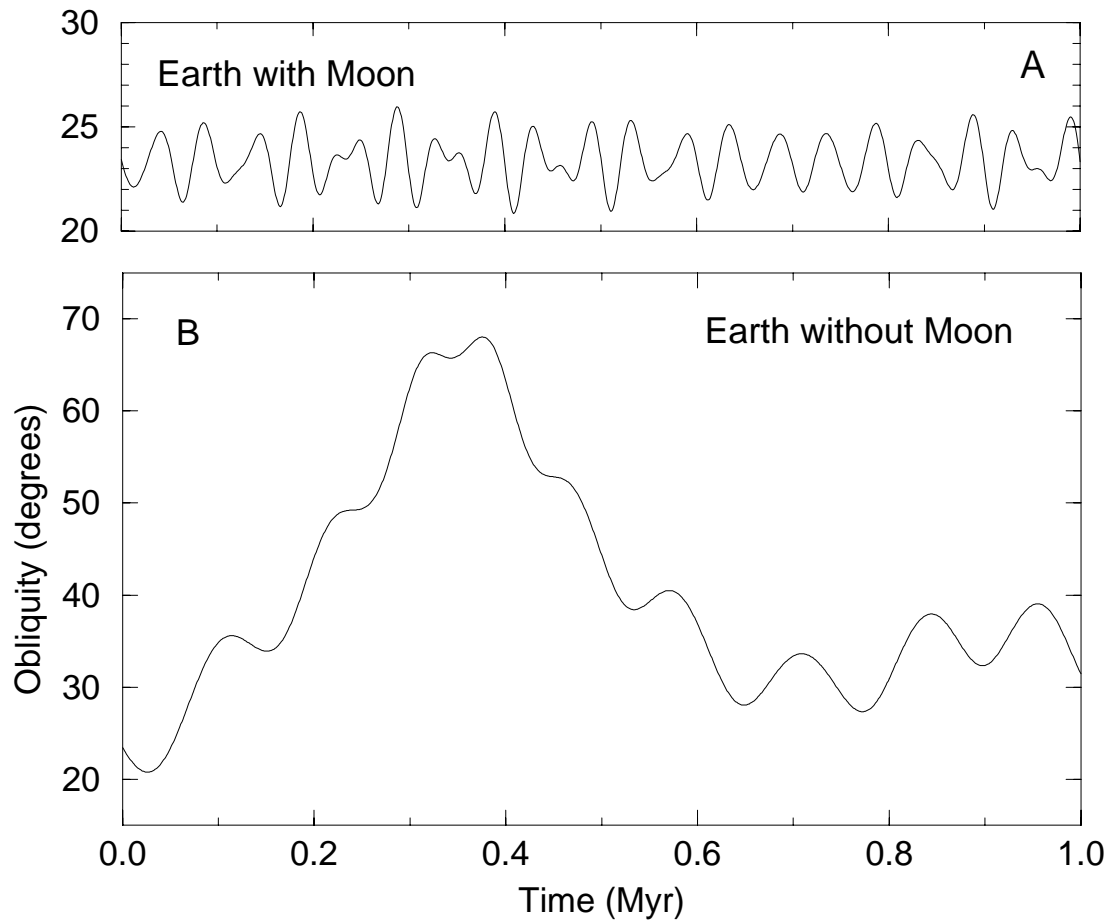


Figure 6.8: Earth's obliquity over 1 Myr with Jupiter at 4.1 AU.

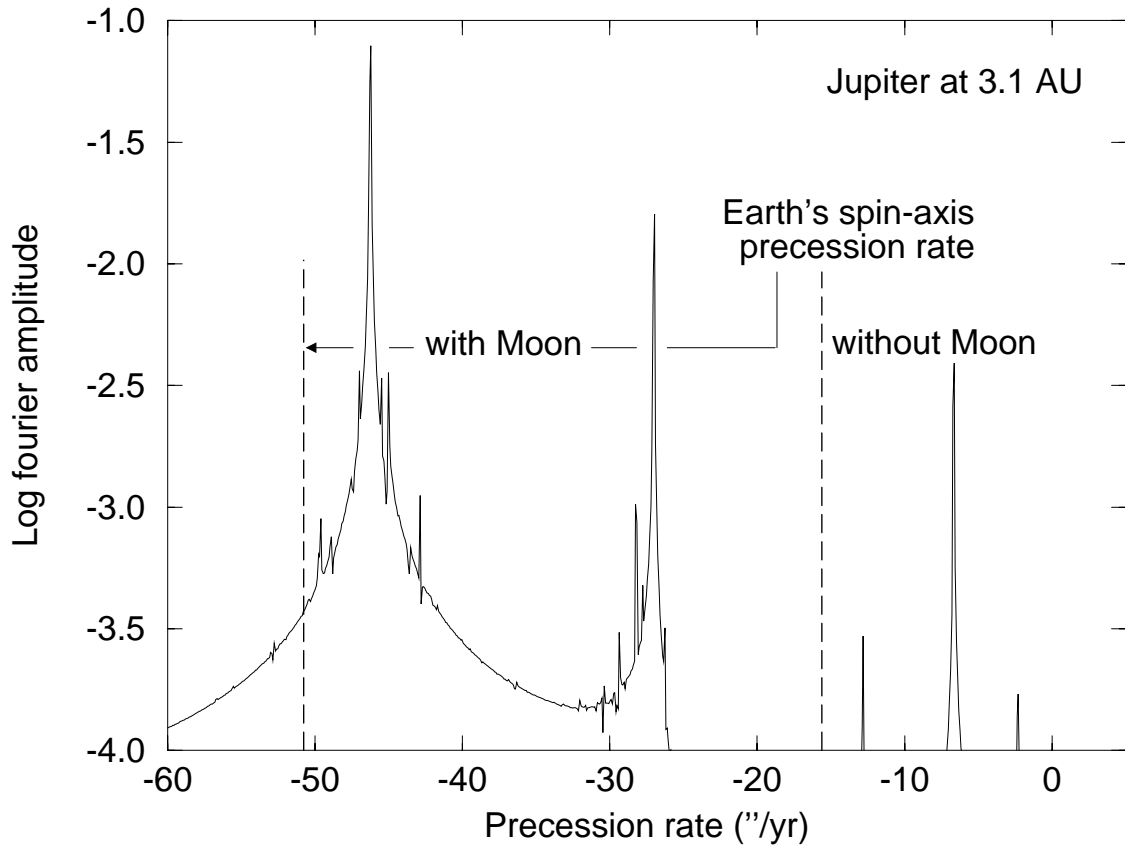


Figure 6.9: Fourier spectrum of Earth's orbital precession frequencies with Jupiter at 3.1 AU. The spin precession rates of Earth with and without the Moon are indicated with vertical dashed lines.

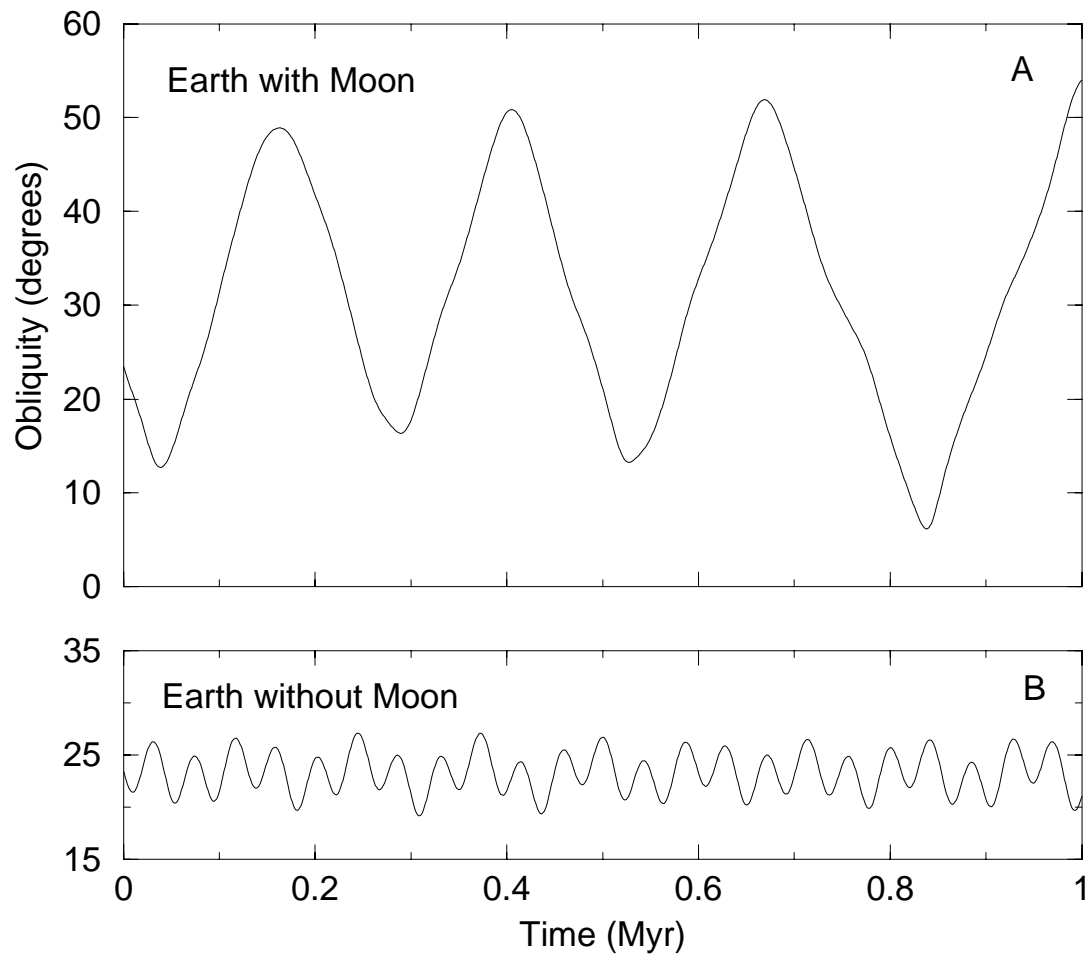


Figure 6.10: Earth's obliquity over 1 Myr with Jupiter at 3.1 AU.

## 6.4 Earth's Position Within the Habitable Zone

The orbital and obliquity integration experiments of the last section were repeated with all the planets in their present positions, but with Earth at a variety of locations within the habitable zone. As discussed in Sec. 1.2 and later in Chapter 2, conservative estimates (KWR) place the HZ inner and outer edges at  $\sim 0.9$  and  $\sim 1.3 - 1.4$  AU, respectively. Optimistically, Earth might be sufficiently warmed by a dense  $\text{CO}_2$  atmosphere beyond 1.4 AU, but the proximity of Mars would make a close-encounter or collision a likely result of such calculations. Between 0.9 AU and 1.4 AU, Earth's obliquity with the Moon present is shown to be remarkably stable (Fig. 6.11a). The largest range in obliquity over 1 Myr is  $\sim 7^\circ$  with Earth at 0.9 AU, which is more than double the size of the present variation. For comparison, the same calculations were performed without the Moon, and the results are shown in Fig. 6.11b. The results reveal a wide region of spin-axis instability extending from 1.0 AU to 1.4 AU, with possible excursions in obliquity of  $45^\circ$  in only 1 Myr. The variation at 0.9 AU is, by contrast, only  $\sim 7^\circ$ , which indicates that obliquity is extremely sensitive to orbital position.

## 6.5 Extrasolar Earths

Whether habitable, terrestrial-sized planets exist around other stars is not known. If such planets are present within the habitable zones of the newly discovered extrasolar planetary systems (e.g., 47 Ursae Majoris, henceforth 47 UMa [Butler and Marcy 1996]), their orbits will be strongly perturbed by the Jovian-sized planets orbiting nearby. The orbital simulation experiments described in Sec. 6.3 showed that the amplitude of Earth's orbital precession rate would grow to over  $\sim 50''\text{yr}^{-1}$  if Jupiter were

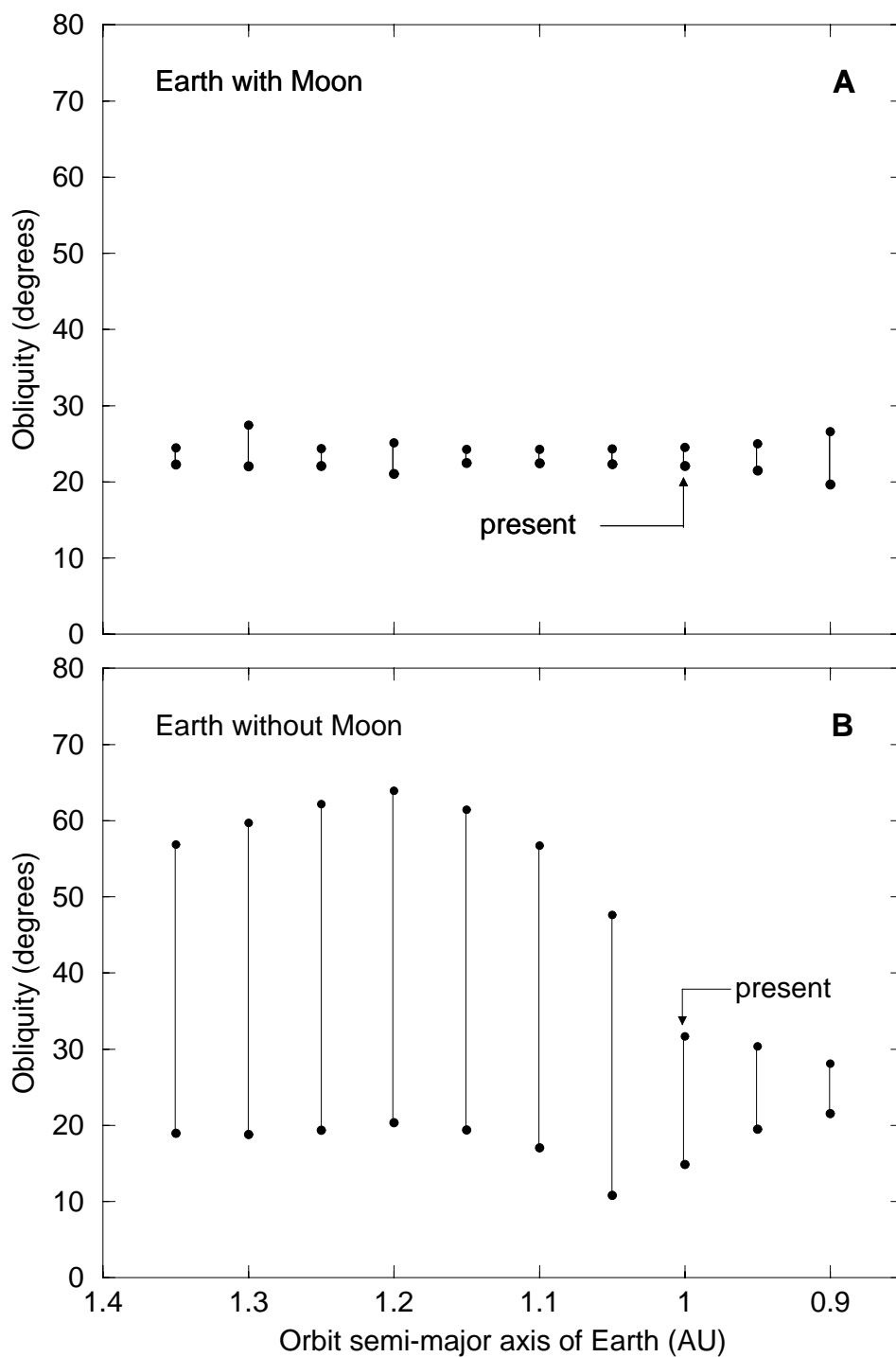


Figure 6.11: Range of Earth's obliquity over 1 Myr as a function of Earth's orbital position within the HZ. All other planets in the Solar System are in the present positions. The results marked *present* with Earth at 1.0 AU correspond to the results shown in Fig. 6.1

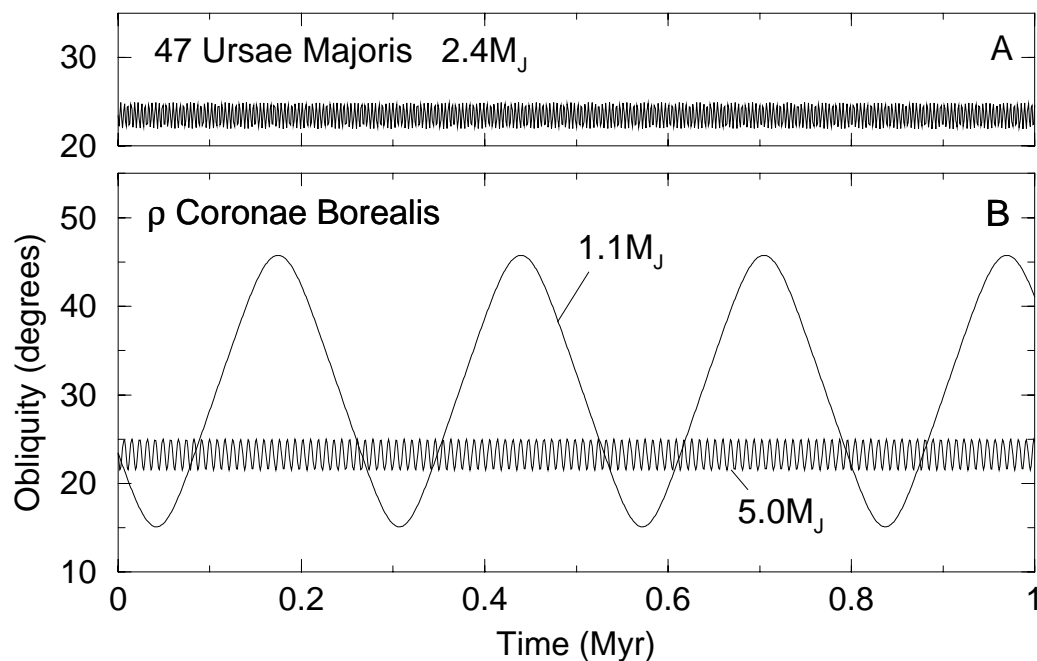


Figure 6.12: Obliquity variations of a hypothetical Earth-like planet orbiting at 1.0 AU from stars: (a) 47 UMa and (b)  $\rho$  CrB. Both planetary systems were assumed to consist of one Jovian-sized planet, with orbital parameters set by observations, and one terrestrial planet with orbital parameters equal to Earth's. The Jovian planet masses were  $2.4 M_J$ ,  $1.1 M_J$ ,  $5.0 M_J$  for the three simulations.

placed at 3.1 AU. More rapid precession is possible for larger Jovian planet masses and/or smaller terrestrial-Jovian planet separations. The planetary companion to the star 47 UMa, for example, has a minimum mass of  $2.1 M_J$  (Jupiter masses) and orbits just beyond the outer edge of the HZ (see Chapter 7) at 2.1 AU. An orbital simulation experiment involving this planet and a hypothetical Earth-sized planet orbiting at a distance of 1.0 AU has revealed orbital precession frequencies for the lesser planet of  $\sim -400'' yr^{-1}$ ! As this rate is much greater than the value for the spin-axis precession, the obliquity is stable with a variation rate of  $-400'' yr^{-1} + 50'' yr^{-1} = -350'' yr^{-1}$ , and a period of 3700 years.

An additional experiment was performed with a hypothetical Earth-sized planet in orbit around the star  $\rho$  Coronae Borealis (henceforth  $\rho$ CrB), whose known giant

planetary companion has a minimum mass of  $1.1 M_J$  and orbits at a distance of 0.23 AU (Noyes et al. 1997). Figure 6.12b shows the behavior of the spin axis to be very sensitive to the mass of  $\rho CrBB$  that is assumed. For a mass of  $1.1 M_J$ , the orbital precession of the lesser planet at 1.0 AU is  $\sim -50'' yr^{-1}$ , which is nearly equal and opposite the assumed rate of spin precession, and the obliquity demonstrates a regular variation between  $15^\circ$  and  $46^\circ$  every 270 Kyr. The amplitude of the variation ( $\sim \sin(I)d\Omega/dt$ ) is constant here, in contrast to the resonant variation shown in Fig. 6.1b, because the inclination  $I$  is also varying much more rapidly than the spin-axis precession. Hence, the amplitude is controlled by the time-averaged inclination which is approximately constant. The mass of  $\rho CrBB$  is not known and it could be as large as  $5.0 M_J$  (or larger). The orbit of an Earth-sized planet in the vicinity of an object of this size was found to precess faster than  $-200'' yr^{-1}$ . As with the case of an Earth around star 47 UMa, the orbital precession dominates the motion and the obliquity is shown in Fig. 6.12b to be rapidly variable, but stable.

These results show that the dynamical behavior of terrestrial-planet spin axes will vary greatly from one system to another. In the case of Earth, the Moon is an important contributor to its spin-axis stability. However, similar planets around other stars may have their spin-axes destabilized by neighboring planets and, so, may be subject to climate problems associated with high obliquity discussed in Chapter 2.

## Chapter 7

# HABITABLE MOONS AROUND EXTRASOLAR GIANT PLANETS

### 7.1 Moons as Life-Supporting Environments

All of the possible planetary objects that have recently been discovered orbiting main sequence stars have a mass at least half that of Jupiter, and are therefore unlikely to be hospitable to Earth-like life. To provide a suitable habitat for life, a planet needs to have a solid or liquid surface near which organisms might dwell, an atmosphere to protect the surface from ionizing radiation, and liquid water to facilitate biochemical reactions (Brack 1993). Jovian-type planets do not satisfy the first criterion and, hence, are unlikely to be inhabited. Rocky planets or moons of giant planets within a habitable zone (Kasting et al. 1993) might conceivably meet these requirements. Figure 7.1 shows that while most of the objects identified so far lie outside of this region, the companions to stars 16 Cygni B and 47 Ursae Majoris may have moons capable of supporting life.

Moons orbiting giant planets face additional problems that an isolated Earth-like planet would not encounter. First, a moon must orbit within a giant planet's Hill sphere, with a radius

$$r_{\text{H}} = \left( \frac{M_{\text{p}}}{3M_{\star}} \right)^{1/3} r, \quad (7.1)$$

to prevent the moon from being lost to the gravitational pull of the parent star. In Eqn. 7.1,  $M_{\text{p}}$  is the mass of the planet,  $M_{\star}$  is the mass of the star, and  $r$  is the

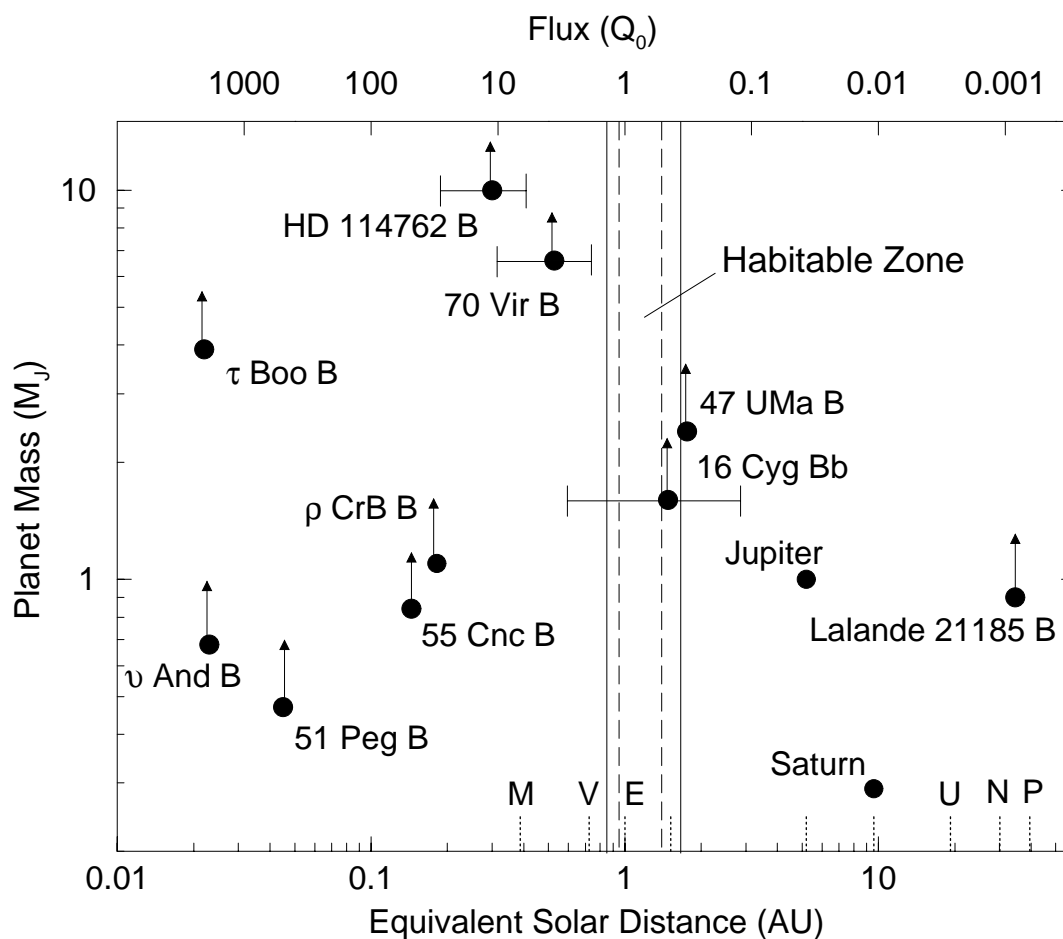


Figure 7.1: Locations of recently discovered or confirmed companions to nearby stars with respect to the HZ. The stars are: 51 Pegasi, 70 Virginis, 47 Ursae Majoris, Lalande 21185, 55( $\rho^1$ ) Cancri,  $\tau$  Boötis,  $\nu$  Andromedae, HD114762, 16 Cygni B (a member of a triple star system—its planet is designated 16 Cygni Bb), and  $\rho$  Coronae Borealis. Reported minimum planet masses are given relative the mass of Jupiter ( $M_J$ ). Planets are plotted according to the mean orbital flux,  $\propto (1 - e^2)^{-1/2}$ , they receive from their stars (upper x-axis) relative to Earth's solar constant  $Q_0 = 1370 \text{ Wm}^{-2}$ . The lower x-axis is the distance each planet would be from the Sun, in AU (astronomical units), to receive an equivalent flux. The positions of the planets in the Solar System are indicated by vertical dotted lines along the lower x-axis. The range of stellar fluxes received by objects in highly eccentric orbits are indicated with horizontal error bars. Conservative and nonconservative HZ limits (Kasting et al. 1993) are indicated by dashed lines and solid lines respectively. Adapted from Williams et al. (1997).

star-planet separation. At 1 AU from the Sun, the Hill-sphere radius of Jupiter is  $\sim 124 R_J$ , so nearly all of Jupiter's present moons (with the exception of eight small satellites beyond  $150 R_J$ ) would remain gravitationally bound at this orbital distance from the Sun. Around a less massive M-star such as Lalande 21185 (Gatewood 1996), with a mass of  $\sim 0.4 M_\odot$  and a HZ inner edge at  $\sim 0.06$  AU, the Hill radius shrinks to  $\sim 40 R_J$ , but Jupiter would still be able to keep all four of its Galilean moons which lie within  $22 R_J$ .

Galilean-moon analogues that orbit close to their planets would become tidally-locked within a few billion years of their formation. Hence, their rotations would last from a few days to a few months, which could lead to large diurnal temperature fluctuations. Moons of planets, or brown dwarfs, on highly eccentric orbits (e.g., 70 Vir B, HD114762 B, 16 Cyg Bb) might also experience large seasonal temperature fluctuations. Additionally, moons forming in a circumplanetary disk might receive different volatile endowments than would planets formed in a circumstellar disk. Lastly, moons orbiting Jovian-type planets would presumably be embedded within the giant planet's magnetosphere, where they would be constantly bombarded by energetic charged particles that could sputter away their atmospheres.

## 7.2 Volatile Endowments

We consider the question of how moons are supplied with volatiles. The terrestrial planets are thought to have received most of their volatiles from bombardment by comets or carbonaceous asteroids (Chyba 1990). If giant planets form in the outer regions of circumstellar disks and then spiral inwards, as suggested by Lin et al. (1996), cometary bombardment would be a likely source of volatiles. (Whether giant planets can retain their moons as they migrate inward is an important, unanswered

question.) Such a model has been proposed for the origin of Titan's atmosphere (Griffith and Zahnle 1995). Titan retained its atmosphere while the Jovian moons did not, perhaps because impacts occurred at lower velocities in the smaller gravitational potential well of Saturn, which resulted in less atmospheric erosion. This suggests that moons orbiting Jupiter-sized planets or larger may have difficulty retaining cometary volatiles.

But moons formed in circumplanetary disks in the outer parts of a stellar nebula may have no need for additional volatiles. Indeed, the problem is just the opposite: Many of these moons may be too volatile-rich. Ganymede and Callisto, which have densities of  $1.8 \text{ g cm}^{-3}$  and  $1.5 \text{ g cm}^{-3}$ , respectively, are at least half water-ice. If brought to 1 AU, the ice would melt and they would be covered with  $\sim 1000$  km of liquid water.

This would not preclude habitability, but it would almost certainly preclude land-based life. Better candidates for producing Earth-analog environments are moons such as Io and Europa (densities of  $3.5 \text{ g cm}^{-3}$  and  $3.0 \text{ g cm}^{-3}$ , respectively) that are composed mostly of rock. Io has been devolatilized by tidally-induced volcanism, but the difference between Europa and the two outermost Galilean moons is considered to be primordial. Europa contains more rock and less ice because the inner region of the circum-Jovian nebula was hotter (Prinn and Fegley 1981). If one assumes that extrasolar giant planets form in the same way, then clearly their inner moons are the most likely to be Earth-like.

## 7.3 Atmospheric Retention

### 7.3.1. Thermal Escape

A habitable moon must also be able to retain its volatiles for billions of years. Its effectiveness in doing so will depend on its mass, the flux of ionizing radiation it receives from its star, and the charged particle flux it receives within the magnetosphere of its planet. For small moons with hot exospheres, thermal (Jeans) escape should be an important loss process. The Jeans escape flux, in units of atoms  $\text{cm}^{-2} \text{sec}^{-1}$ , may be expressed

$$\Phi_{\text{esc}} = \frac{1}{\sqrt{2\pi}} v_s n_c (1 + \lambda_c) e^{-\lambda_c}, \quad (7.2)$$

where  $v_s = (kT/m)$  is related to the mean particle velocity (with  $k$  as the Boltzmann constant,  $T$  as the exospheric temperature, and  $m$  as the particle mass),  $n_c = 1/\sigma H_x$  is the number density of particles in the exosphere (with  $\sigma$  as collisional cross-section of escaping particles,  $H_x = kT/mg_x$  as the scale height at the base of the exosphere, and  $g_x$  as the exospheric gravitational acceleration), and

$$\lambda_c = \frac{GMm}{kTr_c}, \quad (7.3)$$

with  $r_c = R + r_x$  as the height of the exobase from planet center,  $M$  is the mass of the planet or moon, and  $G$  as Newton's gravitational constant. Now, the lifetime of an atmosphere,  $\tau$ , is simply the total particle number  $M_{\text{atm}}/m$  divided by the escape rate in units of particles  $\text{sec}^{-1}$ . The mass of the atmosphere may be obtained from the simple relationship

$$M_{\text{atm}}g = P4\pi R^2, \quad (7.4)$$

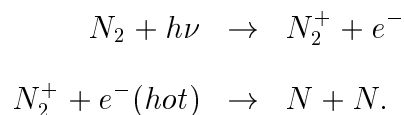
where  $P$  denotes the surface pressure. This enables atmospheric lifetime to be written

$$\tau = \frac{M_{\text{atm}}/m}{\Phi_{\text{esc}}4\pi R^2} = \frac{P}{\Phi_{\text{esc}}gm}. \quad (7.5)$$

So, a moon having a Mars-like density of  $3.9 \text{ g cm}^{-3}$ , an exosphere with its base  $r_x = 1000 \text{ km}$  and a temperature  $T = 2000 \text{ K}$ , similar to Earth's at solar maximum, could retain nitrogen and oxygen (both with  $\sigma \sim 2 \times 10^{-14} \text{ cm}^2$ ) for over 4.5 Gyr if its mass were  $>0.07M_\oplus$ . Loss of O is not necessarily fatal to habitability because  $\text{O}_2$  can be replaced by photosynthesis, and because large reservoirs of O exist in the form of water. Loss of N, though, would be irreversible and could preclude the development of terrestrial-type life. N is needed metabolically by organisms, and  $\text{N}_2$  is a non-toxic buffer gas that reduces flammability of Earth-like ecosystems such as forests (Watson et al. 1978, McKay et al. 1991).

### 7.3.2. Escape by Dissociative Recombination

A second loss process for N, which is important on Mars, is dissociative recombination of  $\text{N}_2^+$  (McElroy 1972). In this process,  $\text{N}_2$  absorbs an ultraviolet photon and loses an electron. A high-energy electron from an earlier ionization then dissociates the  $\text{N}_2^+$  on collision to yield two energetic N atoms, causing one to leave the planet. The reactions may be written



Mars loses nitrogen at a rate of  $5 \times 10^5 \text{ N atoms cm}^{-2} \text{ sec}^{-1}$  (Fox 1993). Scaling the Martian loss rate to an  $\text{N}_2$ -dominated atmosphere, by assuming that the ionization rate is proportional to the  $\text{N}_2$  mixing ratio (0.027 at present), gives an escape flux of  $5 \times 10^5 \text{ N atoms cm}^{-2} \text{ sec}^{-1} / 0.027 = 1.8 \times 10^7 \text{ N atoms cm}^{-2} \text{ sec}^{-1}$ . Now moving Mars to 1 AU from the Sun increases the flux of ionizing photons by  $(1.52 \text{ AU} / 1.0 \text{ AU})^2 = 2.3$  times. Thus, the loss rate from an  $\text{N}_2$ -dominated atmosphere at 1.0 AU from the Sun would be  $\sim 4 \times 10^7 \text{ N atoms cm}^{-2} \text{ sec}^{-1}$ . This would remove  $\sim 17\%$  of Earth's N in

4.5 Gyr. So, moons with Earth-like N endowments would be only marginally affected, but moons with smaller N endowments might lose their atmospheres over time. This loss process would become negligible for moons with masses  $\gtrsim 0.12M_{\oplus}$  because the velocities of the nonthermal N atoms would be too slow for them to escape. Mars' own mass is  $\sim 0.1M_{\oplus}$ , which allows it to lose  $^{14}\text{N}$  efficiently, but not  $^{15}\text{N}$ .

### 7.3.3. Loss of Atmosphere by Sputtering

A potentially even greater threat to atmospheres of moons around giant planets is sputtering by charged particles trapped within the planet's magnetosphere. Titan, which loses less than  $1.2 \times 10^7$  N atoms  $\text{cm}^{-2} \text{sec}^{-1}$  as a consequence of sputtering (Strobel et al. 1992) in the magnetosphere of Saturn ( $\sim 0.3M_{\text{J}}$ ), is only weakly affected. However, higher charged particle densities could exist within the magnetospheres of more massive planets. A moon orbiting within Jupiter's inner magnetosphere, for example, would receive an electron flux of  $4 \times 10^8 \text{ cm}^{-2} \text{sec}^{-1}$  (Van Allen 1976). By comparison, the solar wind particle flux at Mars' orbit is  $4.8 \times 10^5 \text{ cm}^{-2} \text{sec}^{-1}$ , which is thought to sputter away  $\text{CO}_2$  and O at rates  $\sim 2 \times 10^6 \text{ cm}^{-2} \text{sec}^{-1}$  (Kass and Yung 1995). Thus, a non-magnetized moon in a Jovian-like magnetosphere could lose N at a rate of  $\sim 2 \times 10^9 \text{ cm}^{-2} \text{sec}^{-1}$ . This would deplete Earth's  $\text{N}_2$  in only  $\sim 5 \times 10^8$  years.

Atmospheric loss due to sputtering could effectively be eliminated, however, for moons with strong magnetic fields. Until recently, the smallest object in the Solar System known to possess an appreciable magnetic field was Mercury ( $0.06M_{\oplus}$ ). The remarkable new discovery by the Galileo spacecraft of a magnetosphere belonging to Ganymede (Kivelson et al. 1996, Gurnett et al. 1996), which has a mass of  $0.03M_{\oplus}$ , suggests that at least some moons would be immune to this loss process.

## 7.4 Tidal Locking and Spin

Orbital constraints on habitability can be equally significant. Moons with captured rotations would have days which equal their orbital periods. The tidal locking radius for planets of different masses (Peale 1977) is  $r_T = 0.027(P_0 t / Q)^{1/6} M^{1/3}$ . If we assume a primordial moon spin period  $P_0$  of 15 hr, a time  $t$  of 4.5 Gyr, and a tidal dissipation factor  $Q$  of 100, then the 4.5-Gyr tidal locking radius ( $\sim 96 R_J$ ) corresponds to a 116-day orbital period radius. Moons near this limit might experience large diurnal temperature variations, but these moons, including Ganymede ( $15 R_J$ ) and Callisto ( $22 R_J$ ), would be covered by deep, high-heat-capacity oceans which would stabilize their climates over long rotations. Moons closer in (e.g., Europa), having Earth-like atmospheres and surfaces, would experience substantial diurnal temperature swings in continental interiors, but these swings would be greatly moderated in coastal environments.

## 7.5 Eccentric Orbits

Moons belonging to objects in highly eccentric orbits are less likely to be habitable. Objects in highly eccentric orbits are more likely to be brown dwarfs than planets (Boss 1996, Black 1997), unless high orbital eccentricities are a result of interplanetary collisions (Rasio and Ford 1996). Heating from either brown dwarfs or planets would be negligible after the first billion years (Saumon et al. 1996). The companion to the star 16 Cygni B has an orbital eccentricity of  $\sim 0.65$  (Cochran et al. 1996), and the ratio of perihelion flux to aphelion flux is  $[(1 + e)/(1 - e)]^2 \approx 22$ . Land-based life would be hard-pressed to deal with such seasonal fluctuations; however, the amplitudes of damaging seasonal extremes would be greatly reduced on moons possessing dense atmospheres. Hence, at least some moons on such eccentric orbits might still be suitable for life.

## 7.6 Climate Stabilization and the Carbonate-Silicate Cycle

Our discussion of climate to this point has been based on short-term considerations. To remain habitable for an extended time period, an Earth-like planet or moon must have some mechanism to compensate for the gradual brightening of a star as it ages (Kasting et al. 1993). On Earth, such long-term climate regulation is thought to be provided by the carbonate-silicate cycle and its effect on atmospheric  $\text{CO}_2$  (Walker et al. 1981). Cooler (warmer) climatic conditions decrease (increase) the rate of silicate weathering and enhance (diminish) the concentration of the greenhouse gas,  $\text{CO}_2$ . The presence of significant dry land is important in this feedback process because that is where silicate weathering occurs. A second key factor is plate tectonics, which results in subduction and metamorphism of carbonate sediments and return of  $\text{CO}_2$  to the atmosphere. The fact that Mars lost this capability early in its history may be one reason why it is so cold and desolate today (Kasting et al. 1988).

A necessary, but not sufficient, condition for maintaining plate tectonics is the existence of a substantial heat flux from a planet's or moon's interior. Venus, which presumably has an Earth-like heat flux, does not have plate tectonics, perhaps because it has no water (Turcotte 1996). Based on observations, the critical flux probably lies somewhere between that of Earth (Turcotte and Schubert 1982),  $\sim 70 \text{ ergs cm}^{-2} \text{ sec}^{-1}$ , and Mars (Solomon and Head 1990),  $\sim 30 \text{ ergs cm}^{-2} \text{ sec}^{-1}$ .

To obtain an estimate of when enough radiogenic heat is available, we assume that the surface heat flux is proportional to the mass of radioactive material within a moon's interior,  $\propto R^3 \rho e^{-\lambda t}$ , divided by surface area,  $\propto R^2$ , where  $R$  and  $\rho$  are the moon's radius and density, and  $\lambda = 1.5 \times 10^{-10} \text{ yr}^{-1}$  is the decay constant for  $^{238}\text{U}$ . This enables us to express the surface heat flux as  $F_{\text{rad}} \propto R \rho e^{-\lambda t}$ . We further assume that Mars became tectonically inactive 2 Gyr ago (Francis and Wood 1982), which

implies a critical heat flow of  $\sim 40 \text{ ergs cm}^{-2} \text{ sec}^{-1}$ . For a density similar to that of Io, this yields a lower limit of  $\sim 0.23M_{\oplus}$  for a moon capable of sustaining plate tectonics.

## 7.7 Tidal Heating

This “tectonic” lower mass limit might be circumvented if the innermost moons experienced substantial tidal heating, as is true for Io and, to a lesser extent, Europa. The rate of tidal heating is  $F_{\text{tid}} = (9/19)\rho^2 n^5 R^5 e^2 (\mu Q)^{-1}$ , where  $n$  is the moon’s mean motion about the planet,  $\mu$  is the moon’s rigidity ( $6.5 \times 10^{11} \text{ dynes cm}^{-2}$  for Io), and  $e$  is the orbital eccentricity (Peale et al. 1979). Io’s eccentricity is maintained at a finite value (0.004), despite tidal damping, by a 4:2:1 mean-motion resonance with Europa and Ganymede. If such resonances arise naturally during formation, as seems likely (Roy 1988), similar relationships might occur among the moons of extrasolar giant planets. Io’s tidal surface heating is calculated to be  $\sim 41 \text{ ergs cm}^{-2} \text{ sec}^{-1}$ , perhaps enough to drive plate tectonics on a more Earth-like moon. Alternatively, point volcanism of the sort that actually occurs on Io might be sufficient to recycle carbonate rocks and maintain an active carbonate-silicate cycle. So, close-in moons with masses  $< 0.23M_{\oplus}$  could conceivably remain habitable for long time periods. Io itself would not fulfill this criterion because it is too small to retain its volatiles.

In summary, some moons around extrasolar giant planets might be habitable, but only if they are of sufficient size. A  $0.12M_{\oplus}$  moon in an Io-like orbital resonance and possessing a Ganymede-like magnetic field, could conceivably remain habitable for billions of years, given the right amount of stellar insolation. All this suggests that the systems belonging to 47 Ursae Majoris and 16 Cygni B should be considered as possible abodes for extraterrestrial life.

## Chapter 8

# CONCLUSION

### 8.1 Opening Summary

The purpose of this thesis was to outline some of the important factors that might affect whether an extrasolar planet might support life. Such an investigation naturally helps us to also understand the origin, evolution, and eventual demise of Earth's own biosphere. The underlying assumptions made throughout this work are that at least some life-supporting environments around other stars will resemble Earth and that *life* implies organisms that depend on liquid water. To maintain liquid water on its surface, a planet must orbit its star within the habitable zone (HZ), which evolves over time. For a planet to remain within the continuously habitable zone (CHZ) for billions of years, its orbit must be stable. Orbital stability implies that a planet is not subject to large changes in orbital elements such as semi-major axis, eccentricity, and perihelion longitude that can destabilize climate. Climate can also be adversely affected by large changes in the orientation, or *obliquity*, of a planet's spin axis. Earth has benefited from having a relatively stable spin axis throughout much of its history, but some planets might have their climates destabilized by chaotic obliquity variations that allow their obliquities to reach values approaching  $90^\circ$ .

## 8.2 Obliquity and Climate - Chapter 2

An energy-balance climate model was used to show that large areas of Earth might not be habitable if its obliquity were as high as  $90^\circ$ . Long periods of darkness and intense sunlight ( $\sim 90$  days at  $45^\circ$  latitude) might be problematic for photosynthetic life. Other forms of life would have to adapt to rapidly varying temperatures ( $> 0.5^\circ$  K per day) and temperature extremes ( $> 80^\circ\text{C}$ ) over the continents. Similar planets, but with smaller continents or with equatorial supercontinents, would have their unfavorably large seasonal cycles damped by the large heat capacity of their oceans. Planets with polar supercontinents would be largely unsuited for land-based life even at modest ( $23.5^\circ$ ) obliquities.

Habitability is less affected by the size or position of continents on planets with dense,  $\text{CO}_2$ -rich atmospheres. The level of  $\text{CO}_2$  is affected by the amount of sunlight a planet receives from its parent star through the carbonate-silicate feedback loop, which should cause  $p\text{CO}_2$  to increase with orbital distance. At 1.4 AU, Earth's atmosphere would contain 2.1 bars of  $\text{CO}_2$  if the rate of volcanic outgassing remained constant. Aided by the greenhouse effect of its atmosphere, Earth would remain habitable out to distances of 1.40 to 1.46 AU, at which point its surface might be cooled by widespread  $\text{CO}_2$  clouds.

A second benefit of a dense  $\text{CO}_2$  atmosphere is its high thermal inertia, which limits the seasonal temperature variation and latitudinal temperature gradient for planets at high obliquity. Atmospheres that are dynamically similar to Earth's should have their temperature gradients reduced further by more efficient heat transport as a result of their higher surface pressures. All else being equal (e.g., the size and distribution of continents,  $\text{H}_2\text{O}$ -cloud cover, dynamics, etc.), most Earth-like planets occupying the outer HZ around their parent stars should be habitable regardless of their obliquity.

### 8.3 Obliquity-Oblateness Feedback - Chapter 5

Geologic evidence of low-latitude glaciation during the Precambrian Era around 2.2 Ga and 0.8 Ga suggests that Earth's obliquity may have been significantly higher than it is today. This is difficult to explain given Earth's remarkably stable obliquity at present, and even greater stability during the Precambrian when the Earth-Moon separation was smaller. A possible explanation is that Earth's obliquity was  $> 54^\circ$  for much of its history (possibly as a consequence of the giant impact thought to have formed the Moon), which would have made the equator the coldest part of the planet. An explanation for the possible inclination of Earth's spin-axis from high to low obliquity is offered here. The obliquity may have been reduced rapidly near the end of the Precambrian era (0.6 Ga) as a result of a positive feedback between cyclic changes in obliquity and in oblateness from the growth and melting of ice sheets.

Obliquity-oblateness feedback, or *climate friction*, causes a secular drift in obliquity through a time delay between Earth's obliquity oscillation and climatically-induced variations in ice sheet mass, as well as an additional time delay between the ice sheet variation and the isostatic readjustment of the underlying Earth. The rate of obliquity drift is primarily a function of changes to continental ice volume, which may have been considerably amplified during the Late Precambrian when most of the continents are thought to have been situated at high latitude. Under these circumstances, Earth's oblateness may have been reduced by as much as 2.6% during an ice age.

Drift direction is controlled by the response time of climate and ice-volume to obliquity. For phase lags between the sinusoidal obliquity variation and ice-sheet variation in the range  $25^\circ$  to  $206^\circ$ , the drift in obliquity is positive. However, phase lags  $> 206^\circ$  are possible if ice sheets do not begin to melt until after obliquity and polar insolation have peaked. For a phase lag in ice-sheet response of  $230^\circ$ , Earth's obliquity may have been reduced from  $54^\circ$  to  $26^\circ$  in only 100 Myr. If the Earth-Moon momentum was

approximately conserved during this process, the lunar inclination may have grown from  $0^\circ$  (as needed to have the Moon originate from an impact-generated disk aligned with Earth's equator) to  $5\text{-}6^\circ$ , which is the approximate inclination of the lunar orbit today.

## 8.4 Precession and Obliquity - Chapter 6

Earth owes its stable obliquity to the presence of the Moon, as well as to the planetary system in which it resides. This is because the obliquity is a function of the combined rates of precession of a planet's spin axis about its orbit normal and of its orbit normal about the normal to its local invariable plane. If the two precession rates are very different, as in the case of Earth, then the resulting changes to obliquity over a precession cycle are small. When the two rates are approximately equal, however, large and unpredictable variations in obliquity can occur. The rate of spin-axis precession is governed largely by the masses and orbital proximity of satellites, whereas the rate of orbit precession is controlled primarily by the masses and orbits of neighboring planets. At present, Earth's spin axis precesses  $\sim 3$  times as fast as its orbit. However, the rate of spin-axis precession is slowing as a result of the tidal expansion of the lunar orbit, and Earth will enter a spin-orbit resonance in 1-2 Gyr. Earth would be caught in such a resonance today, and its obliquity variation would be considerably amplified, if the Moon were less than half its present mass. Without the Moon, Earth's obliquity would vary by more than  $20^\circ$  in 1 Myr, which is more than six times the present variation.

Planets having Earth-like moons might also be subject to large obliquity fluctuations if they reside in tightly-spaced planetary systems where their orbits are more strongly perturbed than in the Solar System. Orbital simulation experiments show that if Jupiter were moved inward to 4.1 AU, Earth's orbit and spin-axis preces-

sions would be approximately equal so that the obliquity variation would be doubled. Thus, Earth's range in obliquity over 1 Myr would grow to  $\sim 6^\circ$  with the Moon and to  $\sim 50^\circ$  without the Moon. Moving Jupiter inward to 3.1 AU reduces the amplitude of the obliquity variation to  $\sim 6^\circ$  for the moon-less Earth because the orbital precession is now much larger than the spin-axis precession, but Earth with the Moon would have its obliquity variation grow to  $\sim 40^\circ$  as a consequence of precessional resonance. Similar results were obtained with a fictitious Earth in orbit around stars 47 Ursae Majoris having a  $2.4 M_J$  object orbit at 2.1 AU, and around  $\rho$  Coronae Borealis having a  $1.1 M_J$  object orbit at 0.23 AU. In both cases, the Earth-like planet's orbit precession rate is much faster than Earth's is in the Solar System. This poses a problem for an Earth-like planet in the vicinity of  $\rho$  Coronae Borealis B because it would be in a spin-orbit resonance so that the resulting obliquity range would be  $\sim 30^\circ$ . The obliquity of such a planet would be stable (varying only by  $\sim 3^\circ$ ) for larger masses of  $\rho$  Coronae Borealis B or if it did not have a moon.

## 8.5 Moons Around Giant Planets - Chapter 7

Jovian-sized planets have recently been discovered around ten different main-sequence stars. Giant, gaseous planets are unlikely to harbor terrestrial-type life, but their moons might conceivably be habitable if they lie within the HZ. Possible moons around planets 16 Cygni Bb and 47 Ursae Majoris B might satisfy this criterion.

A habitable moon must first form and then be able to retain an atmosphere. Impact-generated atmospheres are most likely to form on large moons (e.g., Titan) born far from their parent stars, where the relative velocities of infalling comets are small. A moon's ability to retain an atmosphere depends primarily on its mass. For an object at 1 AU from its star to retain a  $N_2$  atmosphere for billions of years, it must

be larger than Mars ( $0.1M_{\oplus}$ ), which has lost significant amounts of its primordial nitrogen through dissociative-recombination reactions. Were a moon only slightly larger ( $> 0.12M_{\oplus}$ ), its escape velocity would be high enough to prevent  $^{14}\text{N}$  atoms from being lost by this process. However, all moons orbiting within the charged particle environments of a giant planet's magnetosphere would be susceptible to more rapid loss of atmosphere by sputtering, unless they are shielded by their own magnetic fields, as is Ganymede.

Dynamical factors which might affect habitability are synchronous rotation and orbital eccentricity, which could cause large diurnal and seasonal temperature fluctuations. Water endowments on moons might also be important. Moons formed initially of ice (e.g., Ganymede) would have 1000 km-deep oceans within the HZ. Moons made of more rock (e.g., Europa) would have a better chance of supporting land-based life on dry continents. Finally, long-term climatic stability would be provided a moon that demonstrates an Earth-like carbonate-silicate cycle, which controls levels of  $\text{CO}_2$  and, hence, greenhouse warming through weathering of surface minerals and plate tectonics. Tectonic activity may be sustained by radiogenic heating for 4.5 billion years on moons  $> 0.23M_{\oplus}$ . Smaller moons might also exhibit long-lived plate tectonics if they are heated tidally as a result of resonant interactions with adjacent moons, as is Io.

## 8.6 Directions For Future Research

This thesis has perhaps raised more questions than it has answered. For example: How are terrestrial climates affected by seasonal insolation changes caused by high orbital eccentricity? At what orbital eccentricity are climates destabilized? Also, if  $\text{CO}_2$  clouds can warm a planet's surface, what is the outer edge to the HZ? Would Earth be able to maintain liquid water on its surface out to 2.0 AU, or even 2.5 AU? How

are precession and obliquity affected by high orbital eccentricities and inclinations? How likely is it that a terrestrial planet occupies a habitable zone around a star? What are the possible sizes and orbital separations of moons formed by accretion in a protoplanetary disk? If giant planets migrate inward through gravitational interactions in a protoplanetary disk, do their moons remain bound to them? Conversely, can giant planets capture terrestrial-sized moons as they migrate inward?

The discoveries of extrasolar giant planets within what is the terrestrial-planet region of the Solar System makes it interesting to ask whether there are any terrestrial planets within the HZs around the same stars. The question may be phrased like this: Given the known distribution of Jupiter-sized planets around nearby stars, would an Earth-sized planet within the HZ have a stable orbit for billions of years? Clearly there would be no such stable orbits (ignoring resonances and librations) within the HZ of star 16 Cygni B, whose Jupiter-sized planet 16 Cygni Bb crosses the HZ twice per 802-day orbit. But are there stable terrestrial-planet orbits within the HZs of stars 70 Virginis, 47 Ursae Majoris, or  $\rho$  Coronae Borealis? Short (10 Myr) simulation experiments using the symplectic orbit integrator *SWIFT* show that an Earth-like planet at 1.0 AU around star 70 Virginis would collide with planet 70 Virginis B in only 148 Kyr. Similar experiments involving planets around stars 47 Ursae Majoris and  $\rho$  Coronae Borealis show that Earth would apparently be stable in its present orbit for more than 10 Myr. More work needs to be done to understand how orbital stability of terrestrial planets is affected by Jovian planet mass (which is not well constrained by observations), as well as orbital eccentricity, inclination, and proximity. The results of future simulations will then help to constrain the prospects for finding habitable Earth-like planets in systems around other stars.

## REFERENCE LIST

- Angel, J.R.P. 1994. Ground-based imaging of extrasolar planets using adaptive optics. *Nature* **368**, 203-207.
- Applegate, J.H., Douglas, M.R., Gurael, Y., Sussman, G.J., and Wisdom J. 1986. The outer Solar System for 200 million years. *Astron. J.* **92**, 176-194.
- Bada, J.L., Bigham, C., and Miller, S.L. 1994. Impact melting of frozen oceans on the early Earth: Implications for the origin of life. *Proc. Nat. Acad. Sci.* **91**, 1248-1250.
- Becker, W., and Truemper, J. 1997. The X-ray luminosity of rotation-powered neutron stars. *Astron. Astrophys.* **326**, 682-691.
- Berger, A.L. 1976. Obliquity and precession for the last 5,000,000 years. *Astron. Astrophys.* **51**, 127-135.
- Berger, A.L., Loutre, M.F., and Laskar, J. 1992. Stability of the astronomical frequencies over the earth's history for paleoclimate studies. *Science* **255**, 560-566.
- Berner, R.A., Lasaga, A.C., and Garrels, R.M. 1983. The carbonate-silicate geochemical cycle and its effect on atmospheric carbon dioxide over the past 100 million years. *Amer. J. Sci.* **283**, 641-683.
- Bills, B.G. 1994. Obliquity-oblateness feedback: Are climatically sensitive values of obliquity dynamically unstable? *Geophys. Res. Lett.* **21**, 177-180.
- Black, D.C. 1997. Possible observational criteria for distinguishing brown dwarfs from planets. *Astrophys. J.* **490**, L171.
- Boss, A.P. 1995. Proximity of Jupiter-like planets to low-mass stars. *Science* **267**, 360-362.
- Boss, A.P. 1996a. Extrasolar planets. *Physics Today* **49**, 32-38.
- Boss, A.P. 1996b. Giant planets and dwarfs meet in the middle. *Nature* **379**, 397-398.
- Brack, A. 1993. Liquid water and the origin of life. *Orig. of Life and Evol. of Bios.* **23**, 3-10.

- Bretagnon, P. 1974. Termes a longues periodes dan le systeme solaire. *Astron. Astrophys.* **30**, 141-154.
- Brouwer, D., and Clemence, G.M. 1961. Orbits and masses of planets and satellites. in *Planets and Satellites* (Univ. of Chicago Press, Chicago).
- Brouwer, D., and van Woerkom, A.J.J. 1950. The secular variations of the orbital elements of the principle planets. *Astron. Pap. Amer. Ephem. Naut. Alman.* **13**, 81.
- Budyko, M.I. 1969. The effect of solar radiation variations on the climate of the Earth. *Tellus* **21**, 611-619.
- Butler, R.P., and Marcy, G.W. 1996. A planet orbiting 47 Ursae Majoris. *Astrophys. J.* **464**, L153-L156.
- Butler, R.P., Marcy, G.W., Williams, E., Hauser, H., and Shirts, P. 1996. Three new "51 Pegasi-type" planets. *Astrophys. J.* **474**, L115-L118.
- Caldeira, K., and Kasting, J.F. 1992. Susceptibility of early Earth to irreversible glaciation caused by carbon dioxide clouds. *Nature* **359**, 226-228.
- Cess, R.D. 1976. Climatic change: An appraisal of atmospheric feedback mechanisms employing zonal climatology. *J. Atmos. Sci.* **33**, 1831-1843.
- Chambers, J.E., Wetherill, G.W., and Boss, A.P. 1996. The stability of multi-planet systems. *Icarus* **119**, 261-268.
- Chyba, C.F. 1990. Impact delivery and erosion of planetary oceans in the early inner Solar System. *Nature* **343**, 129-133.
- Cochran, W.D., and Hatzes, A.P. 1996. Radial velocity searches for other planetary systems. *Astrophys. Space Sci.* **241**, 43-60.
- Cochran, W.D., Hatzes, A.P., Butler, R.P., and Marcy, G.W. 1997. The discovery of a planetary companion to 16 Cygni B. *Astrophys. J.* **483**, 457-463.
- Cochran, W.D., Hatzes, A.P., and Hancock, T.J. 1991. Constraints on the companion object to HD 114762. *Astrophys. J.* **380**, L35-L38.
- Colombo, G. 1966. Cassini's second and third laws. *Astron. J.* **71**, 891-896.
- Crowley, T.J., and Baum, S.K. 1993. Effect of decreased solar luminosity on Late Precambrian ice extent. *J. Geophys. Res.* **98**, 16723-16732.

- Danby, J.M.A. 1992. *Fundamentals of Celestial Mechanics, 2nd ed.* (Willmann-Bell, Richmond).
- Dole, S.H. 1964. *Habitable Planets for Man.* (Blaisdell, New York).
- Doyle, L.R. 1996. *Circumstellar Habitable Zones: Proceedings of the First International Conference.* (Travis House, Menlo Park, CA).
- Embleton, B.J. and Williams, G.E. 1986. Low paleolatitude of deposition for late Precambrian periglacial varvites in South Australia: implications for palaeoclimatology. *Earth Planet. Sci. Lett.* **79**, 419-430.
- Evans, D.A. Beukes, N.J., and Kirschvink, J.L. 1997. Low-latitude glaciation in the Palaeoproterozoic era. *Nature* **386**, 262-266.
- Farrell, B.F. 1990. Equable climate dynamics. *J. Atmos. Sci.* **47**, 2986-2995.
- Fernandez, J.A., and Ip, W.-H. 1984. Some dynamical aspects of the accretion of Uranus and Neptune – the exchange of orbital angular momentum with planetesimals. *Icarus* **58**, 109-120.
- Forget, F., and Pierrehumbert, R.T. 1997. Warming early Mars with carbon dioxide clouds that scatter infrared radiation. *Science* **278**, 1273-1276.
- Fox, J.L. 1993. The production and escape of nitrogen atoms on Mars. *J. Geophys. Res.* **98**, 3297-3310.
- Frakes, L.A. 1979. *Climates Throughout Geologic Time* (Elsevier, Amsterdam).
- Francis, P.W., and Wood, C.A. 1982. Absence of silicic volcanism on Mars: implications for crustal composition and volatile abundance. *J. Geophys. Res.* **87**, 9881-9889.
- Gatewood, G 1996. Lalande 21185. *Bull. Amer. Astron. Soc.* **28**, 885.
- Gierasch, P.J., and Toon, O.B. 1973. Atmospheric pressure variation and the climate of Mars. *J. Atmos. Sci.* **30**, 1502-1508.
- Gladman, B. 1993. Dynamics of systems of two close planets. *Icarus* **106**, 247-263.
- Gladman, B., Duncan, M., and Candy, J. 1991. Symplectic integrators for long-term integrations in celestial mechanics. *Celest. Mech.* **52**, 221-240.
- Goldreich, P. 1966. History of the lunar orbit. *Rev. Geophys.* **4**, 411-439.

- Goldstein, H. 1980. *Classical Mechanics, 2nd ed.* (Addison-Wesley, London).
- Gough, D.O. 1981. Solar interior structure and luminosity variations. *Solar Phys.* **74**, 21-34.
- Gray, D.F. 1997. Absence of a planetary signature in the spectra of the star 51 Pegasi. *Nature* **385**, 795-796.
- Gray, D.F. 1998. A planetary companion for 51 Pegasi implied by absence of pulsations in the stellar spectra. *Nature* **391**, 153-154.
- Griffith, C.A., and Zahnle, K. 1995. Influx of cometary volatiles to planetary moons: the atmospheres of 1000 possible Titans. *J. Geophys. Res.* **100**, 16907-16922.
- Guillot, T., Burrows, A., Hubbard, W.B., Lunine, J.I., and Saumon, D. 1996. Giant planets at small orbital distances. *Astrophys. J.* **459**, L35-L38.
- Gurnett, D.A., Kurtin, W.S., Rowe, A., Bolton, S.J., and Kennel C.F. 1996. Evidence for a magnetosphere at Ganymede from plasma-wave observations by the Galileo spacecraft. *Nature* **384**, 535-537.
- Haberle, R.M., McKay, C.P., Tyler, D., and Reynolds, R.T. 1996. Can synchronously rotating planets support an atmosphere? in *Circumstellar Habitable Zones: Proceedings of the First International Conference* (L.R. Doyle ed.) (Travis House, Menlo Park, CA) pp. 29-41.
- Hart, M.H. 1979. Habitable zones about main sequence stars. *Icarus* **37**, 351-357.
- Hartmann, W.K., Phillips, R.J., and Taylor, G.J. 1986. *Origin of the Moon*, (Lunar and Planetary Inst., Houston).
- Hatzes, A.P., Cochran, W.D., and Bakker, E.J. 1998. Further evidence for the planet around 51 Pegasi. *Nature* **391**, 154-156.
- Hecht, J., and Scotese, C.R. 1997. *Ages of the Earth* (MacMillan, New York).
- Hoffert, M.I., Callegari, A.J., Hsieh, C.T., and Ziegler, W. 1981. Liquid water on Mars: an energy balance climate model for CO<sub>2</sub>/H<sub>2</sub>O atmospheres. *Icarus* **47**, 112-129.
- Holland, H.D. 1978. *The Chemistry of the Atmosphere and Oceans*, (John Wiley & Sons, Inc., New York).
- Huang, S.-S. 1959. Occurrence of life in the universe. *Amer. Sci.* **47**, 397-402.

- Huang, S.-S. 1960. Life outside the Solar System. *Sci. Amer.* **202**, 55-63.
- Ida, S., Canup, R.M. and Stewart, G.R. 1997. Lunar accretion from an impact-generated disk. *Nature* **389**, 353-357.
- Imbrie, J., Boyle, E.A., Clemens, S.C., Duffy, A., Howard, W.R., Kukla, G., Kutzback, J., Martinson, D.G., McIntyre, A., Mix, A.C., Molfino, B., Morley, J.J., Peterson, L.C., Pisias, N.G., Prell, W.L., Raymo, M.E., Shackleton, N.J., and Toggweiler, J.R. 1992. On the structure and origin of major glaciation cycles: 1. linear responses to Milankovitch forcing. *Paleoceanography* **7**, 701-738.
- Ito, T., Masuda, K., Hamano, Y. and Matsui, T. 1995. Climate friction: A possible cause for secular drift of Earth's obliquity. *J. Geophys. Res.* **100**, 15147-15161.
- Jacobowitz, H., Smith, W.L. Howell, H.B. Nagle, F.W., and Hickery, J.R. 1979. The first 18 months of planetary radiation budget measurements from Nimbus 6 ERB experiment. *J. Atmos. Sci.* **36**, 501-507.
- Kass, D.M., and Yung, Y.L. 1995. Loss of atmosphere from Mars due to solar wind-induced sputtering. *Science* **268**, 697-699.
- Kasting, J.F. 1988. Runaway and moist greenhouse atmospheres and the evolution of Earth and Venus. *Icarus* **74**, 472-494.
- Kasting, J.F. 1991. CO<sub>2</sub> condensation and the climate of early Mars. *Icarus* **94**, 1-13.
- Kasting, J.F. 1992. Proterozoic climates: The effect of changing atmospheric carbon dioxide concentrations. in *The Proterozoic Biosphere: A Multidisciplinary Study* (eds. Schopf, J.W. and Klein, C.) (Cambridge Univ. Press, Cambridge) pp. 165-168.
- Kasting, J.F. 1996a. Habitable zones around stars: An update. in *Circumstellar Habitable Zones: Proceedings of the First International Conference* (L.R. Doyle ed.) (Travis House, Menlo Park, CA) pp. 17-28.
- Kasting, J.F. 1996b. Planetary atmosphere evolution: Do other habitable planets exist and can we detect them?. *Astrophys. Space Sci.* **241**, 3-24.
- Kasting, J.F., and Ackerman, T.P. 1986. Climatic consequences of very high carbon dioxide levels in the Earth's early atmosphere. *Science* **234**, 1383-1385.
- Kasting, J.F., Toon, O.B., and Pollack, J.B. 1988. How climate evolved on the terrestrial planets. *Sci. Amer.* **256**, 90-97.

- Kasting, J.F., Whitmire, D.P., and Reynolds, R.T. 1993. Habitable zones around main sequence stars. *Icarus* **101**, 108-128.
- Kinoshita, H. 1975. Formulas for precession. *Smithsonian Astrophys. Obs. Special Report* **304**, 1-25.
- Kinoshita, H. 1977. Theory of the rotation of the rigid Earth. *Celestial Mechanics* **15**, 277-326.
- Kirschvink, J.L. Late Proterozoic low-latitude global glaciation: The snowball Earth. 1992. in *The Proterozoic Biosphere: A Multidisciplinary Study* (eds. Schopf, J.W. and Klein, C.) (Cambridge Univ. Press, Cambridge) pp. 51-52.
- Kivelson, M.G., Khurana, K.K., Russell, C.T., Walker, R.J., Warnecke, J., Coroniti, F.V., Polansky, C., Southwood, D.J., and Schubert, G. 1996. Discovery of Ganymede's magnetic field by the Galileo spacecraft. *Nature* **384**, 537-541.
- Kondrat'ev, K.Y.A. 1969. Albedo of the underlying surface and clouds. in *Radiation in the Atmosphere* (K.Y.A. Kondrat'ev) (Academic Press, New York) pp. 411-452.
- Laskar, J., and Robutel, P. 1993. The chaotic obliquity of the planets. *Nature* **361**, 608-614.
- Laskar, J., Joutel, F., and Robutel, P. 1993a. Stabilization of the Earth's obliquity by the Moon. *Nature* **361**, 615-617.
- Laskar, J., Joutel, F., and Robutel, P. 1993b. Orbital, precessional, and insolation quantities for the Earth from -20 Myr to +10 Myr. *Astron. Astrophys.* **270**, 522-533.
- Latham, D.W., Mazeh, T., Stefanik, R.P., Mayor, M., and Burki, G. 1989. The unseen companion of HD 114762: a probable brown dwarf. *Nature* **339**, 38-40.
- Levison, H.F., and M.J. Duncan 1994. The long-term dynamical behavior of short-period comets. *Icarus* **108**, 18-36.
- Lin, D.N.C., Bodenheimer, P., and Richardson, D.C. 1996. Orbital migration of the planetary companion of 51 Pegasi to its present location. *Nature* **380**, 606-607.
- Lindzen, R.S., and Farrell, B. 1977. Some realistic modifications of simple climate models. *J. Atmos. Sci.* **34**, 1487-1501.
- McElroy, M.B. Mars; an evolving atmosphere. 1972. *Science* **175**, 443-445.

- McKay, C.P., Toon, O.B., and Kasting, J.F. 1991. Making Mars habitable. *Nature* **352**, 489-496.
- Marcy, G.W., and Butler, R.P. 1996. A planetary companion to 70 Virginis. *Astrophys. J.* **464**, L147-L151.
- Marcy, G.W., Butler, R.P., Williams, E., Bildsten, L., Graham, J.R. Ghez, A.M., and Jernigan, J.G. 1997. The planet around 51 Pegasi. *Astrophys. J.* **481**, 926-937.
- Marshall, H.G., Walker, J.C.G., and Kuhn, W.R. 1988. Long-term climate change and the geochemical cycle of carbon. *J. Geophys. Res.* **93**, 791-801.
- Mayor, M., and Queloz, D. 1995. A Jupiter-mass companion to a solar-type star. *Nature* **378**, 355-359.
- Mazeh, T., Latham, D.W., and Stefanik, R.P. 1996. Spectroscopic orbits for three binaries with low-mass companions and the distribution of secondary masses near the substellar limit. *Astrophys. J.* **466**, 415-426.
- Meert, J.G., and Van der Voo, R. 1994. The Neoproterozoic (1000-540 Ma) glacial intervals: No more snowball earth? *Earth Planet. Sci. Lett.* **123**, 1-13.
- Mitrovica, J.X. and Forte, A.M. 1995. Pleistocene glaciation and the Earth's precession constant. *Geophys. J. Int.* **121**, 21-32.
- Néron de Surgy, O. and Laskar, J. 1997. On the long term evolution of the spin of the Earth. *Astron. Astrophys.* **318**, 975-989.
- Newhall, X.X., Standish, E.M., and Williams, J.G. 1983. DE 102 - A numerically integrated ephemeris of the moon and planets spanning forty-four centuries. *Astron. Astrophys.* **125**, 150-167.
- North, G.R., Cahalan, R.F., and Coakley, J.A. 1981. Energy balance climate models. *Rev. Geophys. and Space Phys.* **19**, 91-121.
- North, G.R., and Coakley, J.A. 1979. Differences between seasonal and mean annual energy balance model calculations of climate and climate sensitivity. *J. Atmos. Sci.* **36**, 1189-1203.
- North, G.R., Mengel, J.G., and Short, D.A. 1983. Simple energy balance model resolving the seasons and the continents: application to the astronomical theory of the ice ages. *J. Geophys. Res.* **88**, 6576-6586.

- Noyes, R.W., Jha, S., Korzennik, S.G., Krockenberger, M., Nisenson, P., Brown, T.M., Kennelly, E.J., and Horner, S. 1997. A planet orbiting the star Rho Coronae Borealis. *Astrophys. J.* **483**, L111-L114.
- Park, J.K. Paleomagnetic evidence for low-latitude glaciation during deposition of the Neoproterozoic Rapitan Group, Mackenzie Mountains, N.W.T., Canada. 1997. *Can. J. Earth Sci.* **34**, 34-49.
- Peale, S.J. 1977. Rotation histories of the natural satellites. in *Planetary Satellites* (ed. Burns, J.A.) (University of Arizona Press, Tucson) pp. 87-112.
- Peale, S.J. 1997. Expectations from a microlensing search for planets. *Icarus* **127**, 269-289.
- Peale, S.J., Cassen, P., and Reynolds, R.T. 1979. Melting of Io by tidal dissipation. *Science* **203** 892-894.
- Peltier, W.R. 1994. Ice age paleotopography. *Science* **265**, 195-201.
- Peltier, W.R., and Jiang, X. 1994. The precession constant of the Earth: Variations through the ice-age. *Geophys. Res. Lett.* **21**, 2299-2302.
- Podolak, M., Hubbard, W.B., and Pollack, J.B. 1993. Gaseous accretion and the formation of giant planets. in *Protostars and Planets III*. (Arizona Univ., Tucson) pp. 1109-1147.
- Pollack, J.B., Kasting, J.F., Richardson, S.M., and Poliakoff, K. 1987. The case for a wet, warm climate on early Mars. *Icarus* **71**, 203-224.
- Prinn, R.G., and Fegley, B. 1981. Kinetic inhibition of CO and N<sub>2</sub> reduction in circumplanetary nebulae: implications for satellite composition. *Astrophys. J.* **249**, 308-317.
- Quinn, T.R., Tremaine, S., and Duncan, M.J. 1991. A three-million-year integration of the Earth's orbit. *Astron. J.* **101**, 2287-2305.
- Rasio, F.A., and Ford, E.B. 1996. Dynamical instabilities and the formation of extrasolar planetary systems. *Science* **274**, 954-956.
- Rasio, F.A., Tout, C.A., Lubow, S.H., and Livio, M. 1996. Tidal decay of close planetary orbits. *Astrophys. J.* **470**, 1187.
- Rochester, M.G. 1976. The secular decrease of obliquity due to dissipative core-mantle coupling. *Geophys. J. Roy. Astr. Soc.* **46**, 109-126.

- Roy, A.E. 1988. *Orbital Motion, 3rd ed.* (Adam Hilger, Philadelphia).
- Rubincam, D.P. 1975. Tidal friction and the early history of the Moon's orbit. *J. Geophys. Res.* **80**, 1537-1548.
- Rubincam, D.P. Mars: Change in axial tilt due to climate? 1990. *Science* **248**, 720-721.
- Rubincam, D.P. 1993. The obliquity of Mars and "climate friction." *J. Geophys. Res.* **98**, 10827-10832.
- Rubincam, D.P. 1995. Has climate changed Earth's tilt? *Paleoceanography* **10**, 365-372.
- Ryder, G. 1990. Lunar samples, lunar accretion, and the early bombardment of the Moon. *EOS* **71**, 313, 322-323.
- Saumon, D, Hubbard, W.B., Burrows, A, Guillot, T, Lunine, J.I, and Chabrier, G. 1996. A theory of extrasolar giant planets. *Astrophys J.* **460**, 993.
- Schmidt, P.W., and Williams, G.E. 1995. The Neoproterozoic climatic paradox: Equatorial paleolatitude for Marinoan glaciation near sea level in South Australia. *Earth Planet. Sci. Lett.* **134**, 107-124.
- Schubert, G. 1983. General circulation and the dynamical state of the Venus atmosphere. in *Venus* (Hunten, D.M., L. Colin, T.M. Donahue, and V.I. Moroz, eds.) (Univ. of Arizona Press, Tucson) pp. 681-765.
- Segerer, A.H., Burggraf, S., Fiala, G., Huber, G., Huber, R., and Stetter, K.O. 1993. Life in hot springs and hydrothermal vents. *Origins of Life* **23**, 77-90.
- Sellers, W.D. 1965. *Physical Climatology*, Univ. of Chicago Press, London.
- Shklovskii, I.S., and Sagan, C. 1966. *Intelligent Life in the Universe*. (Holden-Day, San Francisco).
- Sleep, N.H., Zahnle, K.J., Kasting, J.F., and Morowitz, H.J. 1989. Annihilation of ecosystems by large asteroid impacts on the early Earth. *Nature* **342**, 139-142.
- Solomon, S.C., and Head, J.W. 1990. Heterogeneities in the thickness of the elastic lithosphere of Mars; constraints on heat flow and internal dynamics. *J. Geophys. Res.* **95**, 11073-11083.
- Stacey, F.D. 1992. *Physics of the Earth, 3rd ed.* (Brookfield Press, Brisbane).

- Stone, P.H. 1972. A simplified radiative-dynamical model for the static stability of rotating atmospheres. *J. Atmos. Sci.* **29**, 405-417.
- Sussman, G.J., and Wisdom, J. 1988. Numerical evidence that the motion of Pluto is chaotic. *Science* **241**, 433-437.
- Taylor, J.H., Manchester, R.N., and Lyne, A.G. 1993. Catalog of 558 pulsars. *Astrophys J. Suppl.* **88**, 529-568.
- Thompson, S.L. and Barron, E.J. 1981. Comparison of Cretaceous and present Earth albedos: Implications for the causes of paleoclimates. *J. Geol.* **89**, 143-167.
- Touma, J., and Wisdom, J. 1993. The chaotic obliquity of Mars. *Science* **259**, 1294-1297.
- Touma, J., and Wisdom, J. 1994a. Evolution of the Earth-Moon system. *Astron. J.* **108**, 1943-1961.
- Touma, J., and Wisdom, J. 1994b. Lie-Poisson integrators for rigid body dynamics in the solar system. *Astron. J.* **107**, 1189-1202.
- Touma, J., and Wisdom, J. 1997. Resonances in the early evolution of the Earth-Moon System. submitted
- Tremaine, S. 1998. Celestial mechanics in new planetary systems. *Bull. Amer. Astron. Soc.* **191**, 02.01
- Turcotte, D.L. 1996. Magellan and comparative planetology. *J. Geophys. Res.* **101**, 4765-4773.
- Turcotte, D.L., and Schubert, G. 1982. *Geodynamics: Applications of Continuum Physics to Geologic Problems*. (John Wiley & Sons, New York) pp. 137-139.
- Van Allen, J.A. 1976. High energy particles in the Jovian magnetosphere. in *Jupiter* (ed. Gehrels, T.) (University of Arizona Press, Tucson) pp. 928-960.
- Walker, J.C.G., Hays, P.B., and Kasting, J.F. 1981. A negative feedback mechanism for the long-term stabilization of Earth's surface temperature. *J. Geophys. Res.* **86**, 9776-9782.
- Walker, J.C.G., and Zahnle, K.J. 1986. Lunar nodal tide and the distance to the Moon during the Precambrian. *Nature* **320**, 600-602.

- Ward, W.R. 1973. Large scale variations in the obliquity of Mars. *Science* **181**, 260-262.
- Ward, W.R. 1974. Climatic variations on Mars: I. Astronomical theory of insolation. *J. Geophys. Res.* **79**, 3375-3386.
- Ward, W.R. 1979. Present obliquity oscillations of Mars: fourth-order accuracy in orbital  $e$  and  $i$ . *J. Geophys. Res.* **84**, 237-241.
- Ward, W.R. 1982. Comments on the long-term stability of the Earth's obliquity. *Icarus* **50**, 444-448.
- Ward, W.R. 1991. Resonant obliquity of Mars? *Icarus* **94**, 160-164.
- Ward, W.R. 1992. Long-term orbital and spin dynamics of Mars. in *Mars* (H. Kieffer, B. Jakosky, and C. Snyder, eds.). Univ. of Arizona Press, Tucson) pp. 298-320.
- Watson, A., Lovelock, J.E., and Margulis, L. 1978. *Biosystems* **10**, 293-298.
- Wetherill, G.W. 1996. The formation and habitability of extra-solar planets *Icarus* **119**, 219-238.
- Williams, D.M. 1997. The susceptibility of Earth-like planets to large obliquity variations. in the proceedings of the workshop on "Planetary Systems: the Long View", 9th Rencontres de Blois, June 22-28 1997; Blois, France. ed. Ludwik Celnikier
- Williams, D.M., and Kasting, J.F. 1997. Habitable planets with high obliquities. *Icarus* **129**, 254-268.
- Williams, D.M., Kasting, J.F., and Caldeira, K. 1996. Chaotic obliquity variations and planetary habitability. in *Circumstellar Habitable Zones—Proceedings of the First International Conference* (L.R. Doyle, ed.) (Travis House, Menlo Park, CA) pp. 43-62.
- Williams, D.M., Kasting, J.F., and Frakes, L.A. Was high obliquity the cause of low-latitude Precambrian glaciation? submitted to *Nature*.
- Williams, D.M., Kasting, J.F., and Wade, R.A. 1997. Habitable moons around extrasolar giant planets. *Nature* **385**, 234-236.
- Williams, G.E. 1975. Late Precambrian glacial climate and the Earth's obliquity. *Geol. Mag.* **112**, 441-465.

- Williams, G.E. 1993. History of the Earth's obliquity. *Earth Sci. Rev.* **34**, 1-45.
- Williams, G.E., and Schmidt, P.W. Paleomagnetism of the Palaeoproterozoic Gowganda and Lorrain formations, Ontario: low paleolatitude for Huronian glaciation. *Earth Planet. Sci. Lett.* in press.
- Williams, J.G. 1994. Contribution to the Earth's obliquity rate, precession, and nutation. *Astron. J.* **108**, 711-724.
- Wisdom, J., and Holman, M. 1991. Symplectic maps for the n-body problem. *Astron. J.* **102**, 1528-1538.
- Wisdom, J., and Holman, M. 1992. Symplectic maps for the n-body problem: stability analysis. *Astron. J.* **104**, 2022-2029.
- Wolszczan, A. 1994. Confirmation of Earth-mass planets orbiting the millisecond pulsar PSR B1257+12. *Science* **264**, 538-542.
- Zhang, H., and Zhang, W. 1985. Palaeomagnetic data, late Precambrian magnetostratigraphy and tectonic evolution of eastern China. *Precam. Res.* **29**, 65-75.

# Curriculum Vitae

Darren M. Williams

May 1998

## Personal Data

Birth Date: 6 April 1970 (Buffalo, New York, U.S.)

Marital Status: married (Jody)

## Degrees Received

1990 A.S. Physics, Jamestown Community College, Jamestown NY

1992 B.S. Physics, University of Pittsburgh

1998 Ph.D. Astronomy and Astrophysics, The Pennsylvania State University

## Work Experience

1989-90 Tutor (physics, mathematics, chemistry)  
Jamestown Community College

1991-92 Undergraduate Research Assistant  
University of Pittsburgh

1992-94 Teaching Assistant

1993-95 Graduate Research Assistant

1993-98 Substitute Astronomy Lecturer

1994-98 Department K-12 Outreach Coordinator

1995-98 NASA Graduate Student Fellow

The Pennsylvania State University

## Publications

Williams, D.M., Kasting, J.F., and Caldeira, K. 1996. Chaotic obliquity variations and planetary habitability. in *Circumstellar Habitable Zones—Proceedings of the First International Conference*. (L. Doyle ed.) (Travis House, Menlo Park, CA).

Williams, D.M., Kasting, J.F., and Wade, R.A. 1997. Habitable moons around extrasolar giant planets. *Nature* **385**, 234-236.

Williams, D.M., and Kasting, J.F. 1997. Habitable planets with high obliquities. *Icarus* **129**, 254-268.

Williams, D.M. 1997. The susceptibility of Earth-like planets to large obliquity variations. in the proceedings of the workshop on "Planetary Systems: the Long View", 9th Rencontres de Blois, June 22-28 1997; Blois, France. ed. Ludwik Celnikier.

Williams, D.M., Kasting, J.F., and Frakes, L.A. 1998. Was high obliquity the cause of low-latitude Precambrian glaciation? *in review*.